Chapter 5
Kirchhoff's Rod Theory

"A new idea, supple in application to a variety of mechanical theories and formalisms, was proposed by DUHEM [1893, 1, Ch. II]: A body is to be regarded as a collection not only of points but also of *directions associated with the points*: These vectors, which we shall call the *directors* of the body, are susceptible of rotations and stretches *independent* of the deformation of material elements."
J. L. Ericksen and C. A. Truesdell [100, Page. 297] commenting on Pierre Duhem's (1861–1916) contribution in [94] to the historical development of theories for rods and shells.

5.1 Introduction

The modeling capabilities of inextensible and elastic strings are limited to situations where complete flexibility is assumed. To develop a model capable of resisting bending and torsion, one needs to put additional structure on the theory of a string. The added ingredients we use are a deformable set of vectors which are associated with each point of the material curve. These vectors are known as directors.[1] In the simplest such rod theory, which we present in this chapter, the two directors, $\mathbf{d}_1$ and $\mathbf{d}_2$, deform rigidly and their projections onto the tangent vector $\mathbf{e}_t$ to the material curve remain constant: $(\mathbf{d}_1 \times \mathbf{d}_2) \cdot \mathbf{e}_t = \text{constant}$. We assume that $\{\mathbf{d}_1, \mathbf{d}_2, \mathbf{e}_t\}$ can be considered as an orthonormal triad which varies with the point of the material curve to which it is associated. It may also be helpful to visualize the vectors $\mathbf{d}_1$ and $\mathbf{d}_2$ remaining parallel to material fibers in the cross section as the rod is deformed.

[1] The terminology "director" was introduced in a seminal paper [100] by Ericksen and Truesdell in 1958. For further discussion on the historical developments following the publication of this paper, see [12, 243, 245].

O.M. O'Reilly, *Modeling Nonlinear Problems in the Mechanics of Strings and Rods*,
Interaction of Mechanics and Mathematics, DOI 10.1007/978-3-319-50598-5_5

In a seminal work [185] published in 1859, Gustav Kirchhoff (1824–1887) proposed a rod theory capable of modeling bending and torsion. The theory is discussed at length in Love's influential treatise [213]. Although Kirchhoff's treatment differs from the modern one we discuss here, the rod theory we present is known as Kirchhoff's rod theory in recognition of his contribution. In the early years of the 20th century, the Cosserat brothers, Eugène (1866–1931) and François (1852–1914), influenced by Duhem [94], formulated Kirchhoff's rod theory using what are now known as directors in [71, 72]. Consequently, the rod theory is also considered as an example of a Cosserat rod theory. Kirchhoff's rod theory is arguably the most popular three-dimensional rod theory in use and has been the subject of a large number of works since the mid-1950s. It has been applied to a wide range of problems including configurations of DNA minicircles (see, e.g., [317, 319, 320]), tendril perversion and vine attachment in plants (see, e.g., [122, 235]), torsional buckling (see, e.g., [164]), and chaotic vibrations of an elastic rod (see, e.g., [78, 79]), among many others. Works on these applications have also been supplemented by an ever increasing body of work, such as [221, 222, 224, 226], examining the linear and nonlinear stability of the equilibrium configurations of the rod and works in computer graphics where this rod theory is used to model strands of hair (see [22, 281, 355] and references therein).

Our exposition of the theory benefits greatly from the aforementioned research and, in particular, the works of Antman [10, 12], Green and Laws [130], and Naghdi and Rubin [246]. In the first part of this chapter, we examine how the introduction of the directors captures the torsional and bending strains. We then explore the types of discontinuities that this rod theory can reproduce. Following our developments with the string, the balance laws are first postulated and then the local forms and jump conditions are derived. Our treatment of this matter parallels the developments for strings and consequently many of the arguments are presented with minimal detail.

Once the balance laws and jump conditions are established, the process of prescribing constitutive relations and examining which of these conditions are nontrivial begins. You will find that the theory promptly reduces to a tractable set of equations which are highly amenable to applications and simplifications. For example, we readily find Euler's theory of the elastica as a special case of the rod theory. In addition, for static configurations of a Kirchhoff rod, the governing ordinary differential equations can often be placed in one-to-one correspondence with the equations governing the attitude of a rigid body.

The chapter concludes with a range of applications of the theory to studying the deformed shape of rods subject to terminal loads. While we cover a spectrum of works on some classic problems, we need to limit our scope to a small fraction of the work that has used Kirchhoff's rod theory. Our hope is that we will have provided the necessary background and a sufficient number of applications for the reader to be able to continue their own exploration and enjoyment of the vast literature discussing applications of this popular rod theory.

5.2 The Directed Curve

Thus far, we have introduced two different types of curves: space curves and material curves. A directed curve is a material curve $\mathscr{L}$ to which at each point a set of directors are defined. The directors represent kinematical quantities pertaining to the cross sections of a rod-like body. Hence, the directed curve serves as a model for a rod-like body. Following the seminal work of the Cosserat brothers in the early 1900s, a directed curve is often known as a Cosserat curve.

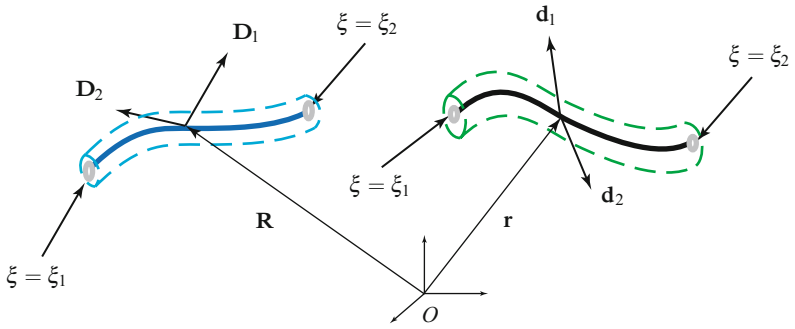

Fig. 5.1 The curve $\mathbf{r}(\xi,t)$ and the vector fields $\mathbf{d}_\alpha(\xi,t)$ at a point along its length. The reference configuration $\mathscr{R}_0$ of the Cosserat (or directed) curve is also shown in this figure.

Referring to Figure 5.1, in its present configuration $\mathscr{R}$, the directed curve is defined by the vector-valued functions $\mathbf{r} = \mathbf{r}(\xi,t)$ and $\mathbf{d}_\alpha = \mathbf{d}_\alpha(\xi,t)$ where $\alpha = 1,2$. Here, ξ is a convected coordinate along the material curve and $\mathbf{r}$ is the position vector of a material point of the curve with respect to a fixed origin. As mentioned previously, the vectors $\mathbf{d}_1$ and $\mathbf{d}_2$ are known as directors.

A reference configuration $\mathscr{R}_0$ of the directed curve is defined by the vector fields $\mathbf{R} = \mathbf{R}(\xi)$ and $\mathbf{D}_\alpha = \mathbf{D}_\alpha(\xi)$. For convenience, we shall assume that ξ is the arc-length parameter of the reference configuration of the material curve. It should be clear that we are assuming that the reference configuration is fixed.

In many treatments, it is common to denote $\frac{\partial \mathbf{r}}{\partial \xi}$ by $\mathbf{d}_3$. This is especially the case with the papers of Green, Naghdi, and Rubin [245, 309]. Similarly, $\frac{\partial \mathbf{R}}{\partial \xi}$ is denoted by $\mathbf{D}_3$. Alternatively, following Antman [12], one defines $\mathbf{d}_3 = \mathbf{d}_1 \times \mathbf{d}_2$ and $\mathbf{D}_3 = \mathbf{D}_1 \times \mathbf{D}_2$. For the rod theory presented in this chapter, it is convenient to use Antman's definition.

5.2.1 An Approximation

Our conception of a rod is primarily as an approximation to a three-dimensional body. In this context, the need to relate quantities associated with the three -dimensional body to the corresponding quantities associated with the rod is crucial

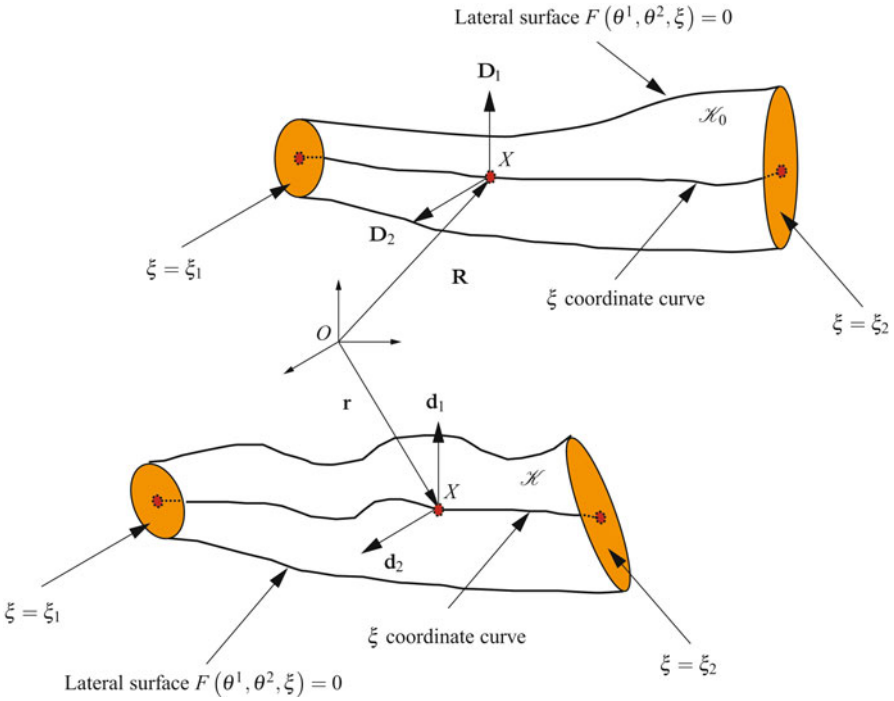

Fig. 5.2 Schematic of the reference $\mathscr{K}_0$ and present $\mathscr{K}$ configurations of a three-dimensional rod-like body whose reference configuration is parameterized using a curvilinear coordinate system. The ends of the body are described by $\theta^3=\xi$ coordinate surfaces, the centerline is described by a ξ coordinate curve where $\theta^1=\theta^2=0$, and the lateral surface of the body is described using the function $F(\theta^1,\theta^2,\xi)$.

in applications. Fortunately, there has been a wealth of work performed on the correspondences between fields associated with the rod theory and those associated with the three-dimensional body that it is modeling. Of particular relevance is the work of Green, Naghdi, and their coworkers [131, 137], which we will now employ.

Consider a three-dimensional rod-like body $\mathscr{B}$ and assign to it a set of curvilinear coordinates θ^i. If we were to model this body using a directed curve, then the following identifications would be made:

$$\xi=\theta^3,\qquad \mathbf{R}^*=\mathbf{R}(\xi)+\sum_{\alpha=1}^{2}\theta^\alpha\mathbf{D}_\alpha(\xi). \tag{5.1}$$

Here, $\mathbf{R}^*$ is the position vector of the material point identified using θ^i (see Figure 5.2). In the present configuration, these choices imply the following approximation:

$$\mathbf{r}^*=\mathbf{r}^*(\theta^i,t)\approx\mathbf{r}(\xi,t)+\sum_{\alpha=1}^{2}\theta^\alpha\mathbf{d}_\alpha(\xi,t). \tag{5.2}$$

This result will be very useful in prescribing kinematical quantities in the sequel.

5.3 Kinematics of Kirchhoff's Rod Theory

For Kirchhoff's rod theory, the material curve $\mathscr{L}$ is assumed to be inextensible: $\frac{\partial \mathbf{r}}{\partial \xi} = \mathbf{e}_t$. Further the cross sections are assumed to remain plane, and the projection of the normal vector to the cross section onto $\mathbf{e}_t$ remains constant. Torsion is accommodated by a rotation of the directors about $\mathbf{e}_t$. To render these statements into a mathematically tractable form, we assume that $\mathbf{D}_1$, $\mathbf{D}_2$, and $\mathbf{D}_3$ define a right-handed orthonormal triad at each ξ:

$$[\mathbf{D}_1, \mathbf{D}_2, \mathbf{D}_3] = 1. \tag{5.3}$$

If we denote a fixed right-handed basis for $\mathbb{E}^3$ by $\{\mathbf{E}_1, \mathbf{E}_2, \mathbf{E}_3\}$, then we can define a rotation tensor $\mathbf{P}_0$:

$$\mathbf{P}_0 = \mathbf{D}_1 \otimes \mathbf{E}_1 + \mathbf{D}_2 \otimes \mathbf{E}_2 + \mathbf{D}_3 \otimes \mathbf{E}_3. \tag{5.4}$$

That is, $\mathbf{D}_i = \mathbf{P}_0 \mathbf{E}_i$. For many reference configurations, we can choose $\mathbf{D}_i$ such that $\mathbf{P}_0 = \mathbf{I}$; some exceptions are for what Love [213] refers to as initially curved rods.

Under a motion of the directed curve, the vectors $\mathbf{d}_i$ retain their relative orientation and magnitude. Consequently,

$$\mathbf{d}_i = \mathbf{P}\mathbf{D}_i, \qquad (i = 1,2,3), \tag{5.5}$$

where $\mathbf{P}$ is a rotation tensor.[2] You should notice that

$$\mathbf{d}_\alpha = \mathbf{P}\mathbf{P}_0\mathbf{E}_\alpha, \qquad \frac{\partial \mathbf{r}}{\partial \xi} = \mathbf{P}\frac{\partial \mathbf{R}}{\partial \xi}, \qquad (\alpha = 1,2). \tag{5.6}$$

These two equations define the constraints on the rod. They are often known as "Kirchhoff's constraints."

The constraints (5.6) imply that

$$\mathbf{d}_\alpha' = (\mathbf{P}(\mathbf{v} + \mathbf{v}_0)) \times \mathbf{d}_\alpha. \tag{5.7}$$

Here, the prime denotes the partial derivative with respect to ξ, and $\mathbf{v}$ and $\mathbf{v}_0$ are axial vectors of skew-symmetric tensors[3]:

$$\mathbf{v} = \mathrm{ax}(\mathbf{K}), \quad \mathbf{K} = \mathbf{P}^T\mathbf{P}', \quad \mathbf{v}_0 = \mathrm{ax}(\mathbf{K}_0), \quad \mathbf{K}_0 = \mathbf{P}_0'\mathbf{P}_0^T. \tag{5.8}$$

---

[2] Recall that an orthogonal tensor $\mathbf{Q}$ has the property that $\mathbf{Q}\mathbf{Q}^T = \mathbf{I}$ and so $\det(\mathbf{Q}) = \pm 1$. A proper-orthogonal tensor $\mathbf{Q}$ has a determinant of 1. From Euler's theorem in rigid body dynamics, proper-orthogonal tensors and rotation tensors are synonymous.

[3] Recall that the axial vector $\mathbf{b}$ of any skew-symmetric tensor $\mathbf{B} = -\mathbf{B}^T$ has the property that $\mathbf{b} \times \mathbf{c} = \mathbf{B}\mathbf{c}$ for any vector $\mathbf{c}$. As a skew-symmetric tensor has three independent components, there is a one-to-one correspondence between $\mathbf{B}$ and its axial vector $\mathbf{b}$ (cf. Eqns. (1.17) and (1.18)).

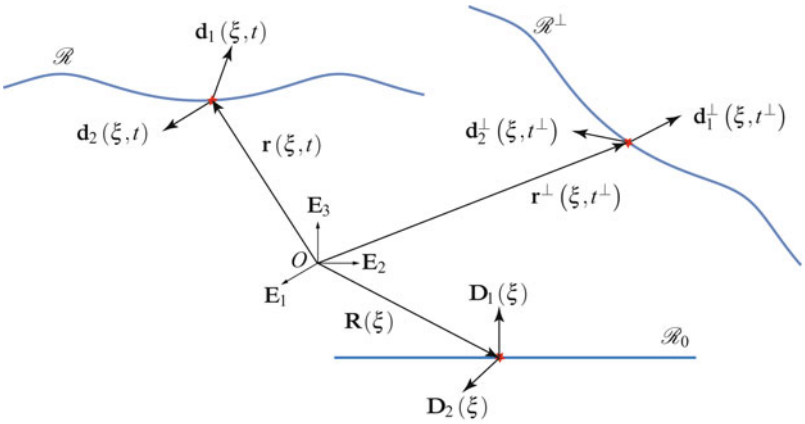

Fig. 5.3 An example of two motions of a directed curve which differ by a rigid body motion. Observe that both motions are relative to the same reference configuration $\mathscr{R}_0$.

The axial vector $\mathbf{v}$ will play a key role in the sequel. We note that the identity

$$\operatorname{ax}\left(\mathbf{Q}\mathbf{B}\mathbf{Q}^T\right) = \det(\mathbf{Q})\,\mathbf{Q}\operatorname{ax}(\mathbf{B}), \tag{5.9}$$

which holds for all orthogonal tensors $\mathbf{Q}$ and all skew-symmetric tensors $\mathbf{B}$, was used to establish (5.7) from (5.6).

Referring to Figure 5.3, we now consider two motions of a directed curve which differ by a rigid body motion:

$$\begin{gathered}\mathbf{r}^\perp\left(\xi,t^\perp\right) = \mathbf{Q}(t)\,\mathbf{r}(\xi,t) + \mathbf{q}(t),\\ \mathbf{d}_1^\perp\left(\xi,t^\perp\right) = \mathbf{Q}(t)\,\mathbf{d}_1(\xi,t), \qquad \mathbf{d}_2^\perp\left(\xi,t^\perp\right) = \mathbf{Q}(t)\,\mathbf{d}_2(\xi,t).\end{gathered} \tag{5.10}$$

As with the previous developments in the theory of a string, $\mathbf{Q}$ is a proper-orthogonal tensor-valued function of time, $\mathbf{q}(t)$ is a vector-valued function of time, and $t^\perp = t + a$ with a being constant. It follows that

$$\mathbf{P}^\perp\left(\xi,t^\perp\right) = \mathbf{Q}(t)\mathbf{P}(\xi,t). \tag{5.11}$$

An easy calculation shows that the tensor $\mathbf{K}$ and its associated axial vector $\mathbf{v}$ are identical at the same material point of the present configurations $\mathscr{R}$ and $\mathscr{R}^\perp$:

$$\mathbf{K}^\perp\left(\xi,t^\perp\right) = \mathbf{K}(\xi,t), \qquad \mathbf{v}^\perp\left(\xi,t^\perp\right) = \mathbf{v}(\xi,t). \tag{5.12}$$

Consequently, $\mathbf{v}$ is used in the sequel as a strain measure. We invite the reader to examine how our remarks pertain to the strain measures $\frac{\partial\theta}{\partial\xi}$ and μ for the extensible elastica.

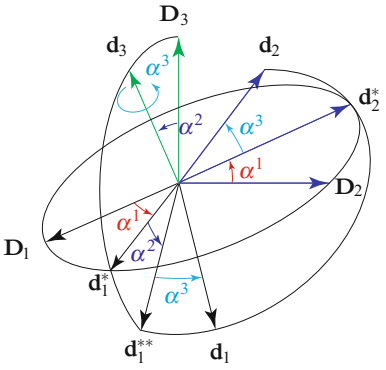

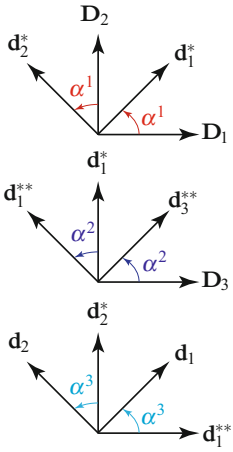

Fig. 5.4 Schematic of a set of 3-2-3 Euler angles that are used to parameterize a rotation from the basis $\{\mathbf{D}_1, \mathbf{D}_2, \mathbf{D}_3\}$ to the basis $\{\mathbf{d}_1, \mathbf{d}_2, \mathbf{d}_3\}$. The three axes of rotation are $\mathbf{e}_1 = \mathbf{D}_3 = \mathbf{d}_3^*$, $\mathbf{e}_2 = \mathbf{d}_2^* = \mathbf{d}_2^{**}$, and $\mathbf{e}_3 = \mathbf{d}_3^{**} = \mathbf{d}_3$ and the inset image is a Handmann's portrait of Leonhard Euler (1707–1783) from 1753. For details on the intermediate bases used to construct the figure, see Eqn. (5.17).

5.3.1 Parameterizations of the Rotation Tensor

To parameterize the rotation tensor $\mathbf{P}$ we follow classic treatments and use a set of Euler angles. Specifically, we incorporate Love's exposition in [213] and, from the 12 possible choices of Euler angles, use a set of 3-2-3 Euler angles to parameterize $\mathbf{P}$.[4] We also supplement Love's exposition with a more modern treatment of the Euler angles from the textbook [265]. Complementing our discussion of the 3-2-3 set of Euler angles, the corresponding developments for a set of 3-2-1 Euler angles are presented in Exercise 5.6 at the end of this chapter.[5] This set of Euler angles is more suited to examining linearized versions of the rod theory presented in this chapter. We also take this opportunity to note that Euler angles are not the sole parameterization for $\mathbf{P}$ in Kirchhoff's rod theory in the literature. Recently, Maddocks and his coworkers [86, 178] have ingeniously used quaternions (also known as the Euler-Rodrigues parameters) to parameterize $\mathbf{P}$ while Simo and Vu-Quoc [327] have used the exponential map. For a discussion of these parameterizations and several others, the interested reader is referred to Shuster's authoritative review [321] on rotations.

[4] The 3-2-3 set of Euler angles is also used in several texts, for example, Ginsberg [115, Section 4.2], Kelvin and Tait [180], Routh [305, 306], and Whittaker [362].

[5] The 3-2-1 set of Euler angles are sometimes known as the Tait-Bryan angles and are prominent in aircraft and vehicle dynamics. The first instance of their development and use dates to the seminal work of Fick and Helmholtz [166, 167] on the kinematics of the eye (see [156, 253] and references therein) in the mid-1800s and Tait's work [336] on rigid body dynamics in 1868.

In the 3-2-3 set of Euler angles, the tensor $\mathbf{P}$ is decomposed into the product of three simple rotations:

$$\mathbf{P} = \mathbf{Q}_{\mathbf{E}}\left(\alpha^3, \mathbf{e}_3\right) \mathbf{Q}_{\mathbf{E}}\left(\alpha^2, \mathbf{e}_2\right) \mathbf{Q}_{\mathbf{E}}\left(\alpha^1, \mathbf{e}_1\right), \tag{5.13}$$

where the function $\mathbf{Q}_{\mathbf{E}}(\theta, \mathbf{i})$ describes a rotation about an axis described by a unit vector $\mathbf{i}$ through a counterclockwise angle θ[6]:

$$\mathbf{Q}_{\mathbf{E}}(\theta, \mathbf{i}) = \cos(\theta)(\mathbf{I} - \mathbf{i} \otimes \mathbf{i}) + \sin(\theta)\text{skew}(\mathbf{i}) + \mathbf{i} \otimes \mathbf{i}. \tag{5.14}$$

The basis $\{\mathbf{e}_1, \mathbf{e}_2, \mathbf{e}_3\}$ is known as the Euler basis. This basis is not orthogonal, and, for the 3-2-3 set of interest here,

$$\begin{aligned}
\mathbf{e}_1 &= \mathbf{D}_3 \\
&= \cos\left(\alpha^2\right)\mathbf{d}_3 - \sin\left(\alpha^2\right)\left(\cos\left(\alpha^3\right)\mathbf{d}_1 - \sin\left(\alpha^3\right)\mathbf{d}_2\right), \\
\mathbf{e}_2 &= \cos\left(\alpha^1\right)\mathbf{D}_2 - \sin\left(\alpha^1\right)\mathbf{D}_1 \\
&= \cos\left(\alpha^3\right)\mathbf{d}_2 + \sin\left(\alpha^3\right)\mathbf{d}_1, \\
\mathbf{e}_3 &= \cos\left(\alpha^2\right)\mathbf{D}_3 + \sin\left(\alpha^2\right)\left(\cos\left(\alpha^1\right)\mathbf{D}_1 + \sin\left(\alpha^1\right)\mathbf{D}_2\right) \\
&= \mathbf{d}_3.
\end{aligned} \tag{5.15}$$

The angles α^1 and α^3 range from 0 to 2π. Because

$$[\mathbf{e}_1, \mathbf{e}_2, \mathbf{e}_3] = -\sin\left(\alpha^2\right), \tag{5.16}$$

in order to ensure that the Euler basis is a basis for $\mathbb{E}^3$, we restrict the second angle $\alpha^2 \in (0, \pi)$. Other perspectives on the singularity when $\alpha^2 = 0, \pi$ might be helpful. First, we note that α^1 and α^2 are polar coordinates for the axis of rotation $\mathbf{e}_3 = \mathbf{d}_3$. Thus, the singularity arises when, for a single value of α^2, multiple values of α^1 are possible. We shall examine two other perspectives shortly.

Referring to Figure 5.4, it is straightforward to transform from $\mathbf{d}_i$ to $\mathbf{D}_i$ and vice versa with the help of two pairs of intermediate bases $\left\{\mathbf{d}_1^*, \mathbf{d}_2^*, \mathbf{d}_3^*\right\}$ and $\left\{\mathbf{d}_1^{**}, \mathbf{d}_2^{**}, \mathbf{d}_3^{**}\right\}$:

$$\begin{aligned}
\begin{bmatrix} \mathbf{d}_1^* \\ \mathbf{d}_2^* \\ \mathbf{d}_3^* \end{bmatrix} &= \begin{bmatrix} \cos\left(\alpha^1\right) & \sin\left(\alpha^1\right) & 0 \\ -\sin\left(\alpha^1\right) & \cos\left(\alpha^1\right) & 0 \\ 0 & 0 & 1 \end{bmatrix} \begin{bmatrix} \mathbf{D}_1 \\ \mathbf{D}_2 \\ \mathbf{D}_3 \end{bmatrix}, \\
\begin{bmatrix} \mathbf{d}_1^{**} \\ \mathbf{d}_2^{**} \\ \mathbf{d}_3^{**} \end{bmatrix} &= \begin{bmatrix} \cos\left(\alpha^2\right) & 0 & -\sin\left(\alpha^2\right) \\ 0 & 1 & 0 \\ \sin\left(\alpha^2\right) & 0 & \cos\left(\alpha^2\right) \end{bmatrix} \begin{bmatrix} \mathbf{d}_1^* \\ \mathbf{d}_2^* \\ \mathbf{d}_3^* \end{bmatrix}, \\
\begin{bmatrix} \mathbf{d}_1 \\ \mathbf{d}_2 \\ \mathbf{d}_3 \end{bmatrix} &= \begin{bmatrix} \cos\left(\alpha^3\right) & \sin\left(\alpha^3\right) & 0 \\ -\sin\left(\alpha^3\right) & \cos\left(\alpha^3\right) & 0 \\ 0 & 0 & 1 \end{bmatrix} \begin{bmatrix} \mathbf{d}_1^{**} \\ \mathbf{d}_2^{**} \\ \mathbf{d}_3^{**} \end{bmatrix}.
\end{aligned} \tag{5.17}$$

[6] The operator skew($\mathbf{i}$) transforms $\mathbf{i}$ into a skew-symmetric tensor such that $\mathbf{i} \times \mathbf{b} = \text{skew}(\mathbf{i})\mathbf{b}$ for any vector $\mathbf{b}$ (cf. Eqn. (1.19)).

After recalling that $\mathbf{P}$ has several representations, including

$$\mathbf{P} = \sum_{i=1}^{3} \mathbf{d}_i \otimes \mathbf{D}_i = \sum_{i=1}^{3}\sum_{k=1}^{3} P_{ik}\mathbf{D}_i \otimes \mathbf{D}_k = \sum_{i=1}^{3}\sum_{k=1}^{3} P_{ik}\mathbf{d}_i \otimes \mathbf{d}_k, \tag{5.18}$$

we note that the three matrices in Eqn. (5.17) can be combined to provide expressions for the components $P_{ik} = (\mathbf{P}\mathbf{D}_k)\cdot\mathbf{D}_i$ of $\mathbf{P}$:

$$\begin{bmatrix} P_{11} & P_{12} & P_{13} \\ P_{21} & P_{22} & P_{23} \\ P_{31} & P_{32} & P_{33} \end{bmatrix} = \begin{bmatrix} c_1c_2c_3 - s_1s_3 & -c_3s_1 - c_1c_2s_3 & c_1s_2 \\ c_2c_3s_1 + c_1s_3 & c_1c_3 - c_2s_1s_3 & s_1s_2 \\ -c_3s_2 & s_2s_3 & c_2 \end{bmatrix}. \tag{5.19}$$

In writing expressions for the components P_{ik}, we have used the helpful abbreviations $c_k = \cos\left(\alpha^k\right)$ and $s_k = \sin\left(\alpha^k\right)$.

It is natural to choose a reference configuration so that $\mathbf{P} = \mathbf{I}$ in an undeformed configuration. However, as we now show, when the 3-2-3 set of Euler angles is used to parameterize $\mathbf{P}$ such a selection is problematic. To proceed, we examine the conditions by which the components of $\mathbf{P}$ in Eqn. (5.19) reduce to $P_{ik} = \delta_{ik}$. It is straightforward to see that these conditions are simply

$$\alpha^2 = 0, \qquad \alpha^1 + \alpha^3 = n\pi, \qquad n = 0, 1, 2, 3, 4. \tag{5.20}$$

Thus, there is no one-to-one correspondence between the 3-2-3 set of Euler angles and the identity tensor. In addition, in order to use the 3-2-3 set of Euler angles to parameterize $\mathbf{P} = \mathbf{I}$ we must set α^2 to one of its singular values and this will present other problems.

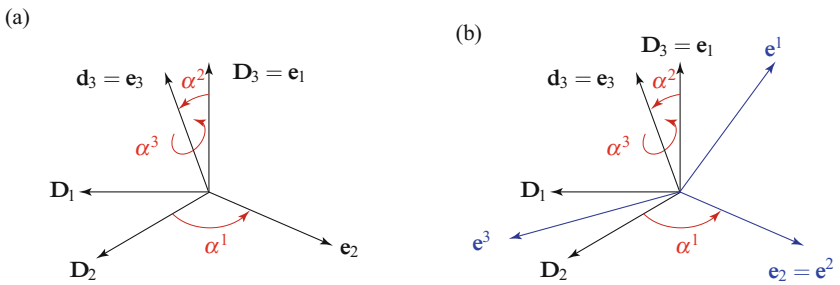

Fig. 5.5 Schematic of the Euler and dual Euler basis vectors associated with a 3-2-3 set of Euler angles. (a) The Euler basis vectors, $\mathbf{e}_1$, $\mathbf{e}_2$, and $\mathbf{e}_3$, and their relation to the Euler angles (cf. Eqn. (5.15)) and (b) the corresponding dual Euler basis vectors, $\mathbf{e}^1$, $\mathbf{e}^2$, and $\mathbf{e}^3$, (cf. Eqn. (5.23)).

In addition to the Euler basis, we also have a companion dual Euler basis. The latter basis has application to representations of moment vectors [262, 270, 271] and we shall exploit this in the sequel. We also note that there is a direct correspondence between the Euler and dual Euler basis sets and covariant and contravariant sets of basis vectors in differential geometry. Given an Euler basis, the corresponding dual

Euler basis vectors are defined by the nine relations

$$\mathbf{e}^k \cdot \mathbf{e}_i = \delta_i^k \qquad (i = 1,2,3, \text{ and } k = 1,2,3), \tag{5.21}$$

where δ_i^k is the Kronecker delta: $\delta_i^k = 1$ if $i = k$ and is otherwise 0. The solution to these nine equations is known in differential geometry (see, e.g., [140, Eqn. (1.9.13)] or [325, Exercise 2.11]):

$$\mathbf{e}^1 = \frac{\mathbf{e}_2 \times \mathbf{e}_3}{(\mathbf{e}_1 \times \mathbf{e}_2) \cdot \mathbf{e}_3}, \qquad \mathbf{e}^2 = \mathbf{e}_2, \qquad \mathbf{e}^3 = \frac{\mathbf{e}_1 \times \mathbf{e}_2}{(\mathbf{e}_1 \times \mathbf{e}_2) \cdot \mathbf{e}_3}. \tag{5.22}$$

The expression for $\mathbf{e}^2$ is greatly simplified because this Euler basis vector is perpendicular to the other two: $\mathbf{e}_1 \perp \mathbf{e}_2$ and $\mathbf{e}_3 \perp \mathbf{e}_2$. With the help of Eqn. (5.22), we now compute the dual Euler basis vectors for the 3-2-3 set of Euler angles:

$$\begin{aligned}
\mathbf{e}^1 &= \frac{\mathbf{e}_2 \times \mathbf{e}_3}{[\mathbf{e}_1, \mathbf{e}_2, \mathbf{e}_3]} = \operatorname{cosec}\left(\alpha^2\right)\left(\sin\left(\alpha^3\right)\mathbf{d}_2 - \cos\left(\alpha^3\right)\mathbf{d}_1\right), \\
\mathbf{e}^2 &= \frac{\mathbf{e}_3 \times \mathbf{e}_1}{[\mathbf{e}_1, \mathbf{e}_2, \mathbf{e}_3]} = \mathbf{e}_2 = \cos\left(\alpha^3\right)\mathbf{d}_2 + \sin\left(\alpha^3\right)\mathbf{d}_1, \\
\mathbf{e}^3 &= \frac{\mathbf{e}_1 \times \mathbf{e}_2}{[\mathbf{e}_1, \mathbf{e}_2, \mathbf{e}_3]} = \cot\left(\alpha^2\right)\left(\cos\left(\alpha^3\right)\mathbf{d}_1 - \sin\left(\alpha^3\right)\mathbf{d}_2\right) + \mathbf{d}_3.
\end{aligned} \tag{5.23}$$

The Euler and dual Euler bases are sketched in Figure 5.5. As a third and final perspective on the Euler angle singularity, we observe from Eqn. (5.23) that the dual Euler basis vectors are not defined when $\alpha^2 = 0, \pi$.

For future reference, we note that the axial vector associated with $\dot{\mathbf{P}}\mathbf{P}^T$ has a simple representation[7]:

$$\boldsymbol{\omega} = \operatorname{ax}\left(\dot{\mathbf{P}}\mathbf{P}^T\right) = \dot{\alpha}^3\mathbf{e}_3 + \dot{\alpha}^2\mathbf{e}_2 + \dot{\alpha}^1\mathbf{e}_1. \tag{5.24}$$

In addition, referring to Eqn. (5.7), we find that

$$\mathbf{P}\left(\mathbf{v} + \mathbf{v}_0\right) = \frac{\partial \alpha^3}{\partial \xi}\mathbf{e}_3 + \frac{\partial \alpha^2}{\partial \xi}\mathbf{e}_2 + \frac{\partial \alpha^1}{\partial \xi}\mathbf{e}_1 + \mathbf{P}\mathbf{v}_0. \tag{5.25}$$

Using the representations for $\mathbf{e}_i$ in terms of $\mathbf{d}_k$ given in Eqn. (5.15), it is straightforward to compute $\mathbf{P}^T\mathbf{e}_i$ and arrive at a representation for $\mathbf{v} + \mathbf{v}_0$.

[7] The axial vectors in Eqns. (5.24) and (5.25) can be computed by direct differentiation of the tensor $\mathbf{P}$ or using the relative angular velocity vector proposed by Casey and Lam [51]. Applications of Casey and Lam's relative angular velocity vector can be found in the textbook [265, Sections 6.7 and 6.8].

5.3.2 Strains

The components of $\mathbf{P}\boldsymbol{\nu}$ with respect to the basis $\{\mathbf{d}_1, \mathbf{d}_2, \mathbf{d}_3 = \mathbf{d}_1 \times \mathbf{d}_2\}$ define three strain measures:

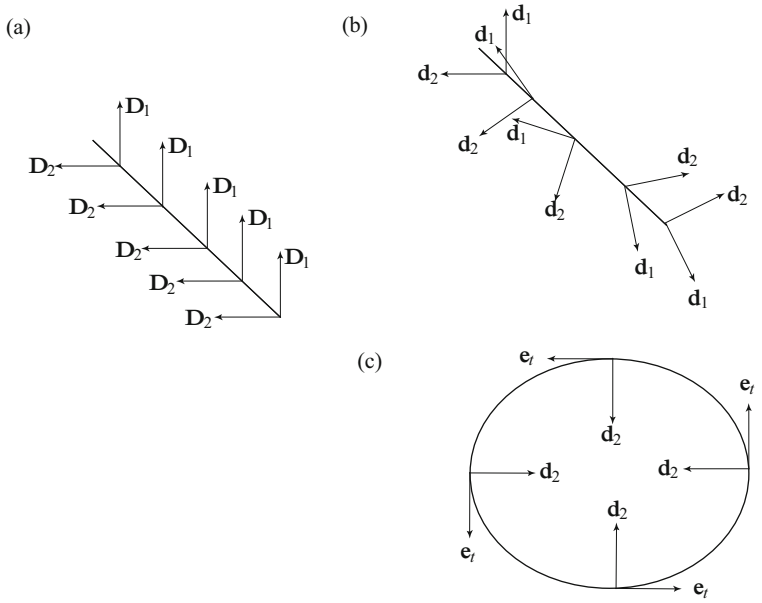

Fig. 5.6 Illustration of the strains for the Kirchhoff rod theory. (a), The reference configuration $\mathscr{R}_0$ of a straight rod; (b), pure torsion $(\nu_1 = 0, \nu_2 = 0, \nu_3 \neq 0)$ of the rod; and (c), pure bending $(\nu_1 \neq 0, \nu_2 = 0, \nu_3 = 0)$ of the rod so that its material curve forms a circle in the present configuration $\mathscr{R}$.

$$\boldsymbol{\nu} = \nu_1 \mathbf{D}_1 + \nu_2 \mathbf{D}_2 + \nu_3 \mathbf{D}_3. \tag{5.26}$$

An alternative set of strain measures are the components of $\mathbf{P}(\mathbf{v} + \mathbf{v}_0)$ with respect to the basis $\{\mathbf{d}_1, \mathbf{d}_2, \mathbf{d}_3 = \mathbf{d}_1 \times \mathbf{d}_2\}$:

$$\mathbf{v} + \mathbf{v}_0 = (\nu_1 + \nu_{0_1})\,\mathbf{D}_1 + (\nu_2 + \nu_{0_2})\,\mathbf{D}_2 + \left(\nu_3 + \nu_{0_3}\right)\mathbf{D}_3. \tag{5.27}$$

This set of strains could be considered as taken relative to a reference configuration where the centerline was straight and the directors were constant. Some authors use $\mathbf{v}$ as a strain measure: particularly for rod models of double-stranded DNA where $\mathbf{v}_0 = \nu_{0_3}\mathbf{E}_3$ (see, e.g., [158, 199, 228]).

The strains ν_1 and ν_2 are associated with the curvature of the centerline and are commonly referred to as curvatures. The question "why are there two curvatures when a space curve only has one?" shall be answered shortly. In addition, ν_3

is known as the torsion. This torsion should not be confused with the geometric torsion τ. We illustrate these bending and torsional strains in Figure 5.6. For the reference configuration $\mathscr{R}_0$ shown in this figure, the intrinsic strains v_{0_k} are zero.

If a set of 3-2-3 Euler angles are used to parameterize $\mathbf{P}$, then, computing the components $\mathbf{P}\mathbf{v}\cdot\mathbf{d}_k$ with the help of Eqns. (5.15), (5.25), and (5.26), we find that[8]

$$\begin{bmatrix} v_1 \\ v_2 \\ v_3 \end{bmatrix} = \begin{bmatrix} -\sin\left(\alpha^2\right)\cos\left(\alpha^3\right) & \sin\left(\alpha^3\right) & 0 \\ \sin\left(\alpha^2\right)\sin\left(\alpha^3\right) & \cos\left(\alpha^3\right) & 0 \\ \cos\left(\alpha^2\right) & 0 & 1 \end{bmatrix} \begin{bmatrix} \frac{\partial\alpha^1}{\partial\xi} \\ \frac{\partial\alpha^2}{\partial\xi} \\ \frac{\partial\alpha^3}{\partial\xi} \end{bmatrix}. \tag{5.28}$$

Inverting the matrix in the above equation or, equivalently, computing $\mathbf{P}\mathbf{v}\cdot\mathbf{e}^k$ with the help of Eqns. (5.23), (5.25), and (5.26), yields expressions for the spatial rates of change of the Euler angles in terms of the strains v_i:

$$\begin{bmatrix} \frac{\partial\alpha^1}{\partial\xi} \\ \frac{\partial\alpha^2}{\partial\xi} \\ \frac{\partial\alpha^3}{\partial\xi} \end{bmatrix} = \begin{bmatrix} -\operatorname{cosec}\left(\alpha^2\right)\cos\left(\alpha^3\right) & \operatorname{cosec}\left(\alpha^2\right)\sin\left(\alpha^3\right) & 0 \\ \sin\left(\alpha^3\right) & \cos\left(\alpha^3\right) & 0 \\ \cot\left(\alpha^2\right)\cos\left(\alpha^3\right) & -\cot\left(\alpha^2\right)\sin\left(\alpha^3\right) & 1 \end{bmatrix} \begin{bmatrix} v_1 \\ v_2 \\ v_3 \end{bmatrix}. \tag{5.29}$$

It should be transparent from the above equations that, while it is easy to correlate the rotation of the directors to the changes in Euler angles, correlating $\frac{\partial\alpha^k}{\partial\xi}$ to the rod strains v_i is nontrivial and, moreover, is impossible when $\alpha^2 = 0, \pi$.

5.3.2.1 An Example

As an illustrative example, we consider the helically plied structures shown in Figure 5.7. Suppose we wish to model the helical plies and the cylindrical structure about which they are wrapped as a single rod. We are then faced with the issue of a choice of reference configuration for such a structure and, with that, a choice of the directors $\mathbf{D}_1$ and $\mathbf{D}_2$. Here, we consider one possible choice where these directors "follow" the helical strand. We emphasize that $\mathbf{R}(\xi)$ for all the three structures shown in Figure 5.7 is the position vector of material points located on the centerline of the cylindrical body. A closely related application will be discussed in Section 5.18 when helical springs, such as the one shown in Figure 5.27, are analyzed using Kirchhoff's rod theory.

To proceed, we choose a fixed unit vector $\mathbf{E}_3$ which is parallel to the axis of the rod in its reference configuration[9]:

$$\mathbf{R}(\xi) = \xi\mathbf{E}_3. \tag{5.30}$$

[8] For the reader comparing our treatment to Love's classic work, the relations (5.28) are identical to [213, Eqn. (8), Page 386].

[9] You may wish to look at our earlier discussion of the helix in Section 3.4.

We assume that the pitch angle of the helix is β, and the equation of the centerline of the helical strand is parameterized using a polar angle ϕ:

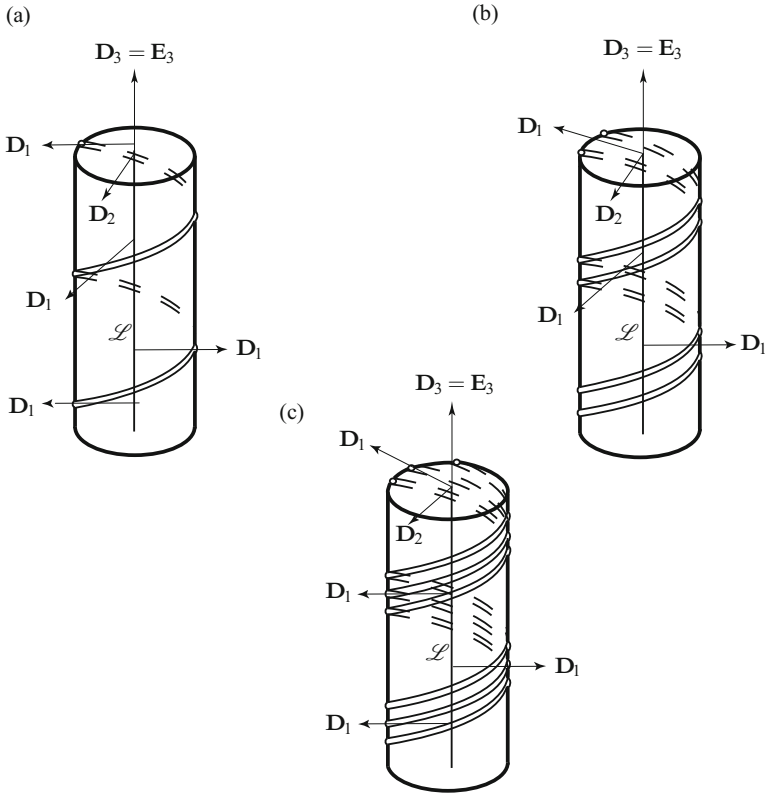

Fig. 5.7 Examples of reference configurations of a cylindrical body with helical plies wound on its lateral surface. Representatives of the referential values of the directors $\mathbf{D}_1$ and $\mathbf{D}_2$ associated with the Cosserat rod that can be used to model the body are also shown in this figure. The material curve $\mathscr{L}$ associated with the rod is the centerline of the cylindrical body. In (a), a single ply; in (b), a two-ply; and in (c), a triple-ply. The two-ply is similar to double-stranded DNA. This figure is adapted from [199].

$$\mathbf{x} = R\left(\cos(\phi)\mathbf{E}_1 + \sin(\phi)\,\mathbf{E}_2\right) + R\tan(\beta)\,\phi\mathbf{E}_3. \tag{5.31}$$

Here, R and $\beta \neq 0$ are constants, and

$$\xi = R\tan(\beta)\,\phi. \tag{5.32}$$

We next prescribe the referential directors:

$$\mathbf{D}_1(\xi) = \cos\left(\frac{\xi}{R\tan(\beta)}\right)\mathbf{E}_1 + \sin\left(\frac{\xi}{R\tan(\beta)}\right)\mathbf{E}_2,$$
$$\mathbf{D}_2(\xi) = -\sin\left(\frac{\xi}{R\tan(\beta)}\right)\mathbf{E}_1 + \cos\left(\frac{\xi}{R\tan(\beta)}\right)\mathbf{E}_2,$$
$$\mathbf{D}_3(\xi) = \mathbf{E}_3. \tag{5.33}$$

With this choice, the material coordinate ξ is chosen to be the arc-length parameter for the reference configuration where $\xi = 0$ when $\phi = 0$. Notice that we can express the representation (5.31) for $\mathbf{x}$ in the compact form

$$\mathbf{x}(\xi) = R\mathbf{D}_1(\xi) + \mathbf{R}(\xi). \tag{5.34}$$

It is straightforward to see that the rotation tensor $\mathbf{P}_0 = \sum_{k=1}^{3} \mathbf{D}_k \otimes \mathbf{E}_k$ corresponds to a rotation about $\mathbf{E}_3$ through an angle $\frac{\xi}{R\tan(\beta)}$. Consequently, the axial vector of $\mathbf{P}_0'\mathbf{P}_0^T$ is

$$\mathbf{v}_0 = v_0\mathbf{E}_3 = \frac{\cot(\beta)}{R}\mathbf{E}_3. \tag{5.35}$$

Thus, the reference configuration of the rod has a constant pretwist $v_0 = \frac{\cot(\beta)}{R}$. This pretwist is often known as the intrinsic twist and can be compared to the geometric torsion $\tau = \frac{\alpha}{R(1+\alpha^2)} = \frac{1}{R}\cos(\beta)\sin(\beta)$ of a helical space curve and the total torsion $T_{\mathrm{w}}(\mathscr{S}, \mathbf{e}_n) = \sin(\beta)$ of a turn of a helical space curve that were discussed in Section 3.4.

5.3.3 Inertias

We suppose that the three-dimensional body that the directed curve is modeling has a mass density per unit volume in a fixed reference configuration of $\rho_0^* = \rho_0^*(\xi, \theta^1, \theta^2)$. The directed curve has a mass per unit length in its reference configuration of $\rho_0 = \rho_0(\xi)$. We prescribe this density and five distinct inertias as follows[10]:

$$\rho_0 = \int_{\mathscr{A}} \rho_0^* da,$$
$$\rho_0 y^{0\alpha} = \int_{\mathscr{A}} \theta^\alpha \rho_0^* da,$$
$$\rho_0 y^{\alpha\beta} = \int_{\mathscr{A}} \theta^\alpha \theta^\beta \rho_0^* da, \tag{5.36}$$

where $\alpha, \beta = 1, 2$ and $da = \sqrt{G}d\theta^1 d\theta^2$. We observe that $y^{12} = y^{21}$ and this symmetry is assumed in the sequel.

[10] A derivation of these results was first presented in [137]. The developments used in [137] can also be found in the text [309].

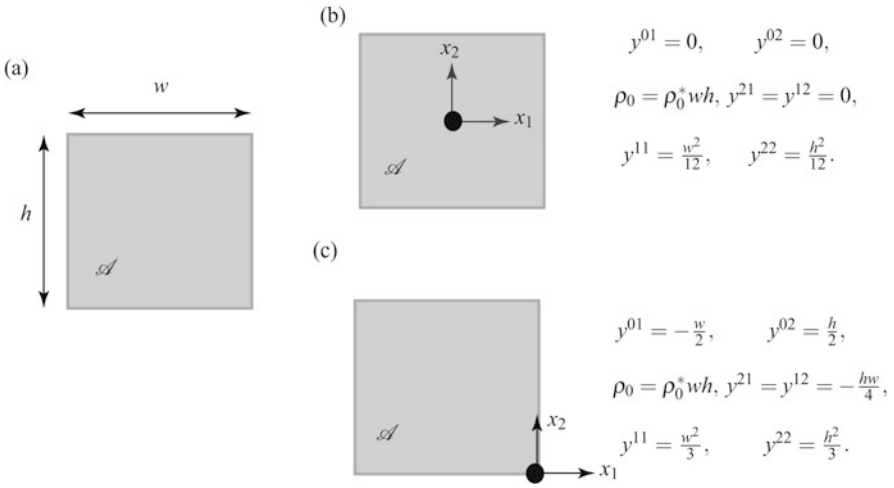

Fig. 5.8 Computation of the coefficients $y^{0\alpha}$ and $y^{\alpha\beta}$ using Eqn. (5.36) for a homogeneous rod with rectangular cross sections in the reference configuration $\mathscr{R}_0$. (a), Geometry of the cross section; (b), the case where the centerline is chosen to pass through the center of the cross section; and (c), the case where the centerline is chosen to pass through a corner point.

The integrals in Eqn. (5.36) are taken over the cross section $\mathscr{A}$ of the reference configuration of the rod-like body that the directed curve is modeling. These cross sections correspond to $\theta^3 = \xi$ coordinate surfaces. That is, θ^1 and θ^2 are curvilinear coordinates which parameterize the cross sections of the rod (see Section 5.2.1 and Figure 5.2), and the point $(\theta^1, \theta^2) = (0,0)$ on each section corresponds to the material point of the directed curve.

Suppose a set of Cartesian coordinates are used to parameterize the reference configuration of the rod-like body: $\theta^1 = x_1$, $\theta^2 = x_2$, $\theta^3 = x_3$, $\sqrt{G} = 1$, and $da = dx_1 dx_2$. As shown in Figure 5.8(b), if we assume that the centerline is the line at the intersection of the planes $x_1 = 0$ and $x_2 = 0$, then, for the case of a homogeneous rod with a rectangular cross section of width w and height h,

$$\rho_0 = \rho_0^* wh, \qquad y^{0\alpha} = 0, \qquad y^{12} = 0,$$

$$\rho_0 y^{11} = \rho_0^* I_2 = \rho_0^* \left(\frac{hw^3}{12} \right), \qquad \rho_0 y^{22} = \rho_0^* I_1 = \rho_0^* \left(\frac{wh^3}{12} \right). \tag{5.37}$$

Here, I_2 is the second moment of area of the cross section about the x_2 axis. You should notice that if the centerline is chosen to pass through one of the corners of the cross section, then this will alter the values of $y^{0\alpha}$ and $y^{\alpha\beta}$. We refer the interested

reader to Figure 5.8(c) for an example of a situation where the centerline is chosen to pass through one of the corners on the lower lateral surface of a rod-like body with a rectangular cross section.[11]

5.4 Further Kinematics and Discontinuities

Because the directors in Kirchhoff's rod theory behave as part of an orthonormal triad, the kinematics in this rod theory are particularly rich in representations. For example, differentiating Eqn. $(5.6)_1$ with respect to t, we find that

$$\dot{\mathbf{d}}_\alpha = \boldsymbol{\omega} \times \mathbf{d}_\alpha. \tag{5.38}$$

Here, $\boldsymbol{\omega}$ is the axial vector of a skew-symmetric tensor:

$$\boldsymbol{\omega} = \omega_1 \mathbf{d}_1 + \omega_2 \mathbf{d}_2 + \omega_3 \mathbf{d}_3 = \operatorname{ax}\left(\dot{\mathbf{P}}\mathbf{P}^T\right). \tag{5.39}$$

Concerning the vector $\mathbf{v}$, it is interesting (and not surprising) to note that the time derivative of $\mathbf{v}$ and the arc-length derivative of $\boldsymbol{\omega}$ are related:

$$\dot{\mathbf{v}} = \mathbf{P}^T \boldsymbol{\omega}', \qquad \boldsymbol{\omega}' = \mathbf{P}\dot{\mathbf{v}}. \tag{5.40}$$

To establish these compatibility relations, one uses Eqn. (5.9), the fact that $\dot{\mathbf{v}}_0 = \mathbf{0}$, and the skew-symmetries of $\mathbf{P}^T\dot{\mathbf{P}}$ and $\mathbf{P}^T\mathbf{P}'$. The relations (5.40) will be used later to help establish constitutive relations for the rod.

The discontinuities that are inherent in the rod theory can be categorized as those associated with the translation of the material curve and those associated with the rotation of the cross sections. The former are considered by examining the discontinuities in the time- and ξ-derivatives of $\mathbf{r}$ while the latter are encompassed by discontinuities in the time- and ξ-derivatives of the rotation tensor $\mathbf{P}\mathbf{P}_0$. To proceed, we first assume that $\mathbf{r}$ and $\mathbf{d}_\alpha$ are continuous functions of ξ:

$$[\![\mathbf{r}]\!]_\gamma = \mathbf{0}, \qquad [\![\mathbf{d}_1]\!]_\gamma = \mathbf{0}, \qquad [\![\mathbf{d}_2]\!]_\gamma = \mathbf{0}. \tag{5.41}$$

That is, the centerline of the rod has no breaks and the directors vary continuously with ξ. As a consequence of the continuity of $\mathbf{d}_1$ and $\mathbf{d}_2$, it follows that $\mathbf{d}_3$ and $\mathbf{P}$ are also continuous:

$$[\![\mathbf{d}_3]\!]_\gamma = \mathbf{0}, \qquad [\![\mathbf{P}]\!]_\gamma = \mathbf{0}. \tag{5.42}$$

Thus, the centerline of the rod cannot have any kinks.

For rods, we have the velocity $\mathbf{v}_\gamma$, which is identical to one presented earlier for strings:

[11] As discussed by Naghdi [244], the freedom to make such a selection can be advantageous for formulating contact problems. It can also be advantageous when attempting to develop rod models for deformable bodies as in [286].

$$\mathbf{v}_\gamma = \lim_{\sigma\to 0}\left(\frac{d}{dt}\mathbf{r}\left(\gamma(t)\pm\sigma,t\right)\right) = \mathbf{v}^+ + \dot{\gamma}\mathbf{r}'^+ = \mathbf{v}^- + \dot{\gamma}\mathbf{r}'^-, \tag{5.43}$$

where $\sigma > 0$. That is,

$$\mathbf{v}_\gamma = \left\{\mathbf{v} + \dot{\gamma}\mathbf{r}'\right\}_\gamma. \tag{5.44}$$

This velocity vector describes the shock speed experienced by the material curve relative to a fixed observer.

The velocity vector of the directors and the derivatives $\mathbf{d}'_\alpha$ can also experience discontinuities. Such behavior can be associated with the deformation of the cross sections of the rod, as opposed to the centerline of the rod. The discontinuities in $\dot{\mathbf{d}}_\alpha$ and $\mathbf{d}'_\alpha$ are not independent. As with the vector $\mathbf{r}$, we correlate left-sided and right-sided calculations of $\dot{\mathbf{d}}_\alpha$ and $\mathbf{d}'_\alpha$ to find two equivalent representations for each of the vectors $\mathbf{w}_{1_\gamma}$ and $\mathbf{w}_{2_\gamma}$. For instance,

$$\mathbf{w}_{1_\gamma} = \lim_{\sigma\to 0}\left(\frac{d}{dt}\mathbf{d}_1\left(\gamma(t)\pm\sigma,t\right)\right) = \dot{\mathbf{d}}_1^+ + \dot{\gamma}\mathbf{d}_1'^+ = \dot{\mathbf{d}}_1^- + \dot{\gamma}\mathbf{d}_1'^-. \tag{5.45}$$

That is,

$$\begin{aligned}\mathbf{w}_{1_\gamma} &= \left\{\dot{\mathbf{d}}_1 + \dot{\gamma}\mathbf{d}_1'\right\}_\gamma \\ &= \left\{\left(\boldsymbol{\omega} + \dot{\gamma}\mathbf{P}\left(\mathbf{v}+\mathbf{v}_0\right)\right)\times\mathbf{d}_1\right\}_\gamma.\end{aligned} \tag{5.46}$$

In arriving at the final expression, we used Eqn. (5.38) and the identity $\mathbf{d}'_1 = \left(\mathbf{P}\left(\mathbf{v}+\mathbf{v}_0\right)\right)\times\mathbf{d}_1$.

Although $[\![\mathbf{d}_\alpha]\!]_\gamma = \mathbf{0}$ implies that $[\![\mathbf{P}\mathbf{P}_0\mathbf{E}_\alpha]\!]_\gamma = \mathbf{0}$, we cannot expect $\mathbf{v}$ and $\boldsymbol{\omega}$ to be continuous at a point of discontinuity. Indeed, it is possible, and useful, to calculate the velocity $\boldsymbol{\omega}_\gamma$ by examining the time derivative of $\mathbf{P}\left(\xi=\gamma(t),t\right)\mathbf{P}_0\left(\xi=\gamma(t)\right)$:

$$\begin{aligned}\boldsymbol{\omega}_\gamma &= \mathrm{ax}\left(\left(\left(\dot{\mathbf{P}}\mathbf{P}_0 + \dot{\gamma}\left(\mathbf{P}'\mathbf{P}_0 + \mathbf{P}\mathbf{P}_0'\right)\right)\mathbf{P}_0^T\mathbf{P}^T\right)^+\right) \\ &= \mathrm{ax}\left(\left(\left(\dot{\mathbf{P}}\mathbf{P}_0 + \dot{\gamma}\left(\mathbf{P}'\mathbf{P}_0 + \mathbf{P}\mathbf{P}_0'\right)\right)\mathbf{P}_0^T\mathbf{P}^T\right)^-\right) \\ &= \left(\boldsymbol{\omega} + \dot{\gamma}\det\left(\mathbf{P}\right)\mathbf{P}\left(\mathbf{v}+\mathbf{v}_0\right)\right)^+ \\ &= \left(\boldsymbol{\omega} + \dot{\gamma}\det\left(\mathbf{P}\right)\mathbf{P}\left(\mathbf{v}+\mathbf{v}_0\right)\right)^-,\end{aligned} \tag{5.47}$$

where we used the definitions $(5.8)_{1,2}$ and (5.38) and the identity (5.9). It can be concluded from Eqn. (5.47) that

$$\boldsymbol{\omega}_\gamma = \left\{\boldsymbol{\omega} + \dot{\gamma}\mathbf{P}\left(\mathbf{v}+\mathbf{v}_0\right)\right\}_\gamma,$$

$$\boldsymbol{\omega}^{+} + \dot{\gamma}(\mathbf{P}(\mathbf{v}+\mathbf{v}_0))^{+} = \boldsymbol{\omega}^{-} + \dot{\gamma}(\mathbf{P}(\mathbf{v}+\mathbf{v}_0))^{-}. \tag{5.48}$$

These results clearly parallel those we found for $\mathbf{v}_\gamma$, $\mathbf{w}_{1_\gamma}$, and $\mathbf{w}_{2_\gamma}$. We also observe the useful identities

$$\mathbf{w}_{1_\gamma} = \boldsymbol{\omega}_\gamma \times \mathbf{d}_1(\gamma,t), \qquad \mathbf{w}_{2_\gamma} = \boldsymbol{\omega}_\gamma \times \mathbf{d}_2(\gamma,t). \tag{5.49}$$

To establish these results from Eqn. (5.46), the facts that $\{\mathbf{d}_\alpha\} = \mathbf{d}_\alpha(\gamma,t)$ were used.

It follows from the definitions of the velocity $\mathbf{v}_\gamma$ and angular velocity $\boldsymbol{\omega}_\gamma$ that

$$[\![\mathbf{v}]\!]_\gamma = -\left[\left[\mathbf{r}'\right]\right]_\gamma \dot{\gamma}, \qquad [\![\boldsymbol{\omega}]\!]_\gamma = -[\![\mathbf{P}(\mathbf{v}+\mathbf{v}_0)]\!]_\gamma \dot{\gamma}. \tag{5.50}$$

These conditions are crucial in establishing an alternative form of the jump condition arising from the balance of energy.

5.5 Momenta and Kinetic Energy

We define the linear momentum $\mathbf{G}$ per unit length of ξ of the rod by the expression

$$\mathbf{G} = \rho\mu\left(\dot{\mathbf{r}} + \sum_{\alpha=1}^{2} y^{0\alpha}\dot{\mathbf{d}}_\alpha\right). \tag{5.51}$$

Supplementing this momentum, we define the two director momenta per unit length of ξ:

$$\begin{aligned}\mathbf{L}^1 &= \rho\mu\left(y^{01}\dot{\mathbf{r}} + \sum_{\alpha=1}^{2} y^{1\alpha}\dot{\mathbf{d}}_\alpha\right),\\ \mathbf{L}^2 &= \rho\mu\left(y^{02}\dot{\mathbf{r}} + \sum_{\alpha=1}^{2} y^{2\alpha}\dot{\mathbf{d}}_\alpha\right).\end{aligned} \tag{5.52}$$

To examine the physical interpretations of these three momenta, we can, without loss in generality, set $y^{0\alpha} = 0$. Then, $\mathbf{G}$ can be identified as the linear momentum of the material curve, and $\mathbf{L}^\alpha$ can be identified as the linear momenta of the cross sections of the rod.

The material momentum of a segment (ξ_1, ξ_2) of the directed curve is defined as the integral of the material momentum P, $\int_{\xi_1}^{\xi_2} \mathsf{P}\, d\xi$, where

$$\mathsf{P} = -\left(\mathbf{r}' \cdot \mathbf{G} + \mathbf{d}_1' \cdot \mathbf{L}^1 + \mathbf{d}_2' \cdot \mathbf{L}^2\right). \tag{5.53}$$

This momentum is sometimes referred to as the pseudomomentum and first appeared in the literature in [264]. You should notice how the expression for P simplifies to that presented earlier for a string (see Eqn. (1.44)).

The kinetic energy of a segment (ξ_1, ξ_2) of the directed curve is defined as $\int_{\xi_1}^{\xi_2} T d\xi$ where the kinetic energy density T is

$$T = \frac{1}{2}\left(\dot{\mathbf{r}} \cdot \mathbf{G} + \dot{\mathbf{d}}_1 \cdot \mathbf{L}^1 + \dot{\mathbf{d}}_2 \cdot \mathbf{L}^2\right). \tag{5.54}$$

Note that we are not imposing inextensibility here, so we leave μ arbitrary.

The angular momentum relative to O of a segment (ξ_1, ξ_2) of the directed curve is

$$\mathbf{H}_O = \int_{\xi_1}^{\xi_2} \mathbf{h}_O d\xi, \tag{5.55}$$

where

$$\mathbf{h}_O = \mathbf{r} \times \mathbf{G} + \mathbf{d}_1 \times \mathbf{L}^1 + \mathbf{d}_2 \times \mathbf{L}^2. \tag{5.56}$$

Because, $\dot{\mathbf{d}}_\alpha = \boldsymbol{\omega} \times \mathbf{d}_\alpha$, we can also define inertia tensors $\mathbf{J}_R$ and $\mathbf{J}_{R_0}$:

$$\begin{aligned}
\mathbf{J}_{R_0} &= \rho\mu\left(y^{11} + y^{22}\right)\mathbf{I} - \sum_{\alpha=1}^{2}\sum_{\beta=1}^{2} \rho\mu y^{\alpha\beta}\mathbf{D}_\alpha \otimes \mathbf{D}_\beta, \\
\mathbf{J}_R &= \rho\mu\left(y^{11} + y^{22}\right)\mathbf{I} - \sum_{\alpha=1}^{2}\sum_{\beta=1}^{2} \rho\mu y^{\alpha\beta}\mathbf{d}_\alpha \otimes \mathbf{d}_\beta.
\end{aligned} \tag{5.57}$$

It should be noted that

$$\mathbf{J}_R = \mathbf{P}\mathbf{J}_{R_0}\mathbf{P}^T, \tag{5.58}$$

a result which parallels that for the inertia tensors of a rigid body (cf., e.g., [48]). We also note that the inertia tensor can be used to write a compact expression for a portion of the kinetic energy density of the rod:

$$\sum_{\alpha=1}^{2}\sum_{\beta=1}^{2} \rho\mu y^{\alpha\beta}\dot{\mathbf{d}}_\alpha \cdot \dot{\mathbf{d}}_\beta = \mathbf{J}_R\boldsymbol{\omega} \cdot \boldsymbol{\omega}. \tag{5.59}$$

The inertia tensor $\mathbf{J}_R$ is equivalent to that for a lamella with $\mathbf{d}_1 \times \mathbf{d}_2$ normal to the plane of this infinitesimally thin body. It is left as an exercise to show how T and $\mathbf{h}_O$ can be partially expressed in terms of $\mathbf{J}_R$.

5.6 A Strain Energy Function

The directed curve associated with the Kirchhoff rod theory is capable of resisting bending in two directions and torsion. We use the skew-symmetric tensor $\mathbf{K}$ to help define the associated strains. As a consequence, the strain energy function per unit mass is assumed to be a function of the three strains ν_i and (if the rod is not homogeneous) possibly ξ:

$$\psi = \psi(\nu_1, \nu_2, \nu_3, \xi). \tag{5.60}$$

It is important to note that the material time derivative of this function has the following representations:

$$\begin{aligned}\dot{\psi} &= \sum_{i=1}^{3} \frac{\partial \psi}{\partial \nu_i} \dot{\nu}_i \\ &= \frac{\partial \psi}{\partial \boldsymbol{\nu}} \cdot \dot{\boldsymbol{\nu}} \\ &= \left(\mathbf{P} \frac{\partial \psi}{\partial \boldsymbol{\nu}} \right) \cdot \frac{\partial \boldsymbol{\omega}}{\partial \xi}. \end{aligned} \tag{5.61}$$

We used the notation $\frac{\partial \psi}{\partial \boldsymbol{\nu}} = \sum_{i=1}^{3} \frac{\partial \psi}{\partial \nu_i} \mathbf{D}_i$ and the identity $(5.40)_1$ to obtain these representations. They will play an important role when we find constitutive equations. Calculation of a representation for $\rho_0 \dot{\psi}$ where

$$\psi = \hat{\psi} \left(\nu_1 - \nu_{0_1}, \nu_2 - \nu_{0_2}, \nu_3 - \nu_{0_3}, \xi \right) \tag{5.62}$$

and a proof that $\hat{\psi}$ is invariant under superposed rigid body motions are left as exercises.

It is common to consider Taylor series expansions of ψ about the reference configuration $\nu_i = 0$:

$$\begin{aligned} 2\rho_0 \psi (\nu_1, \nu_2, \nu_3, \xi) = 2\rho_0 \psi (0,0,0,\xi) &+ \sum_{i=1}^{3} \sum_{k=1}^{3} A_{ik} (\xi) \nu_i \nu_k \\ &+ \sum_{i=1}^{3} \sum_{k=1}^{3} \sum_{r=1}^{3} B_{ikr} (\xi) \nu_i \nu_k \nu_r + \cdots . \end{aligned} \tag{5.63}$$

The coefficients A_{ik} and B_{ikr} will depend both on the geometric properties of the cross sections and the constitution of the rod-like body that the rod is modeling. It is standard to invoke material symmetry arguments, such as those presented in [12, 158, 198, 228], to reduce the number of coefficients. These arguments along with the assumptions that the rod-like body is isotropic, linearly elastic, that the reference configuration is straight and unstressed, and that the directors $\mathbf{D}_{1,2}$ are chosen to be parallel to the principal axis of the area moment of inertia tensor for the cross section, are used to motivate the most popular form of the expansion of $\rho_0 \psi$ in the literature which dates to Kirchhoff in 1859 [185]:

$$2\rho_0 \psi = EI_1 \nu_1^2 + EI_2 \nu_2^2 + \mathscr{D} \nu_3^2. \tag{5.64}$$

In this equation, E is Young's modulus, I_α are second moments of area, and $\mathscr{D}$ is the torsional rigidity. Rods whose strain energy function are given by Eqn. (5.64) with $I_1 = I_2$ are sometimes referred to as (transversely) isotropic.[12]

[12] We discuss this matter in additional detail in Section 6.4.3 of Chapter 6.

It is convenient to recall the parameters EI_α and $\mathscr{D}$ for a selection of geometries that can be found in the literature on linear elasticity [328]. First, for a straight rod with a circular cross section of radius r, it is known that

$$EI_1 = EI_2 = \frac{\pi E r^4}{4}, \qquad \mathscr{D} = \frac{EI_1}{1+\nu}. \tag{5.65}$$

For a straight rod with an elliptical cross section of semi-axes a and b,

$$EI_1 = \frac{\pi E a b^3}{4}, \qquad EI_2 = \frac{\pi E b a^3}{4}, \qquad \mathscr{D} = \left(\frac{E}{2(1+\nu)}\right)\frac{\pi a^3 b^3}{a^2+b^2}. \tag{5.66}$$

Finally, for a straight rod with a square cross section of width w,

$$EI_1 = EI_2 = \frac{E w^4}{12}, \qquad \mathscr{D} \approx \frac{27 EI_1}{32(1+\nu)}. \tag{5.67}$$

In general, closed-form solutions for $\mathscr{D}$ are only available for a limited number of cross sections.

5.7 Balance Laws for the Rod Theory

Preparatory to writing the conservation laws for the directed curve, we record some additional notation. Associated with the inertia of $\mathscr{R}$ is its mass density $\rho = \rho(\xi,t)$. Pertaining to forces, $\mathbf{n} = \mathbf{n}(\xi,t)$ is the contact force, $\mathbf{m} = \mathbf{m}(\xi,t)$ is the contact moment, and $\mathbf{f} = \mathbf{f}(\xi,t)$ and $\mathbf{l}^\beta = \mathbf{l}^\beta(\xi,t)$ are the respective assigned force and assigned director forces per unit mass. We also define the contact material force C and assigned material force b. For the prescription of the former,[13]

$$\mathsf{C} = \rho\mu\psi - \mathbf{n}\cdot\mathbf{r}' - \mathbf{m}\cdot(\mathbf{P}(\mathbf{v}+\mathbf{v}_0)) - T. \tag{5.68}$$

If we ignore the directors and set $\mathbf{m} = \mathbf{0}$, then this prescription reduces to the one we presented earlier for a string (see Eqn. (1.69)). We also remark that for static problems involving rods where $\rho\mu\psi$ has the classic quadratic form (5.64), C is identical to an energy integral used to establish solutions for boundary-value problems.[14]

[13] The prescription (5.68) is a generalization of Eqn. $(56)_1$ in [264] to the case of an intrinsically curved rod.

[14] See, e.g., [213, Eqn. (3), Section 260] or the more recent work [164, Eqn. (20)].

5.7.1 Assigned Forces, Assigned Director Forces, and Assigned Moments

It is convenient to be able to prescribe the assigned force fields in terms of the three-dimensional body force $\rho_0^*\mathbf{b}$ acting on the rod and surface tractions $\mathbf{t}$ acting on the lateral surface of the rod.[15] The prescriptions are, with evident parallels to the prescriptions (5.36) for the inertia coefficients,

$$\begin{aligned}\rho_0\mathbf{f} &= \int_{\mathscr{A}} \mathbf{b}\rho_0^* da + \oint_{\partial\mathscr{A}} \mathbf{t} du,\\ \rho_0\mathbf{l}^\alpha &= \int_{\mathscr{A}} \mathbf{b}\theta^\alpha\rho_0^* da + \oint_{\partial\mathscr{A}} \mathbf{t}\theta^\alpha du.\end{aligned} \tag{5.69}$$

Here, $\partial\mathscr{A}$ is the boundary of the cross section, ρ_0^* is the mass density per unit volume, and u is the arc-length parameter on this boundary.

The force $\rho_0\mathbf{f}$ is the resultant of the body force and surface traction at a value of ξ (i.e., at a particular cross section). You should also notice that

$$\begin{aligned}\sum_{\alpha=1}^{2} \mathbf{d}_\alpha \times \rho_0\mathbf{l}^\alpha &= \sum_{\alpha=1}^{2} \mathbf{d}_\alpha \times \int_{\mathscr{A}} \mathbf{b}\theta^\alpha\rho_0^* da + \sum_{\alpha=1}^{2} \mathbf{d}_\alpha \times \oint_{\partial\mathscr{A}} \mathbf{t}\theta^\alpha du\\ &= \sum_{\alpha=1}^{2} \int_{\mathscr{A}} \theta^\alpha \mathbf{d}_\alpha \times \mathbf{b}\rho_0^* da + \sum_{\alpha=1}^{2} \oint_{\partial\mathscr{A}} \theta^\alpha \mathbf{d}_\alpha \times \mathbf{t} du.\end{aligned} \tag{5.70}$$

Consequently, we can consider $\sum_{\alpha=1}^{2} \mathbf{d}_\alpha \times \rho_0\mathbf{l}^\alpha$ as the moment (relative to the material point ξ on the centerline) of the body force and surface tractions acting on rod-like body (see Section 5.2.1 and Eqn. (5.2)). That is,

$$\mathbf{m}_a = \sum_{\alpha=1}^{2} \mathbf{d}_\alpha \times \rho_0\mathbf{l}^\alpha, \tag{5.71}$$

where $\mathbf{m}_a$ denotes the applied or assigned moment.

A selection of three examples where $\rho_0\mathbf{f}$ and $\rho_0\mathbf{l}^\alpha$ are computed using the prescriptions (5.69) are shown in Figure 5.9. In these examples, the tractions $\mathbf{t}_A$, $\mathbf{t}_B$, and $\mathbf{t}_C$ are applied to lateral surface of a rod whose cross section in the present configuration is assumed to be a rectangle of height h and width w. In this situation, $\theta^1 = x_1$ and $\theta^2 = x_2$. The line integrals $\oint_{\partial\mathscr{A}} \mathbf{t} du$ and $\oint_{\partial\mathscr{A}} \mathbf{t}\theta^\alpha du$ are evaluated by taking the path in a counterclockwise manner around the perimeter of the rectangle:

[15] A derivation of these results was first presented in [137] and is based on the approximation (5.2): $\mathbf{r}^* = \mathbf{r}(\xi,t) + \sum_{\alpha=1}^{2} \theta^\alpha \mathbf{d}_\alpha(\xi,t)$. However, the derivation is difficult to follow. A recent treatment by [309] is far more transparent (see also [260] and Section 7.12 in Chapter 7).

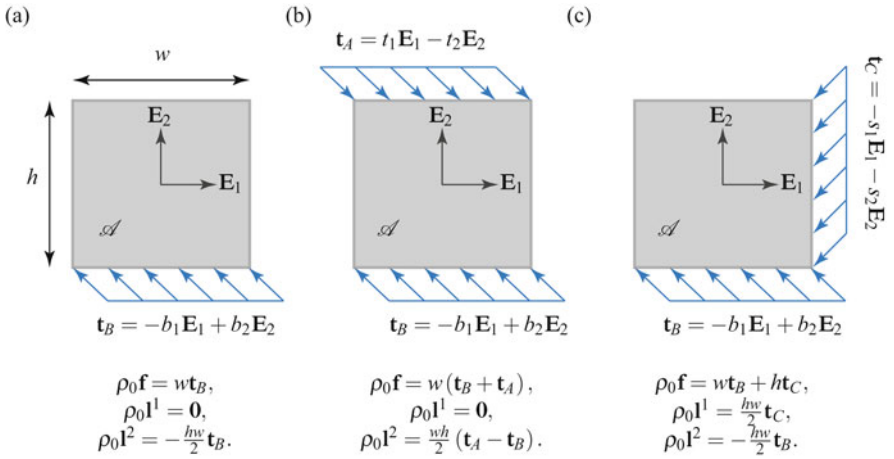

Fig. 5.9 Three examples of the computation of $\rho_0\mathbf{f}$ and $\rho\mathbf{l}^\alpha$ using Eqn. (5.69) (or, equivalently, Eqn. (7.38)). The cross section $\mathscr{A}$ of the rod in the present configuration is assumed to be rectangular in shape with $\mathbf{d}_1 = \mathbf{E}_1$ and $\mathbf{d}_2 = \mathbf{E}_2$ in the examples shown. The corresponding moments $\mathbf{m}_a$ are presented in Eqn. (5.74).

$$\begin{aligned}\oint_{\partial\mathscr{A}} \mathbf{q}\,du &= \int_{-w/2}^{w/2} \mathbf{q}\,dx_1 + \int_{-h/2}^{h/2} \mathbf{q}\,dx_2 - \int_{w/2}^{-w/2} \mathbf{q}\,dx_1 - \int_{h/2}^{-h/2} \mathbf{q}\,dx_2 \\ &= \int_{-w/2}^{w/2} \mathbf{q}\,dx_1 + \int_{-h/2}^{h/2} \mathbf{q}\,dx_2 + \int_{-w/2}^{w/2} \mathbf{q}\,dx_1 + \int_{-h/2}^{h/2} \mathbf{q}\,dx_2, \end{aligned} \tag{5.72}$$

where $\mathbf{q}$ is an arbitrary integrable function and the arc-length parameter $du = \pm dx_1$ or $du = \pm dx_2$. For all three examples shown in Figure 5.9, suppose a gravitational force in the $-\mathbf{E}_2$ direction acts on the rod, then the corresponding assigned forces are

$$\rho_0\mathbf{f} = -\rho_0 g\mathbf{E}_2, \qquad \rho_0\mathbf{l}^1 = \mathbf{0}, \qquad \rho_0\mathbf{l}^2 = \mathbf{0}. \tag{5.73}$$

We take this opportunity to note that prescriptions for $\rho_0\mathbf{f}$ of the type presented here were previously used in the examples discussed in Chapter 2 for strings. Other instances of the prescriptions (5.69) can be found in the application of Green and Naghdi's rod theory to contact problems in [247, 251].

For the moment $\mathbf{m}_a$ associated with the assigned force and assigned director forces in Figure 5.9, we assume for simplicity that the present configurations are such that $\mathbf{d}_1 = \mathbf{E}_1$ and $\mathbf{d}_2 = \mathbf{E}_2$. Then, using the prescription (5.71) for $\mathbf{m}_a$, we find for the respective examples that

$$\begin{aligned}\mathbf{m}_a &= -\frac{1}{2}hwb_1\mathbf{E}_3, \\ \mathbf{m}_a &= -\frac{1}{2}hw(b_1 + t_1)\mathbf{E}_3, \\ \mathbf{m}_a &= -\frac{1}{2}hw(b_1 + s_2)\mathbf{E}_3. \end{aligned} \tag{5.74}$$

As expected these moments are clockwise. It is also comforting to observe that if the applied tractions in Figure 5.9(b) are such that $t_1 = -b_1$, then the assigned moment will vanish (as expected).

As with the earlier developments of the theory of an elastic string, here we are motivated by the works of Green and Naghdi [132] and Marshall and Naghdi [230], among others, and admit singular supplies at a specific material point $\xi = \gamma(t)$.[16] The four supplies are those for momentum, $\mathbf{F}_\gamma$, material momentum, B_γ, angular momentum relative to O, $\mathbf{M}_{O_\gamma}$, and energy rate, Φ_{E_γ}. For a rod theory incorporating growth or decay, one could also consider supplies of mass and inertia but we do not consider these here.

5.7.2 Conservation Laws

We adopt the following balance laws for any fixed material segment (ξ_1, ξ_2) of the material curve. First, we record the conservations of mass and inertia:

$$\begin{aligned} \frac{d}{dt}\int_{\xi_1}^{\xi_2} \rho\,\mu\, d\xi &= 0, \\ \frac{d}{dt}\int_{\xi_1}^{\xi_2} \rho y^{0\alpha}\,\mu\, d\xi &= 0, \\ \frac{d}{dt}\int_{\xi_1}^{\xi_2} \rho y^{\alpha\beta}\,\mu\, d\xi &= 0. \end{aligned} \tag{5.75}$$

The balance of linear momentum is

$$\frac{d}{dt}\int_{\xi_1}^{\xi_2} \rho\left(\dot{\mathbf{r}} + y^{0\alpha}\dot{\mathbf{d}}_\alpha\right)\mu\, d\xi = \int_{\xi_1}^{\xi_2} \rho\mu\mathbf{f}\, d\xi + [\mathbf{n}]_{\xi_1}^{\xi_2} + \int_{\xi_1}^{\xi_2} \mathbf{F}_\gamma\,\delta(\xi-\gamma)\, d\xi, \tag{5.76}$$

where $\delta(\cdot)$ is the Dirac delta distribution. The balance of angular (or moment of) momentum relative to O is

$$\begin{aligned} \frac{d\mathbf{H}_O}{dt} = [\mathbf{r}\times\mathbf{n} + \mathbf{m}]_{\xi_1}^{\xi_2} &+ \int_{\xi_1}^{\xi_2} (\mathbf{r}\times\mathbf{f} + \mathbf{d}_\alpha\times\mathbf{l}^\alpha)\,\rho\,\mu\, d\xi \\ &+ \int_{\xi_1}^{\xi_2} \mathbf{M}_{O_\gamma}\,\delta(\xi-\gamma)\, d\xi. \end{aligned} \tag{5.77}$$

As with the string, one has a balance of material momentum:

$$\frac{d}{dt}\int_{\xi_1}^{\xi_2} \mathsf{P}\, d\xi = [\mathsf{C}]_{\xi_1}^{\xi_2} + \int_{\xi_1}^{\xi_2} \mathsf{b}\, d\xi + \int_{\xi_1}^{\xi_2} \mathsf{B}_\gamma\,\delta(\xi-\gamma)\, d\xi. \tag{5.78}$$

[16] For ease of exposition and without loss of generality, we assume that there is at most one such point.

One also has the balance of energy:

$$\frac{d}{dt}\int_{\xi_1}^{\xi_2}(\psi\rho\,\mu+T)\,d\xi = [\mathbf{n}\cdot\mathbf{v}+\mathbf{m}\cdot\boldsymbol{\omega}]_{\xi_1}^{\xi_2}+\int_{\xi_1}^{\xi_2}\left(\mathbf{f}\cdot\mathbf{v}+\mathbf{l}^{\alpha}\cdot\dot{\mathbf{d}}_{\alpha}\right)\rho\,\mu d\xi + \int_{\xi_1}^{\xi_2}\Phi_{\mathrm{E}_\gamma}\,\delta(\xi-\gamma)\,d\xi. \tag{5.79}$$

The similarities in structure between these balance laws and those we presented earlier for a string and the elastica should be noted.

5.8 Local Balance Laws and Jump Conditions

In the balance laws, we assume that there is one point of discontinuity. Consequently, with the help of the Leibnitz rule, we can follow the procedure discussed in Section 1.5.3 and establish local forms of the balance laws and jump conditions.

5.8.1 Local Balance Laws

In the interests of brevity, and because the procedure is so similar to the one we used for the string, we do not give details here of the procedure discussed to establish the following local forms of the balance laws from Eqns. (5.75)–(5.79). Instead, we just quote the final results:

$$\begin{gathered}
\rho_0 = \rho_0(\xi) = \rho\mu,\\
y^{0\alpha} = y^{0\alpha}(\xi),\\
y^{\alpha\beta} = y^{\alpha\beta}(\xi),\\
\rho_0\ddot{\mathbf{r}} + \rho_0 y^{0\alpha}\ddot{\mathbf{d}}_{\alpha} = \rho_0\mathbf{f} + \frac{\partial\mathbf{n}}{\partial\xi},\\
\mathbf{d}_1\times\dot{\mathbf{L}}^1 + \mathbf{d}_2\times\dot{\mathbf{L}}^2 = \mathbf{m}_a + \frac{\partial\mathbf{m}}{\partial\xi} + \frac{\partial\mathbf{r}}{\partial\xi}\times\mathbf{n},\\
\dot{\mathsf{P}} = \mathsf{C}' + \mathsf{b},\\
\rho_0\dot{\psi} = \mathbf{m}\cdot\frac{\partial\boldsymbol{\omega}}{\partial\xi} + \mathbf{n}\cdot\left(\frac{\partial\mathbf{v}}{\partial\xi} - \boldsymbol{\omega}\times\frac{\partial\mathbf{r}}{\partial\xi}\right).
\end{gathered} \tag{5.80}$$

To establish these laws, we used mass conservation and the linear and angular momentum balances to simplify the local form of the energy balance.[17] We also used the identity $\dot{\mathbf{d}}_{\alpha}\cdot\mathbf{a} = (\boldsymbol{\omega}\times\mathbf{d}_{\alpha})\cdot\mathbf{a} = (\mathbf{d}_{\alpha}\times\mathbf{a})\cdot\boldsymbol{\omega}$ for any vector $\mathbf{a}$.

[17] Some of the details and manipulations involved are outlined in Exercises 5.2 and 5.3.

5.8.2 Jump Conditions

From the balance laws (5.75)–(5.79), we find that the following jump conditions must hold at $\xi = \gamma(t)$:

$$\begin{gathered}
[\![\rho_0]\!]_\gamma \dot{\gamma} = 0, \\
\left[\!\left[\rho_0 y^{0\alpha}\right]\!\right]_\gamma \dot{\gamma} = 0, \\
\left[\!\left[\rho_0 y^{\alpha\beta}\right]\!\right]_\gamma \dot{\gamma} = 0, \\
[\![\mathbf{n} + \dot{\gamma}\mathbf{G}]\!]_\gamma + \mathbf{F}_\gamma = \mathbf{0}, \\
[\![\mathbf{r} \times \mathbf{n} + \mathbf{m}]\!]_\gamma + [\![\mathbf{h}_O]\!]_\gamma \dot{\gamma} + \mathbf{M}_{O_\gamma} = \mathbf{0}, \\
[\![\mathsf{C} + \mathsf{P}\dot{\gamma}]\!]_\gamma + \mathsf{B}_\gamma = 0, \\
[\![\mathbf{n} \cdot \mathbf{v} + \mathbf{m} \cdot \boldsymbol{\omega}]\!]_\gamma + [\![T + \rho_0 \psi]\!]_\gamma \dot{\gamma} + \Phi_{\mathrm{E}_\gamma} = 0.
\end{gathered} \tag{5.81}$$

Notice that it was assumed that $[\![\mathbf{r}]\!]_\gamma = \mathbf{0}$ and $[\![\mathbf{d}_\alpha]\!]_\gamma = \mathbf{0}$.

We can also invoke some of the jump conditions in order to simplify those associated with momentum and energy. For example, using the identity

$$\begin{aligned}
[\![\mathbf{h}_O]\!]_\gamma &= \left[\!\left[\mathbf{r} \times \mathbf{G} + \mathbf{d}_1 \times \mathbf{L}^1 + \mathbf{d}_2 \times \mathbf{L}^2\right]\!\right]_\gamma \\
&= \mathbf{r}(\gamma, t) \times [\![\mathbf{G}]\!]_\gamma + \left[\!\left[\mathbf{d}_1 \times \mathbf{L}^1 + \mathbf{d}_2 \times \mathbf{L}^2\right]\!\right]_\gamma,
\end{aligned} \tag{5.82}$$

we can use the jump condition $[\![\mathbf{n}]\!]_\gamma + [\![\mathbf{G}]\!]_\gamma \dot{\gamma} + \mathbf{F}_\gamma = \mathbf{0}$ to express the jump condition associated with the balance of angular momentum as

$$[\![\mathbf{m}]\!]_\gamma + \left[\!\left[\mathbf{d}_1 \times \mathbf{L}^1 + \mathbf{d}_2 \times \mathbf{L}^2\right]\!\right]_\gamma \dot{\gamma} + \mathbf{M}_{O_\gamma} - \mathbf{r}(\gamma, t) \times \mathbf{F}_\gamma = \mathbf{0}. \tag{5.83}$$

The moment $\mathbf{M}_{O_\gamma} - \mathbf{r}(\gamma, t) \times \mathbf{F}_\gamma$ can be interpreted as a moment relative to the point $\xi = \gamma$ on the material curve as opposed to the moment $\mathbf{M}_{O_\gamma}$ relative to O.[18] Consequently, we define

$$\mathbf{M}_\gamma = \mathbf{M}_{O_\gamma} - \mathbf{r}(\gamma, t) \times \mathbf{F}_\gamma, \tag{5.84}$$

which is the singular supply of angular momentum relative to the material point $\xi = \gamma$ on the material curve. As with $\mathbf{M}_{O_\gamma}$, the supply $\mathbf{M}_\gamma$ can also be interpreted as a moment.

To simplify the jump condition arising from the energy balance, we use the jump conditions from the balances of material momentum, linear momentum, and angular momentum to show that

[18] As we saw earlier for a string, the jump condition (5.83) simplifies to $\mathbf{M}_{O_\gamma} - \mathbf{r}(\gamma, t) \times \mathbf{F}_\gamma = \mathbf{0}$ (i.e., $\mathbf{M}_\gamma = \mathbf{0}$ when the directors are ignored (cf. Eqn. (1.87))). As mentioned in an earlier chapter, the physical interpretation of this result is that a string can neither transmit nor resist a moment, so application of a nonzero $\mathbf{M}_\gamma$ at $\xi = \gamma$ is not feasible.

$$\begin{aligned}\mathsf{B}_\gamma\dot{\gamma}+\mathbf{F}_\gamma\cdot\mathbf{v}_\gamma+\mathbf{M}_\gamma\cdot\boldsymbol{\omega}_\gamma = &-[\![\mathsf{P}\dot{\gamma}+\mathsf{C}]\!]_\gamma\dot{\gamma}-[\![\mathbf{n}+\dot{\gamma}\mathbf{G}]\!]_\gamma\cdot\mathbf{v}_\gamma\\ &-\left[\!\left[\mathbf{m}+\left(\mathbf{d}_1\times\mathbf{L}^1+\mathbf{d}_2\times\mathbf{L}^2\right)\dot{\gamma}\right]\!\right]_\gamma\cdot\boldsymbol{\omega}_\gamma. \qquad (5.85)\end{aligned}$$

Using the definition of C and repeated use of the identities (1.58) and (5.50), the right-hand side simplifies dramatically and we arrive at the identity[19]

$$\mathsf{B}_\gamma\dot{\gamma}+\mathbf{F}_\gamma\cdot\mathbf{v}_\gamma+\mathbf{M}_\gamma\cdot\boldsymbol{\omega}_\gamma = -[\![\mathbf{n}\cdot\mathbf{v}+\mathbf{m}\cdot\boldsymbol{\omega}]\!]_\gamma-[\![T+\rho_0\psi]\!]_\gamma\dot{\gamma}. \qquad (5.86)$$

With this identity, it is easy to see that the jump condition $(5.81)_7$ is equivalent to

$$\mathsf{B}_\gamma\dot{\gamma}+\mathbf{F}_\gamma\cdot\mathbf{v}_\gamma+\mathbf{M}_\gamma\cdot\boldsymbol{\omega}_\gamma = \Phi_{\mathrm{E}_\gamma}. \qquad (5.87)$$

As expected, if we ignore the moment term in this equation, then we arrive at the form of this identity that we found in an earlier chapter for a string.

5.9 Constitutive Relations

For the elastic rod (elastic directed curve), the constitutive relations for $\mathbf{m}$ and $\mathbf{n}$ are obtained by assuming that the local balance of energy $(5.80)_6$ is identically satisfied. The procedure we use has evident parallels to the ones used for strings in Section 1.6 of Chapter 1, for the elastica in Section 4.3.1 of Chapter 4, and, in Section 8.6 of Chapter 8, for a three-dimensional continuum.

The local form of the energy balance is

$$\rho_0\dot{\psi} = \mathbf{m}\cdot\frac{\partial\boldsymbol{\omega}}{\partial\xi}+\mathbf{n}\cdot\left(\frac{\partial\mathbf{v}}{\partial\xi}-\boldsymbol{\omega}\times\frac{\partial\mathbf{r}}{\partial\xi}\right). \qquad (5.88)$$

We also need to use the fact that $\frac{\partial\mathbf{r}}{\partial\xi}$ is the unit tangent vector which is perpendicular to $\mathbf{d}_\alpha$. These facts are expressed in the constraint $(5.6)_2$. Differentiating this constraint we would find that

$$\frac{\partial\mathbf{v}}{\partial\xi} = \boldsymbol{\omega}\times\frac{\partial\mathbf{r}}{\partial\xi}. \qquad (5.89)$$

Using our previous expression for $\dot{\psi}$ (see Eqn. (5.61)), we find that

$$\left(\rho_0\mathbf{P}\frac{\partial\psi}{\partial\mathbf{v}}-\mathbf{m}\right)\cdot\frac{\partial\boldsymbol{\omega}}{\partial\xi} = 0. \qquad (5.90)$$

[19] A key calculation used to arrive at the simplification is discussed in Exercise 5.7.

Assuming that $\mathbf{m}$ is independent of $\frac{\partial \boldsymbol{\omega}}{\partial \xi}$, and that the above equation holds for all $\frac{\partial \boldsymbol{\omega}}{\partial \xi}$, we conclude that

$$\mathbf{m} = \rho_0 \mathbf{P} \frac{\partial \psi}{\partial \mathbf{v}} = \sum_{i=1}^{3} \rho_0 \frac{\partial \psi}{\partial v_i} \mathbf{d}_i, \qquad \mathbf{n} = \sum_{i=1}^{3} n_i \mathbf{d}_i, \tag{5.91}$$

where $n_i = n_i(\xi, t)$. Observe that $\mathbf{n}$ is absent from Eqn. (5.90) and this explains why the constitutive relations for $\mathbf{n}$ are independent of the partial derivatives of the strain energy function. The components n_k of $\mathbf{n}$ can be considered as constraint responses whose function is to ensure that the constraints that the centerline of the rod is inextensible, and the cross sections of the rod retain their orientation relative to the centerline. We shall explore this interpretation in further detail in Section 7.11 of Chapter 7.

For the special strain energy function discussed earlier,

$$2\rho_0 \psi = EI_1 v_1^2 + EI_2 v_2^2 + \mathscr{D} v_3^2, \tag{5.92}$$

the constitutive relations for the contact moment are

$$\mathbf{m} = EI_1 v_1 \mathbf{d}_1 + EI_2 v_2 \mathbf{d}_2 + \mathscr{D} v_3 \mathbf{d}_3. \tag{5.93}$$

When the rod is undeformed in its reference configuration ($\mathbf{D}_i = \mathbf{E}_i$, and $v_{0_i} = 0$), then the constitutive equations (5.93) are those discussed in Kirchhoff [185] and repeated in Love [213]. If $v_{0_i} \neq 0$, then Eqn. (5.93) can also be used, provided it is understood that the total strain (relative to an undeformed reference configuration) is $v_i + v_{0_i}$. When the rod has a so-called kinetic symmetry $I_1 = I_2$, the relations (5.93) simplify - this often happens for rods with circular or square cross sections.

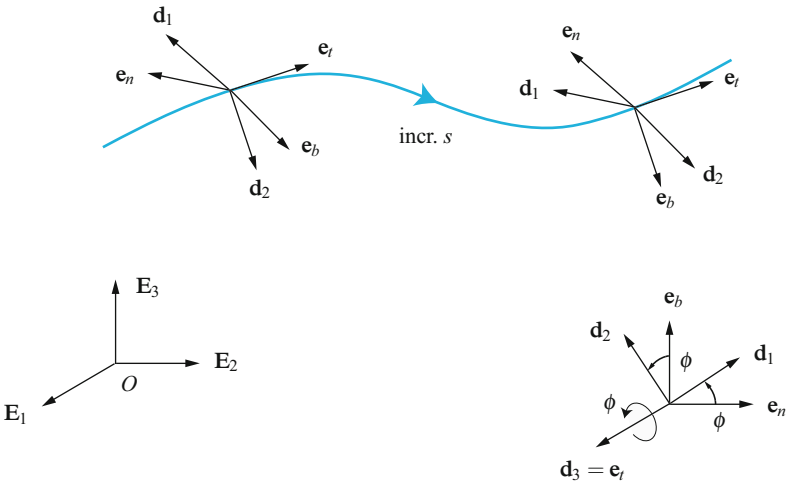

Fig. 5.10 Illustration of the evolution of the Frenet triad and the directors $\mathbf{d}_1$ and $\mathbf{d}_2$ along a directed curve.

5.10 Twist, Torsion, and Tortuosity

The material curve associated with the directed curve can, at each instant, be associated with a space curve $\mathscr{S}$. It is natural to question how $\mathbf{v}+\mathbf{v}_0$ and $\mathbf{PP}_0$ for the directed curve is related to $\boldsymbol{\omega}_{\mathrm{SF}}$, $\boldsymbol{\omega}_{\mathrm{B}}$, and $\mathbf{Q}_{\mathrm{SF}}$ for $\mathscr{S}$. We turn to discussing these matters here.

Recall that for a space curve $\mathscr{S}$ in Euclidean three-dimensional space $\mathbb{E}^3$ (see Figure 5.10), we can define the position vector of a point on the curve:

$$\mathbf{r}=\mathbf{r}(s)=x_1(s)\mathbf{E}_1+x_2(s)\mathbf{E}_2+x_3(s)\mathbf{E}_3. \tag{5.94}$$

The Frenet triad to this curve is the set of three vectors $\{\mathbf{e}_t,\mathbf{e}_n,\mathbf{e}_b\}$. These vectors satisfy the Serret-Frenet relations (1.2). Another set of vectors that can be defined at each point on the curve is the Bishop frame $\{\mathbf{e}_t,\mathbf{B}_1,\mathbf{B}_2\}$. You may also recall that using the Darboux vector $\boldsymbol{\omega}_{\mathrm{SF}}=\tau\mathbf{e}_t+\kappa\mathbf{e}_b$, the Serret-Frenet relations can be expressed in a compact form. Here, τ is the geometric torsion of the space curve and κ is the curvature. The corresponding angular velocity vector associated with the Bishop frame is $\boldsymbol{\omega}_{\mathrm{B}}=\kappa_{B_1}\mathbf{B}_2-\kappa_{B_2}\mathbf{B}_1=\kappa\mathbf{e}_b$ (cf. Eqn. (3.7)).

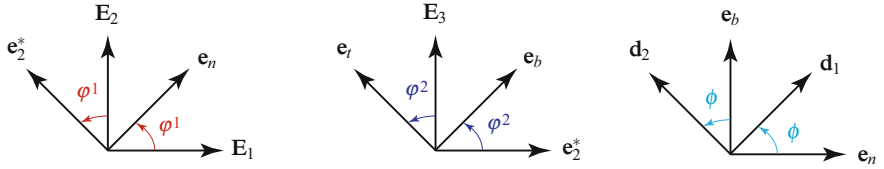

Fig. 5.11 Schematic of the three rotations used to parameterize $\mathbf{Q}_{\mathrm{SF}}$ and $\mathbf{Q}_{\mathrm{t}}$ (cf. Eqn. (5.97)). The unit vector $\mathbf{e}_2^*=\cos\left(\varphi^1\right)\mathbf{E}_2-\sin\left(\varphi^1\right)\mathbf{E}_1$. The rotations used in the parameterization are equivalent to the parameterization of the compound rotation $\mathbf{Q}_{\mathrm{t}}\mathbf{Q}_{\mathrm{SF}}$ using a set of 3-1-3 Euler angles.

Now, the directors associated with (Kirchhoff's) directed curve remain tangent to the centerline: $\frac{\partial\mathbf{r}}{\partial\xi}=\mathbf{e}_t$. Consequently, $\mathbf{e}_n$ and $\mathbf{e}_b$ are coplanar with $\mathbf{d}_1$ and $\mathbf{d}_2$. We can therefore deduce that

$$\mathbf{d}_1=\mathbf{Q}_{\mathrm{t}}\mathbf{e}_n,\qquad \mathbf{d}_2=\mathbf{Q}_{\mathrm{t}}\mathbf{e}_b, \tag{5.95}$$

where $\mathbf{Q}_{\mathrm{t}}$ is a rotation tensor corresponding to a rotation about the unit tangent vector $\mathbf{e}_t$ through an angle ϕ. This rotation tensor has multiple equivalent representations:

$$\begin{aligned}\mathbf{Q}_{\mathrm{t}}&=\mathbf{Q}_{\mathbf{E}}\left(\phi,\mathbf{e}_t\right)\\&=\mathbf{d}_1\otimes\mathbf{e}_n+\mathbf{d}_2\otimes\mathbf{e}_b+\mathbf{d}_3\otimes\mathbf{e}_t\\&=\cos(\phi)\left(\mathbf{d}_1\otimes\mathbf{d}_1+\mathbf{d}_2\otimes\mathbf{d}_2\right)+\sin(\phi)\left(\mathbf{d}_2\otimes\mathbf{d}_1-\mathbf{d}_1\otimes\mathbf{d}_2\right)+\mathbf{d}_3\otimes\mathbf{d}_3\\&=\cos(\phi)\left(\mathbf{e}_n\otimes\mathbf{e}_n+\mathbf{e}_b\otimes\mathbf{e}_b\right)+\sin(\phi)\left(\mathbf{e}_b\otimes\mathbf{e}_n-\mathbf{e}_n\otimes\mathbf{e}_b\right)+\mathbf{e}_t\otimes\mathbf{e}_t.\end{aligned} \tag{5.96}$$

Here, ϕ is a counterclockwise angle of rotation and the function $\mathbf{Q_E}$ was defined earlier in Eqn. (5.14).

Several results now follow immediately:

$$\mathbf{P}\mathbf{P}_0 = \mathbf{Q}_\mathrm{t}\mathbf{Q}_\mathrm{SF}, \tag{5.97}$$

where

$$\mathbf{Q}_\mathrm{SF} = \mathbf{e}_t \otimes \mathbf{E}_3 + \mathbf{e}_n \otimes \mathbf{E}_1 + \mathbf{e}_b \otimes \mathbf{E}_2. \tag{5.98}$$

We parameterize $\mathbf{Q}_\mathrm{SF}$ with a pair of rotations illustrated in Figure 5.11:

$$\mathbf{Q}_\mathrm{SF} = \mathbf{Q_E}\left(\varphi^2, \mathbf{e}_n\right)\mathbf{Q_E}\left(\varphi^1, \mathbf{E}_3\right), \tag{5.99}$$

where

$$\mathbf{e}_n = \cos\left(\varphi^1\right)\mathbf{E}_1 + \sin\left(\varphi^1\right)\mathbf{E}_2. \tag{5.100}$$

Further, using methods similar to what was used earlier with the 3-2-3 set of Euler angles, we can conclude that

$$\mathbf{P}\left(\mathbf{v}+\mathbf{v}_0\right) = \boldsymbol{\omega}_\mathrm{SF} + \frac{\partial\phi}{\partial s}\mathbf{e}_t = \boldsymbol{\omega}_\mathrm{B} + \left(\tau + \frac{\partial\phi}{\partial s}\right)\mathbf{e}_t. \tag{5.101}$$

Hence,

$$\begin{aligned}
v_3 + v_{0_3} &= \tau + \frac{\partial\phi}{\partial s} = \frac{\partial\varphi^1}{\partial s}\cos\left(\varphi^2\right) + \frac{\partial\phi}{\partial s}, \\
v_1 + v_{0_1} &= \kappa\sin(\phi) = \frac{\partial\varphi^1}{\partial s}\sin\left(\varphi^2\right)\sin(\phi) + \frac{\partial\varphi^2}{\partial s}\cos(\phi), \\
v_2 + v_{0_2} &= \kappa\cos(\phi) = \frac{\partial\varphi^1}{\partial s}\sin\left(\varphi^2\right)\cos(\phi) - \frac{\partial\varphi^2}{\partial s}\sin(\phi).
\end{aligned} \tag{5.102}$$

In the context of the differential geometry of curves on surfaces, the relations (5.102) are known as Bonnet's theorem and Meusnier's theorem, respectively (see [188]). For Kirchhoff's rod theory, they were first written down by Love in 1892 (see [213, Section 253]). Here, we have supplemented his relations with a representation using φ^1 and φ^2. We observe from the relation $(5.102)_1$ that if $v_3 + v_{0_3} = 0$, then the frame $\{\mathbf{e}_t, \mathbf{d}_1, \mathbf{d}_2\}$ can be considered a Bishop frame.

It is a common error to assume that $\tau = v_3 + v_{0_3}$. We follow Love and call ϕ the angle of twist. To interpret ϕ in this manner, imagine a straight rod ($\tau = 0$) and twist it between its ends. Possibly to avoid confusion with (geometric) torsion, Love defines the tortuosity Σ as $\Sigma = \frac{1}{\tau}$ and uses Σ exclusively (see Table 5.1).

Referring to our earlier discussion in Section 1.3.4 from Chapter 1, φ^2 will be constant for a helix:

$$\cos\left(\varphi^2\right) = R\alpha\frac{\partial\theta}{\partial s} = R\tan(\gamma)\frac{\partial\theta}{\partial s}. \tag{5.103}$$

Table 5.1 The notation of Love [213, Chapter XVIII] and its correlation to the notation used in this book.

Love's notation	Our notation	Terminology
Σ	$\frac{1}{\tau}$	tortuosity
f	$\phi - \frac{3\pi}{2} + 2n\pi$	angle of twist
ψ	α^1	Euler angle
θ	α^2	Euler angle
ϕ	α^3	Euler angle
κ	ν_1	bending strain
κ'	ν_2	bending strain
τ	ν_3	torsional strain
ρ	$\frac{1}{\kappa}$	radius of curvature
N	$\mathbf{n}\cdot\mathbf{d}_1$	shear force
N'	$\mathbf{n}\cdot\mathbf{d}_2$	shear force
T	$\mathbf{n}\cdot\mathbf{e}_t$	tension
A, B, and C	EI_2, EI_1, and $\mathscr{D}$	rigidities

In addition, from the relations (5.102) and the earlier representation (1.34) for $\boldsymbol{\omega}_{\mathrm{SF}}$, we conclude that

$$\kappa = \frac{\partial \varphi^1}{\partial s}\sin\left(\varphi^2\right), \qquad \tau = \frac{\partial \varphi^1}{\partial s}\cos\left(\varphi^2\right), \qquad \frac{\partial \theta}{\partial s} = \frac{\partial \varphi^1}{\partial s}. \tag{5.104}$$

The angle θ in this discussion was used in the representation $\mathbf{r} = R\mathbf{e}_r + R\alpha\theta\mathbf{E}_3$ that appeared throughout Chapter 1.

5.11 Summary of the Governing Equations for Kirchhoff's Rod Theory

To summarize the equations governing Kirchhoff's rod theory, we have the following jump conditions:

$$\begin{gathered}
[\![\mathbf{r}]\!]_\gamma = \mathbf{0}, \qquad [\![\mathbf{P}\mathbf{P}_0]\!]_\gamma = \mathbf{0}, \\
[\![\rho_0]\!]_\gamma \dot{\gamma} = 0, \qquad \left[\left[\rho_0 y^{0\alpha}\right]\right]_\gamma \dot{\gamma} = 0, \qquad \left[\left[\rho_0 y^{\alpha\beta}\right]\right]_\gamma \dot{\gamma} = 0, \\
[\![\mathbf{n} + \mathbf{G}\dot{\gamma}]\!]_\gamma + \mathbf{F}_\gamma = \mathbf{0}, \\
[\![\mathsf{C} + \mathsf{P}\dot{\gamma}]\!]_\gamma + \mathsf{B}_\gamma = 0, \\
[\![\mathbf{m}]\!]_\gamma + \left[\left[\mathbf{d}_1 \times \mathbf{L}^1 + \mathbf{d}_2 \times \mathbf{L}^2\right]\right]_\gamma \dot{\gamma} + \mathbf{M}_\gamma = \mathbf{0}.
\end{gathered} \tag{5.105}$$

These are supplemented by the partial differential equations

$$\dot{\mathbf{G}} = \rho_0 \mathbf{f} + \frac{\partial \mathbf{n}}{\partial \xi},$$

$$\rho_0 \left(\sum_{\alpha=1}^{2} \mathbf{d}_\alpha \times y^{0\alpha} \ddot{\mathbf{r}} + \sum_{\alpha=1}^{2} \sum_{\beta=1}^{2} \mathbf{d}_\alpha \times y^{\alpha\beta} \ddot{\mathbf{d}}_\beta \right) = \mathbf{m}_a + \frac{\partial \mathbf{m}}{\partial \xi} + \frac{\partial \mathbf{r}}{\partial \xi} \times \mathbf{n}. \tag{5.106}$$

To close this system of equations, constitutive relations for $\mathbf{m}$ need to be supplied while $\mathbf{n}$ is considered to be indeterminate:

$$\mathbf{m} = \rho_0 \mathbf{P} \frac{\partial \psi}{\partial \mathbf{v}} = \sum_{i=1}^{3} \rho_0 \frac{\partial \psi}{\partial v_i} \mathbf{d}_i, \qquad \mathbf{n} = \sum_{i=1}^{3} n_i \mathbf{d}_i. \tag{5.107}$$

The jump condition arising from the energy balance is not listed above as it is used to relate the mechanical powers of the singular supplies:

$$\mathsf{B}_\gamma \dot{\gamma} + \mathbf{F}_\gamma \cdot \mathbf{v}_\gamma + \mathbf{M}_\gamma \cdot \boldsymbol{\omega}_\gamma = \Phi_{\mathrm{E}_\gamma}. \tag{5.108}$$

Given the appropriate boundary and initial conditions, the preceding equations serve to enable the calculation of $\mathbf{r}$ and $\mathbf{P}$ (or equivalently $\mathbf{d}_\alpha$) for a directed curve.

5.12 Relation to the Theory of the Elastica

We may consider the elastica as a restricted theory. The adjective "restricted" is used here in the sense that the rod's motion is planar and torsional deformations, among others, are not accommodated. An alternative viewpoint is to consider the theory as a member of a hierarchy of constrained theories. From this perspective, we note that the theory of the elastica presented in Chapter 4 can also be obtained from Kirchhoff's theory by assuming that the motion of the material curve is planar, $\mathbf{r} = x\mathbf{E}_1 + z\mathbf{E}_3$, that the rotation tensor $\mathbf{P}_0 = \mathbf{I}$, and that the rotation tensor $\mathbf{P}$ corresponds to a rotation about $\mathbf{E}_2 = \mathbf{D}_2$ through an angle θ:

$$\begin{aligned} \mathbf{P} &= \mathbf{d}_1 \otimes \mathbf{E}_1 + \mathbf{d}_2 \otimes \mathbf{E}_2 + \mathbf{d}_3 \otimes \mathbf{E}_3 \\ &= \cos(\theta)\,(\mathbf{d}_1 \otimes \mathbf{d}_1 + \mathbf{d}_3 \otimes \mathbf{d}_3) + \sin(\theta)\,(\mathbf{d}_1 \otimes \mathbf{d}_3 - \mathbf{d}_3 \otimes \mathbf{d}_1) + \mathbf{d}_2 \otimes \mathbf{d}_2. \end{aligned} \tag{5.109}$$

One also needs to make the identifications $\mathbf{E}_1 \to \mathbf{A}_2$, $\mathbf{E}_2 \to \mathbf{A}_3$, and $\mathbf{E}_3 \to \mathbf{A}_1$. The vectors associated with the rotation $\mathbf{P}$ are

$$\boldsymbol{\omega} = \dot{\theta} \mathbf{E}_2, \qquad \mathbf{P}\mathbf{v} = v_2 \mathbf{E}_2 = \theta' \mathbf{E}_2. \tag{5.110}$$

Further, the inertias $y^{0\alpha}$ and $y^{12} = y^{21}$ are set to zero.

It is interesting to note that when the motion of the Kirchhoff rod is planar, then the frame $\{\mathbf{e}_t, \mathbf{d}_1, \mathbf{d}_2\}$ is a Bishop frame with $\kappa_{B_1} = \theta'$ and $\kappa_{B_2} = 0$ for the space curve $\mathscr{S}$ occupied by the material curve $\mathscr{L}$ in the present configuration.

5.13 A Terminally Loaded Rod and a Kinetic Analogue

As a first application of the rod theory, we consider a stationary inextensible rod of length ℓ which is loaded by forces at its ends[20]:

$$\mathbf{n}\left(0^{+},t\right)=-\mathbf{F}_{0},\qquad \mathbf{n}\left(\ell^{-},t\right)=-\mathbf{F}_{0}, \tag{5.111}$$

where $\mathbf{F}_0$ is constant. Supplementing these conditions are three independent conditions from the following twelve boundary values:

$$\alpha^{k}\left(0^{+},t\right),\qquad \alpha^{k}\left(\ell^{-},t\right),\qquad \nu_{k}\left(0^{+},t\right),\qquad \nu_{k}\left(\ell^{-},t\right). \tag{5.112}$$

For example, if a rod is clamped at $\xi=0$ and free from external moments at $\xi=\ell$, then $\alpha^{k}(0^{+},t)$ are prescribed, and, with the possible help of constitutive relations (5.91), $\nu_{k}(\ell^{-},t)$ are prescribed. Alternatively, if a moment $\mathbf{M}_{\ell}$ is applied at $\xi=\ell$, then $\mathbf{m}(\ell^{-},t)=\mathbf{M}_{\ell}$ and Eqn. (5.91) are used to prescribe $\nu_{k}(\ell^{-},t)$.

In the absence of assigned body forces and moments (i.e., $\mathbf{f}=\mathbf{0}$ and $\mathbf{m}_{a}=\mathbf{0}$) and assuming the problem at hand remains static, we can solve for $\mathbf{n}$ from the local form of the balance of linear momentum $(5.106)_1$:

$$\mathbf{n}(\xi)=-\mathbf{F}_{0},\qquad \xi\in(0,\ell). \tag{5.113}$$

The local form of the balance of angular momentum $(5.106)_2$ reduces to

$$\frac{\partial\mathbf{m}}{\partial\xi}=\frac{\partial\mathbf{r}}{\partial\xi}\times\mathbf{F}_{0}. \tag{5.114}$$

Indeed, the balance laws (5.106) both yield conservations:

$$\mathbf{n}^{'}=\mathbf{0},\qquad \left(\mathbf{m}+\mathbf{r}\times\mathbf{n}\right)^{'}=\mathbf{0}. \tag{5.115}$$

That is, the contact force $\mathbf{n}$ and the contact moment relative to a fixed point O are both constant functions of ξ. If the rod is homogeneous, as shown in Exercise 5.5, $\mathsf{b}_{\mathrm{p}}=0$, and we have the additional conservation

$$\mathsf{C}^{'}=0,\ \text{where}\ \mathsf{C}=\rho_{0}\psi-\mathbf{n}\cdot\mathbf{r}^{'}-\mathbf{m}\cdot\left(\mathbf{P}\left(\mathbf{v}+\mathbf{v}_{0}\right)\right). \tag{5.116}$$

We emphasize that the conservations (5.115) apply independently of the form of the strain energy function $\rho_0\psi$.

Assuming that the strain energy function of the rod is (cf. Eqn. (5.64))

$$2\rho_{0}\psi=EI_{1}\nu_{1}^{2}+EI_{2}\nu_{2}^{2}+\mathscr{D}\nu_{3}^{2}, \tag{5.117}$$

we find using Eqn. $(5.107)_1$ that

$$\mathbf{m}=EI_{1}\nu_{1}\mathbf{d}_{1}+EI_{2}\nu_{2}\mathbf{d}_{2}+\mathscr{D}\nu_{3}\mathbf{d}_{3}. \tag{5.118}$$

[20] The jump conditions $[\![\mathbf{n}]\!]_{\gamma}+\mathbf{F}_{\gamma}=\mathbf{0}$ and $[\![\mathbf{m}]\!]_{\gamma}+\mathbf{M}_{\gamma}=\mathbf{0}$ where $\gamma=0$ and $\gamma=\ell$ are used to compute the boundary conditions on $\mathbf{n}$ and $\mathbf{m}$.

Taking the $\mathbf{d}_i$ components of the balance of angular momentum leads to three scalar equations for $\nu_k(\xi)$:

$$\begin{aligned}(EI_1\nu_1)' - (EI_2 - \mathscr{D})\,\nu_2\nu_3 &= -\mathbf{F}_0\cdot\mathbf{d}_2,\\ (EI_2\nu_2)' - (\mathscr{D} - EI_1)\,\nu_3\nu_1 &= \mathbf{F}_0\cdot\mathbf{d}_1,\\ (\mathscr{D}\nu_3)' - (EI_1 - EI_2)\,\nu_1\nu_2 &= 0.\end{aligned} \tag{5.119}$$

To determine the deformed state of the rod, the differential equations (5.119) are supplemented by an appropriate combination of six boundary conditions on the Euler angles α^k and the strains ν_k, an Euler angle parameterization of the rotation tensor $\mathbf{P}$, and a description of the reference configuration of the rod. For instance, if a 3-2-3 set of Euler angles are used to parameterize $\mathbf{P}$ then the differential equations (5.119) are supplemented by the ordinary differential equations (5.29) relating ν_k to the rates of change of the Euler angles.

5.13.1 Kirchhoff's Kinetic Analogue

The equations (5.119) are identical in form to Euler's equations for the motion of a rigid body which is free to rotate about a fixed point O where the body is subject to a force $\mathbf{F}_0$ acting at the center of mass $\bar{X}$ and the position of the center of mass is a unit length along one of the principal axes of the rigid body. This correspondence is known as the kinetic analogue and was first noted by Kirchhoff in his seminal paper [185] from 1859. It has enabled researchers, such as the authors of [164, 170, 178, 319], to leverage the considerable body of work on rigid body dynamics problems such as the Lagrange top, the asymmetric top, and the moment-free motion of a rigid body to gain insight into $\mathbf{d}_k(\xi)$ (see Figure 5.12). Indeed, in some of the applications considered in the remainder of this chapter, the kinetic analogue will play a prominent role.

As with the corresponding analogue for the elastica that was discussed in Section 4.4 of Chapter 4, once $\mathbf{P}$ is known, it remains to integrate $\mathbf{r}' = \mathbf{d}_3$ with respect to ξ to determine the shape $\mathbf{r}(\xi)$ of the deformed material curve. Recently, it has come to be appreciated that this integration is greatly facilitated by conservation laws.[21] To elaborate, $\mathbf{n}$ is constant for the terminally loaded rod and so the local form of the balance of angular momentum $(5.115)_2$ can be integrated:

$$\mathbf{m} - \mathbf{r}\times\mathbf{F}_0 = \mathbf{c}, \tag{5.120}$$

[21] The reader is referred to Kehrbaum and Maddocks [178] for a lucid discussion of this integration along with commentary on the works of Ilyukhin [170], Langer and Singer [196], and Shi and Hearst [319].

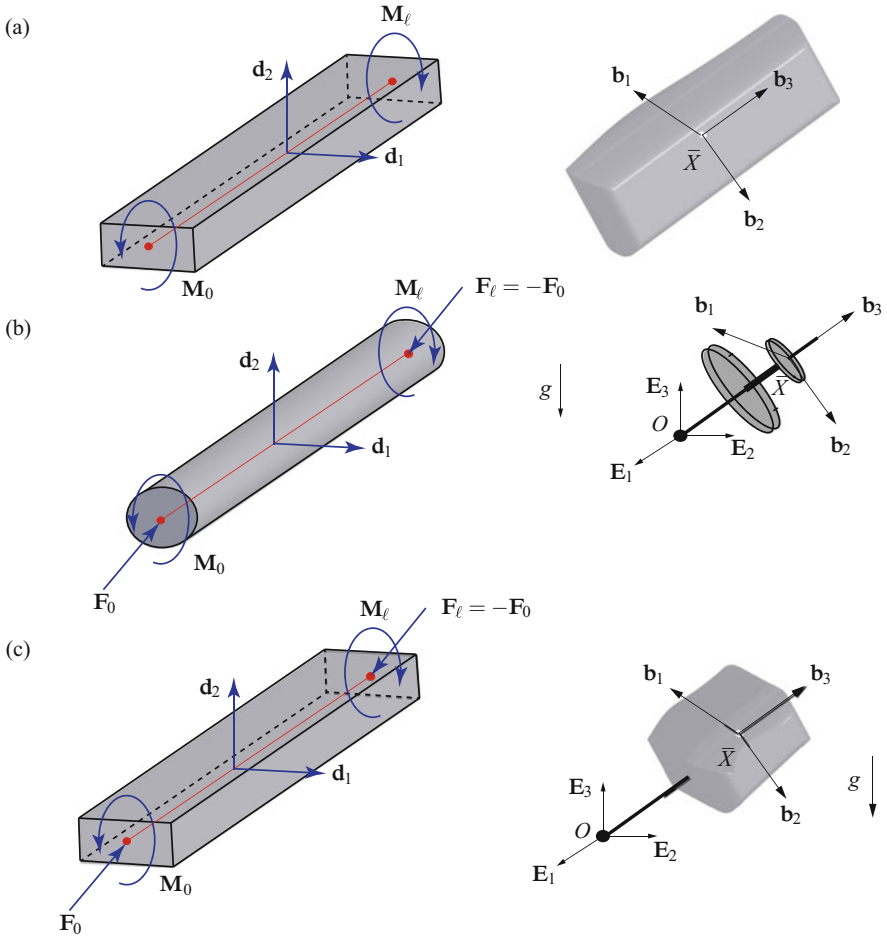

Fig. 5.12 Three cases of Kirchhoff's kinetic analogue: (a), moment-free motion of a rigid body is analogous to a rod deformed by the action of (terminally applied) moments; (b), motion of a heavy symmetric top (Lagrange top) that is connected to a fixed point O by a ball and socket joint and is subject to a gravitational loading is analogous to a rod with $I_1 = I_2$ deformed by terminally applied forces and moments; and (c), motion of an asymmetric heavy rigid body that is connected to a fixed point O by a ball and socket joint and is subject to a gravitational loading is analogous to a terminally loaded rod which has distinct flexural and torsional stiffnesses. The body-fixed basis $\{\mathbf{b}_1, \mathbf{b}_2, \mathbf{b}_3\}$ corotates with the rigid body. In Kirchhoff's kinetic analogue, the behavior of $\mathbf{b}_k(t)$ is placed in one-to-one correspondence with the vectors $\mathbf{d}_i$: $\mathbf{b}_i = \mathbf{d}_i$ and $\xi = t$.

where $\mathbf{c}$ is a constant. If we temporarily choose the fixed right-handed orthogonal basis $\{\mathbf{A}_1, \mathbf{A}_2, \mathbf{A}_3\}$ such that $\mathbf{F}_0 = -n\mathbf{A}_3$, then

$$X = \mathbf{r} \cdot \mathbf{A}_1 = \frac{1}{n}(\mathbf{m} - \mathbf{c}) \cdot \mathbf{A}_2, \qquad Y = \mathbf{r} \cdot \mathbf{A}_2 = -\frac{1}{n}(\mathbf{m} - \mathbf{c}) \cdot \mathbf{A}_1. \tag{5.121}$$

Whence, if $\mathbf{m}(\xi)$ is known, then the plane projection of $\mathbf{r}$ can be determined immediately. By way of contrast, the $\mathbf{A}_3$ component of $\mathbf{r}$ is then obtained by integrating $\mathbf{r}' \cdot \mathbf{A}_3$ with respect to ξ. In applications of the rod theory to terminally loaded rods where $\rho_0 \psi$ is given by the classic functional form (5.64) with $EI_1 = EI_2$, the relations (5.121) are used to explain why the planar projection of $\mathbf{r}$ is bounded to lie in a circular domain (cf. [319, Page 5191]).

5.14 The Simplest Problem: Bending and Torquing into a Helical Shape

As one of our first applications of Kirchhoff's rod theory, let us consider a homogeneous, linearly elastic, inextensible rod where $I_1 = I_2$. The rod is loaded at its ends by a pair of constant moments:

$$\mathbf{F}_0 = -\mathbf{0}, \qquad \mathbf{M}_0 = -\mathbf{M}_A, \qquad \mathbf{F}_\ell = \mathbf{0}, \qquad \mathbf{M}_\ell = \mathbf{M}_B. \tag{5.122}$$

It is preferable at this point not to provide any additional details on $\mathbf{M}_{A,B}$. We now proceed to establish the classic result that the deformed shape of the centerline of the rod is a helical space curve and the rod has a constant twist. This result is a natural extension to the corresponding result for an elastica: the centerline of an elastica loaded at its ends with equal and opposite applied moments will have the shape of a circular arc.[22]

The assumption that $EI_1 = EI_2 = EI$ enables the governing equations for $\nu_k(\xi)$ to simplify dramatically from (5.119):

$$\begin{aligned} \nu_1' - (1-\beta)\,\nu_2\nu_3 &= 0, \\ \nu_2' - (\beta-1)\,\nu_3\nu_1 &= 0, \\ \nu_3' &= 0. \end{aligned} \tag{5.123}$$

We have introduced a parameter

$$\beta = \frac{\mathscr{D}}{EI}, \tag{5.124}$$

which is the ratio of torsional to bending stiffnesses in the rod. For a rod with a circular cross section of radius r, $\mathscr{D} = \frac{EI}{2(1+\nu)}$ where ν is Poisson's ratio and $I = \frac{\pi r^4}{2}$, and so $\beta \leq 0.5$.

The equations (5.123) have an exact solution:

$$\begin{bmatrix} \nu_1(\xi) \\ \nu_2(\xi) \end{bmatrix} = \begin{bmatrix} \cos(\delta\xi) & \sin(\delta\xi) \\ -\sin(\delta\xi) & \cos(\delta\xi) \end{bmatrix} \begin{bmatrix} \nu_1(0) \\ \nu_2(0) \end{bmatrix}, \tag{5.125}$$

[22] See the discussion pertaining to Exercise 4.2 on Page 183.

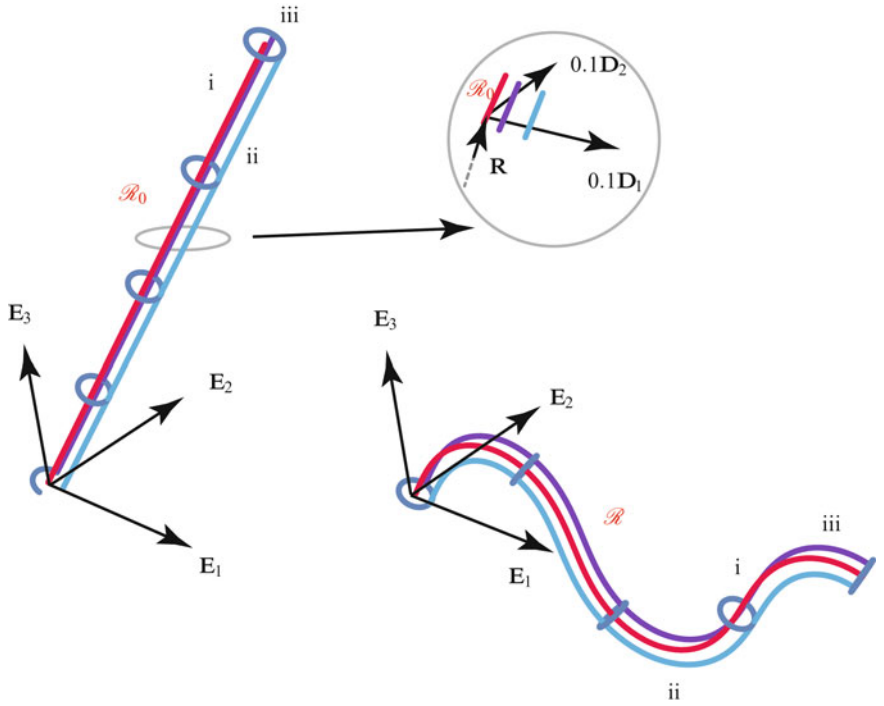

Fig. 5.13 Representative examples of the deformation of material curves from the bending and twisting of a rod with terminal moments. Reference and present configurations of three material curves are shown: (i) $\mathbf{R}(\xi)$, (ii) $\mathbf{R}+0.1\mathbf{D}_1$, and (iii) $\mathbf{R}+0.1\mathbf{D}_2$ are the chosen curves in the reference configuration. Their counterparts in the present configuration are (i) $\mathbf{r}(\xi)$, (ii) $\mathbf{r}+0.1\mathbf{d}_1$, and (iii) $\mathbf{r}+0.1\mathbf{d}_2$. The inset image shows the directors in the reference configuration. Observe that the material curve $\mathscr{L}$ in the reference configuration $\mathscr{R}_0$ is deformed into a helical curve in the present configuration.

where

$$\nu_3(\xi) = \nu_3(0), \qquad \delta = (1-\beta)\,\nu_3(0). \tag{5.126}$$

To interpret the resulting shape of the material line, we first rewrite the solutions for $\nu_\alpha(\xi)$ as

$$\begin{aligned} \nu_1(\xi) &= \sqrt{\nu_1^2(0)+\nu_2^2(0)}\,\sin(\delta\xi+\varphi_0), \\ \nu_2(\xi) &= \sqrt{\nu_1^2(0)+\nu_2^2(0)}\,\cos(\delta\xi+\varphi_0), \end{aligned} \tag{5.127}$$

where the angle φ_0 is given by

$$\tan(\varphi_0) = \frac{\nu_1(0)}{\nu_2(0)}. \tag{5.128}$$

Appealing to Bonnet and Meusnier's theorems (5.102) from Section 5.10, we conclude that the space curve formed by the material curve is a helix with a curvature κ and torsion τ which are given by the following expressions:

$$\begin{aligned}\kappa &= \sqrt{v_1^2(\xi)+v_2^2(\xi)} = \sqrt{v_1^2(0)+v_2^2(0)},\\ \tau &= v_3(\xi) - \frac{\partial\phi}{\partial\xi} = \beta v_3(0) = \left(\frac{\mathscr{D}}{EI}\right) v_3(0).\end{aligned} \tag{5.129}$$

In addition, the angle of twist of the rod is

$$\phi(\xi) = \delta\xi + \phi(0) = \left(1 - \frac{\mathscr{D}}{EI}\right) v_3(0)\xi + \phi(0), \qquad \varphi_0 = \phi(0). \tag{5.130}$$

Thus, under terminal moments, the centerline of the rod deforms into a circular helix and the directors twist about the helical curve at a constant rate. The torques needed to achieve this state can be computed with the help of the constitutive relations:

$$\begin{aligned}\mathbf{M}_A &= -EI\left(v_1(0)\mathbf{d}_1(0) + v_2(0)\mathbf{d}_2(0)\right) - \mathscr{D}v_3(0)\mathbf{d}_3(0),\\ \mathbf{M}_B &= EI\left(v_1(\ell)\mathbf{d}_1(\ell) + v_2(\ell)\mathbf{d}_2(\ell)\right) + \mathscr{D}v_3(0)\mathbf{d}_3(\ell).\end{aligned} \tag{5.131}$$

The radius R and parameter α for the helical curve formed by the centerline can be found from Eqn. (5.129) with the help of Eqn. (1.35): we leave this as an exercise for the interested reader.

As an example of a rod twisted into a helical form, consider the initially straight rod shown in Figure 5.13. The rod in question is assumed to have the material properties

$$\beta = \frac{\mathscr{D}}{EI} = 0.5, \qquad \ell = 4. \tag{5.132}$$

To avoid singularities in the 3-2-3 Euler angles that are used to parameterize $\mathbf{d}_k(\xi)$, the reference configuration is chosen so that $\mathbf{R}(\xi)$ describes a straight line, $\mathbf{P}_0 = \mathbf{I}$, and the rotation tensor $\mathbf{P}$ is a constant rotation with $\alpha^1 = \alpha^3 = 0$ and $\alpha^2 = \frac{\pi}{8}$. The end $\xi = 0$ is subject to an applied moment,

$$\mathbf{M}_A = -3EI\mathbf{d}_1(0) - 3\mathscr{D}\mathbf{d}_3(0), \tag{5.133}$$

and the directors are assumed to have the initial values

$$\begin{aligned}\mathbf{d}_1(0) &= \cos\left(\frac{\pi}{8}\right)\mathbf{E}_1 - \sin\left(\frac{\pi}{8}\right)\mathbf{E}_3,\\ \mathbf{d}_2(0) &= \mathbf{E}_2,\\ \mathbf{d}_3(0) &= \cos\left(\frac{\pi}{8}\right)\mathbf{E}_3 + \sin\left(\frac{\pi}{8}\right)\mathbf{E}_1.\end{aligned} \tag{5.134}$$

Integrating (5.29) and (5.123), the Euler angles α^k and, with the help of (5.19), the directors $\mathbf{d}_\alpha(\xi)$ and the tangent vector $\mathbf{r}'(\xi) = \mathbf{d}_3(\xi)$ can be computed. An additional integration of $\mathbf{d}_3(\xi)$ provides $\mathbf{r}(\xi)$. An applied moment $\mathbf{M}_B$ at $\xi = \ell$ is

needed for equilibrium and this moment can be determined from the computed values of $v^k(\ell^-)$ and $\mathbf{d}_k(\ell^-)$. The results of these computations are displayed in Figure 5.13. In addition, to the shape of the deformed material curve $\mathscr{L}$, the deformed shape of two other material curves, $\mathbf{r}+0.1\mathbf{d}_1$ and $\mathbf{r}+0.1\mathbf{d}_2$, and five circular cross sections are shown.

It is natural to ask if helical solutions are possible for rods modeled using Kirchhoff's rod theory where the symmetry $I_1 = I_2$ is absent? The affirmative answer to this question can be found in a recent paper by Chouaieb et al. [60] where the search for helical solutions, that was initiated by Kirchhoff, is completed.

5.15 Hockling of Cables, Loop Formation, and Localized Buckling

The next set of problems we consider pertain to an initially straight rod which has the symmetry $EI_1 = EI_2$. In addition to the terminal moments that deformed the rod in the previous section, the rod is also subject to terminal forces. For this rod, depending on the loading and boundary conditions, we will find some of the helical solutions just discussed as well as more complex spatial shapes of the material curve such as those shown in Figure 5.14. These solutions find application to a wide range of models for problems including the looping and hockling of marine cables [75] and the supercoiling of DNA [319, 320]. The model we present is nonlinear. However, as discussed in Love [213, Section 272(d)] the model can be linearized to provide a model for the vibration of a shaft of finite length that is subject to combined thrust and torsion. Such a model was famously employed by Greenhill [141] in 1883 to examine the buckling instability in the driveshafts of ships.

We assume that the terminal loading is given by Eqn. (5.111), the strain energy function is prescribed as in the classic functional form (5.64), and the reference configuration is chosen so that $\mathbf{D}_i = \mathbf{E}_i$ with $\mathbf{E}_3$ taken to be parallel to the direction of the terminal loading:

$$\mathbf{F}_0 = F_0\mathbf{E}_3, \qquad \mathbf{F}_\ell = F_\ell\mathbf{E}_3, \qquad F_0 = -F_\ell. \tag{5.135}$$

The kinetic analogue for this problem is a symmetric rigid body which is free to rotate about a fixed point O and is subject to a gravitational force (see Figure 5.12(b)). In recognition of the seminal work performed on this problem in the 1780s by Joseph-Louis Lagrange (1736–1813), the rigid body dynamics problem is known as the Lagrange top.[23] The gravitational force is analogous to the terminal load $F_\ell\mathbf{E}_3$ and the pair of conserved angular momenta are analogous to conserved components of the contact moment $\mathbf{m}$ in the rod.

[23] Lagrange's original work is presented in [191, 192, Sections IX.34–IX.41]. Other treatments of this problem can be found in Arnold [15, Section 30], Lewis et al. [205], Marsden and Ratiu [229, Chapter 1], and Whittaker [362, Sections 71–73].

The highlights of the analysis of this example include the demonstration of buckling of a twisted, initially straight rod subject to tensile end loads and terminal moments into a pair of helical forms. We also show the evolution of the handedness of the helical forms as a loading parameter is varied and discuss the presence of a localized buckling solution corresponding to a homoclinic orbit in the state space of a reduced system governing the evolution of the Euler angle $\alpha^2(\xi)$. We are fortunate to be able to leverage a large literature on this problem and shall cite several works in the sequel. However, two aspects of our analysis are novel. First, the discussion of the changing handedness of the helical forms has not been discussed in the literature. Second, we show how the dual Euler basis can be used to obtain physically meaningful representations for the contact moment $\mathbf{m}$ in the rod and asymptotic estimates for the terminal moments $\mathbf{M}_0$ and $\mathbf{M}_\ell$.

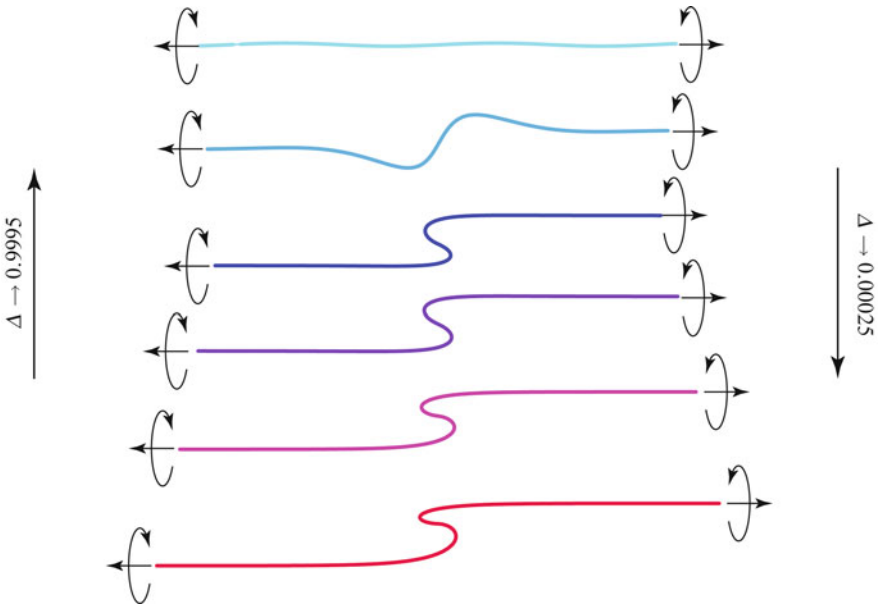

Fig. 5.14 Deformation of a twisted, initially straight rod as the terminal forces $\mathbf{F}_\ell = F_\ell \mathbf{E}_3 = -\mathbf{F}_0$ and terminal moments (proportional to a parameter c) are varied in a particular manner. The variation of the loading is captured by a dimensionless parameter $\Delta = \frac{c^2}{4F_\ell EI}$ which is decreased from 0.9995 to 0.00025 for the results shown. The planar projections of the deformed centerlines are shown in additional detail in Figure 5.18.

5.15.1 Development of the Reduced Dynamical System

The strains v_k of the rod are again governed by the differential equations (5.119) supplemented by the ordinary differential equations (5.29). However, this formulation of the equations governing the rod is not very amenable to analysis and it is more convenient to consider the components of $\frac{\partial \mathbf{m}}{\partial \xi} = -\frac{\partial \mathbf{r}}{\partial \xi} \times \mathbf{F}_\ell$ projected onto the Euler basis for the 3-2-3 set of Euler angles:

$$\left\{\mathbf{e}_1 = \mathbf{E}_3, \mathbf{e}_2 = \cos\left(\alpha^3\right)\mathbf{d}_2 + \sin\left(\alpha^3\right)\mathbf{d}_1, \mathbf{e}_3 = \mathbf{d}_3\right\}. \tag{5.136}$$

That is,

$$\begin{aligned}
\frac{\partial}{\partial \xi}\left(\mathbf{m}\cdot\mathbf{E}_3\right) &= -\left(\mathbf{d}_3 \times F_\ell \mathbf{E}_3\right)\cdot\mathbf{E}_3,\\
\frac{\partial}{\partial \xi}\left(\mathbf{m}\cdot\mathbf{e}_2\right) - \mathbf{m}\cdot\mathbf{e}_2' &= -\left(\mathbf{d}_3 \times F_\ell \mathbf{E}_3\right)\cdot\mathbf{e}_2,\\
\frac{\partial}{\partial \xi}\left(\mathbf{m}\cdot\mathbf{d}_3\right) - \mathbf{m}\cdot\mathbf{d}_3' &= -\left(\mathbf{d}_3 \times F_\ell \mathbf{E}_3\right)\cdot\mathbf{d}_3.
\end{aligned} \tag{5.137}$$

The resulting three second-order differential equations for the Euler angles are equivalent to Lagrange's equations of motion.[24] Expanding the components of $\mathbf{m}$ in the above equations, one finds that

$$\begin{aligned}
&\frac{\partial}{\partial \xi}\left(\left(\mathscr{D}\cos^2\left(\alpha^2\right) + EI\sin^2\left(\alpha^2\right)\right)\frac{\partial \alpha^1}{\partial \xi} + \mathscr{D}\cos\left(\alpha^2\right)\frac{\partial \alpha^3}{\partial \xi}\right) = 0,\\
&EI\frac{\partial^2 \alpha^2}{\partial \xi^2} + \mathscr{D}\frac{\partial \alpha^1}{\partial \xi}\frac{\partial \alpha^3}{\partial \xi}\sin\left(\alpha^2\right) + \left(\frac{\mathscr{D} - EI}{2}\right)\frac{\partial \alpha^1}{\partial \xi}\frac{\partial \alpha^1}{\partial \xi}\sin\left(2\alpha^2\right) = F_\ell \sin\left(\alpha^2\right),\\
&\frac{\partial}{\partial \xi}\left(\mathscr{D}\left(\frac{\partial \alpha^1}{\partial \xi}\cos\left(\alpha^2\right) + \frac{\partial \alpha^3}{\partial \xi}\right)\right) = 0.
\end{aligned} \tag{5.138}$$

The first and third of these equations lead to the conclusion that the following pair of components of the contact moment $\mathbf{m}$ are conserved along the rod:

$$\begin{bmatrix} c_F = \mathbf{m}\cdot\mathbf{E}_3 \\ c_S = \mathbf{m}\cdot\mathbf{d}_3 \end{bmatrix} = \begin{bmatrix} \mathscr{D}\cos^2\left(\alpha^2\right) + EI\sin^2\left(\alpha^2\right) & \mathscr{D}\cos\left(\alpha^2\right) \\ \mathscr{D}\cos\left(\alpha^2\right) & \mathscr{D} \end{bmatrix} \begin{bmatrix} \frac{\partial \alpha^1}{\partial \xi} \\ \frac{\partial \alpha^3}{\partial \xi} \end{bmatrix}, \tag{5.139}$$

where c_F and c_S are constants. That is, the component of $\mathbf{m}$ in the direction of $\mathbf{F}_\ell$ is conserved, the component of $\mathbf{m}$ along the axis of symmetry $\mathbf{d}_3$ of the rod is conserved, and the moment vector $\mathbf{m}$ has the representation[25]

$$\mathbf{m} = c_F\mathbf{e}^1 + c_S\mathbf{e}^3 + m_2\mathbf{e}^2, \tag{5.140}$$

[24] See Exercise 5.8 for further details on the Lagrangian and the specific form of Lagrange's equations of interest here.

[25] The application here of the dual Euler basis vectors to explain the terminal loading on the rod is novel and, to the best of our knowledge, has not appeared previously in the vast literature on terminally loaded rods.

where expressions for the dual Euler basis vectors can be found in Eqn. (5.23). Observe that the only component of $\mathbf{m}$ that varies along the rod is in the $\mathbf{e}^2 = \mathbf{e}_2 = \cos\left(\alpha^3\right)\mathbf{d}_2 + \sin\left(\alpha^3\right)\mathbf{d}_1$ direction. It is interesting to also note that $\mathbf{e}_2$ is perpendicular to the axis of symmetry $\mathbf{d}_3$ and the applied forces $\mathbf{F}_0 = F_0\mathbf{E}_3$ and $\mathbf{F}_\ell = F_\ell\mathbf{E}_3$. As noted previously, these conservations are precisely analogous to the conservation of two distinct components of the angular momentum of a symmetric rigid body freely rotating about a fixed point while subject to a gravitational force.

Of particular interest in the sequel is the limiting behavior of the moment $c\mathbf{e}^1 + c\mathbf{e}^3$ as the angle α^2 approaches 0. As c is a constant, it suffices to compute the limiting value of the sum of the dual Euler basis vectors:

$$\lim_{\alpha^2\to 0}\left(\mathbf{e}^1+\mathbf{e}^3\right) = \lim_{\alpha^2\to 0}\left(\mathbf{d}_3 - \frac{1-\cos\left(\alpha^2\right)}{\sin\left(\alpha^2\right)}\left(\cos\left(\alpha^3\right)\mathbf{d}_1 - \sin\left(\alpha^3\right)\mathbf{d}_2\right)\right). \tag{5.141}$$

That is,

$$\lim_{\alpha^2\to 0}\left(\mathbf{e}^1+\mathbf{e}^3\right) = \mathbf{E}_3. \tag{5.142}$$

We shall use this result in the sequel to explore asymptotic limits of terminal moments applied to the rod.

The expressions for the conservations (5.139) can be inverted to yield $\frac{\partial\alpha^1}{\partial\xi}$ and $\frac{\partial\alpha^3}{\partial\xi}$ as functions of α^2, $\mathscr{D}$, EI, c_S, and c_F:

$$\begin{bmatrix} \frac{\partial\alpha^1}{\partial\xi} \\ \frac{\partial\alpha^3}{\partial\xi} \end{bmatrix} = \begin{bmatrix} \frac{\operatorname{cosec}^2\left(\alpha^2\right)}{EI} & -\frac{\cot\left(\alpha^2\right)\operatorname{cosec}\left(\alpha^2\right)}{EI} \\ -\frac{\cot\left(\alpha^2\right)\operatorname{cosec}\left(\alpha^2\right)}{EI} & \frac{1}{\mathscr{D}} + \frac{\cot^2\left(\alpha^2\right)}{EI} \end{bmatrix} \begin{bmatrix} c_F = \mathbf{m}\cdot\mathbf{E}_3 \\ c_S = \mathbf{m}\cdot\mathbf{d}_3 \end{bmatrix}. \tag{5.143}$$

Observe that once $\alpha^2(\xi)$ is known, then (5.143) can be integrated (often numerically) to determine $\alpha^1(\xi)$ and $\alpha^3(\xi)$.

To find the differential equation governing $\alpha^2(\xi)$ that accommodates the conservations of $\mathbf{m}\cdot\mathbf{E}_3$ and $\mathbf{m}\cdot\mathbf{d}_3$, we follow a classic procedure developed by Routh [305] which is known as Routhian reduction. The first step of the reduction is to use the pair of conservations (5.143) to eliminate $\frac{\partial\alpha^1}{\partial\xi}$ and $\frac{\partial\alpha^3}{\partial\xi}$ from the differential equation $(5.138)_2$. After some rearranging and algebraic manipulations, the following two-parameter family of ordinary differential equations for $\alpha^2(\xi)$ is obtained:

$$EI\frac{\partial^2\alpha^2}{\partial\xi^2} + \frac{\left(c_F c_S\left(1+\cos^2\left(\alpha^2\right)\right) - \left(c_F^2+c_S^2\right)\cos\left(\alpha^2\right)\right)}{EI\sin^3\left(\alpha^2\right)} = F_\ell\sin\left(\alpha^2\right). \tag{5.144}$$

This set of differential equations can be expressed in the compact form[26]

$$EI\frac{\partial^2\alpha^2}{\partial\xi^2} = -\frac{\partial U}{\partial\alpha^2}, \tag{5.145}$$

where the function

$$U = U\left(c_S, c_F, \alpha^2\right) = \frac{\left(c_F - c_S\cos\left(\alpha^2\right)\right)^2}{2EI\sin^2\left(\alpha^2\right)} + F_\ell\cos\left(\alpha^2\right). \tag{5.146}$$

Analysis of Eqn. (5.144) is facilitated in the sequel both with the help of dimensionless variables,

$$x = \frac{\xi}{\hat{\ell}}, \qquad \hat{c}_F = \frac{c_F\hat{\ell}}{EI}, \qquad \hat{c}_S = \frac{c_S\hat{\ell}}{EI}, \qquad \hat{F}_\ell = \frac{F_\ell\hat{\ell}^2}{EI}, \tag{5.147}$$

and the extensive body of work that has been performed on the corresponding differential equations for the Lagrange top. In order to accommodate rods of infinite length and to enable simplification of differential equations in the sequel, the length scale $\hat{\ell}$ will not necessarily be chosen to equal the length ℓ of the rod.

We henceforth consider instances where $c_S = c_F = c$. In this case, the moment components in the directions of $\mathbf{d}_3$ and $\mathbf{F}_0$ are equal and the differential equation (5.144) simplifies dramatically:

$$EI\frac{\partial^2\alpha^2}{\partial\xi^2} + \frac{c^2\left(1-\cos\left(\alpha^2\right)\right)^2}{EI\sin^3\left(\alpha^2\right)} = F_\ell\sin\left(\alpha^2\right). \tag{5.148}$$

The differential equation (5.148) is analogous to the reduced dynamical system used to demonstrate the well-known stabilization of a vertical upright top (sleeping top) as it is spun at successively faster speeds. The forthcoming bifurcation as c^2 increases corresponds to this stabilization.

5.15.2 The Straight Rod and a Pair of Rods Bent into a Helical Form

After examining the conditions governing the equilibria $\left(\alpha^2 = \alpha_0^2, \frac{\partial\alpha^2}{\partial\xi} = 0\right)$ of Eqn. (5.148), it can be shown that for $c^2 > 4F_\ell EI$ only one equilibrium is present, while for $c^2 < 4F_\ell EI$, three equilibria are present[27]:

[26] This classic result can be used to show that the solutions to the second-order differential equation (5.144) conserve $\frac{EI}{2}\left(\frac{\partial\alpha^2}{\partial\xi}\right)^2 + U$ and can be expressed in terms of Weierstrassian elliptic functions. For further details on this integration and the Routhian reduction procedure that can be used to establish Eqn. (5.144), the exposition in Whittaker [362, Section 71] is highly recommended.

[27] For details on this calculation, see Exercise 5.9.

$$\alpha_0^2 = 0, \qquad \alpha_0^2 = \pm \arccos\left(-1 + 2\sqrt{\Delta}\right). \tag{5.149}$$

Here, we have found it convenient to define a parameter Δ:

$$\Delta = \frac{c^2}{4F_\ell EI}. \tag{5.150}$$

For the equilibria where $\alpha_0^2 \neq 0$, we note from Eqn. (5.143) that $\frac{\partial \alpha^1}{\partial \xi}$ and $\frac{\partial \alpha^3}{\partial \xi}$ are constant throughout the equilibrium state of the rod:

$$\frac{\partial \alpha^1}{\partial \xi} = \alpha_0^{1'} = \frac{c}{2EI}\frac{1}{\sqrt{\Delta}}, \qquad \frac{\partial \alpha^3}{\partial \xi} = \alpha_0^{3'} = \frac{c}{\mathscr{D}} - \frac{c}{EI}\left(1 - \frac{1}{2\sqrt{\Delta}}\right). \tag{5.151}$$

Referring to Figure 5.15 where the solutions are plotted, it is obvious that when $4F_\ell EI = c^2$ a (pitchfork) bifurcation occurs. For both types of equilibria, $\mathbf{n} = F_\ell \mathbf{E}_3$, and, as $\mathbf{m}\cdot\mathbf{e}_2 = EI\frac{\partial \alpha^2}{\partial \xi}$, the moment component $\mathbf{m}\cdot\mathbf{e}^2 = \mathbf{m}\cdot\mathbf{e}_2 = 0$.

For the first type of equilibrium $\mathbf{d}_3 = \mathbf{E}_3$ and the centerline of the rod is straight with $\alpha_0^2 = 0$. Invoking the identity (5.142), we conclude that the terminal moments at the ends of the rod are $\mp c\mathbf{E}_3$. We also observe that these moments are parallel to the terminal forces $\mathbf{F}_0 = -F_\ell \mathbf{E}_3 = -\mathbf{F}_\ell$. The bifurcation of this solution as Δ drops below 1 has close similarities to Greenhill's famed buckling formula for a straight rod of finite length ℓ.[28] Here, however, we also have the unusual situation that the terminal loadings of the rod are tensile. In other words, a combination of tensile loads and torque can produce buckling in a straight rod.

With the help of the relations (5.15) for the Euler basis vectors, for the second type of equilibrium we find that

$$\begin{aligned}\mathbf{P}\mathbf{v} &= \alpha_0^{1'}\mathbf{E}_3 + \alpha_0^{3'}\mathbf{d}_3 \\ &= -\alpha_0^{1'}\sin\left(\alpha_0^2\right)\cos\left(\alpha^3\right)\mathbf{d}_1 + \alpha_0^{1'}\sin\left(\alpha_0^2\right)\sin\left(\alpha^3\right)\mathbf{d}_2 \\ &\quad + \left(\alpha_0^{3'} + \cos\left(\alpha_0^2\right)\alpha_0^{1'}\right)\mathbf{d}_3.\end{aligned} \tag{5.152}$$

Invoking Bonnet and Meusnier's theorems (5.102) from Section 5.10, using the fact that

$$1 + \cos\left(\alpha_0^2\right) = 2\sqrt{\Delta} = \sqrt{\frac{c^2}{F_\ell EI}}, \tag{5.153}$$

and employing the relations (5.139), it can be shown that the centerline of the rod has constant curvature and constant torsion and that the directors twist at a constant rate about this centerline:

[28] Greenhill's development of [141, Eqn. (1)] forms the basis for Exercise 5.12 at the end of this chapter. We note that the bifurcation at hand cannot be predicted as a limit of his criterion (see Eqn. (5.252)) when the length of the rod $\ell \to \infty$.

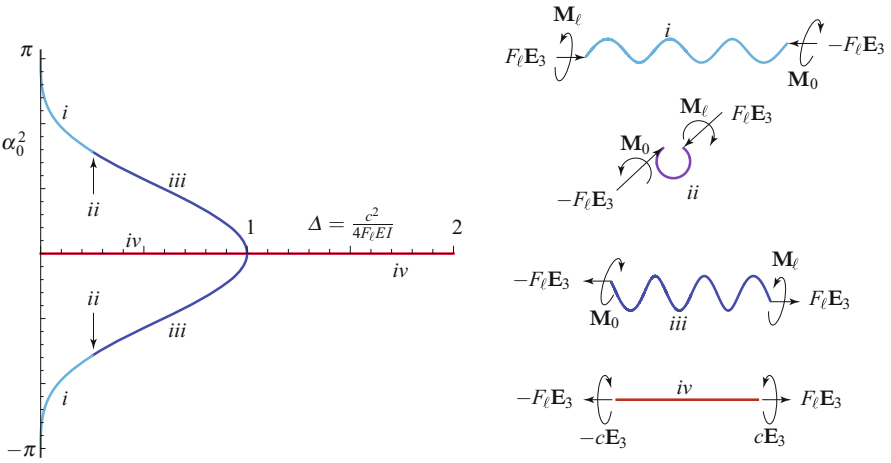

Fig. 5.15 The equilibria α_0^2 of Eqn. (5.148) as a function of the dimensionless parameter $\Delta = \frac{c^2}{4F_\ell EI}$ when $c = c_S = c_F$. The trivial branch corresponds to the straight equilibrium of the rod (labeled *iv* in the figure). For $\Delta < 1/4$, the nontrivial branches correspond to rods whose centerlines are helical curves (labeled *i* in the figure). As $\Delta = 1/4$, the centerlines of these rods become plane circles (labeled *ii* in the figure), and we observe that the helical curves (labeled *iii* in the figure) now change handedness as Δ increases past $1/4$. The parameter value $\Delta = 1/4$ corresponds to the force parameter $F_\ell = c^2/EI$ and $\alpha_0^2 = \pm\frac{\pi}{2}$.

$$\begin{aligned}
\phi &= \alpha^3 - \operatorname{sgn}\left(\alpha_0^{1'}\sin\left(\alpha_0^2\right)\right)\frac{\pi}{2},\\
\kappa &= \left|\alpha_0^{1'}\sin\left(\alpha_0^2\right)\right| = \left|\left(\frac{\sin\left(\alpha_0^2\right)}{1+\cos\left(\alpha_0^2\right)}\right)\frac{c}{EI}\right|,\\
\tau &= \alpha_0^{1'}\cos\left(\alpha_0^2\right) = \left(\frac{\cos\left(\alpha_0^2\right)}{1+\cos\left(\alpha_0^2\right)}\right)\frac{c}{EI}.
\end{aligned} \tag{5.154}$$

That is, the centerline of the rod is bent into a helix. We can use the identity (5.101) with Eqn. (5.154) to show that the axis of the helix is parallel to the terminal loadings $\mathbf{F}_\ell = -\mathbf{F}_0 = F_\ell\mathbf{E}_3$:

$$\begin{aligned}
\boldsymbol{\omega}_{\mathrm{SF}} &= \mathbf{P}\mathbf{v} - \frac{\partial\phi}{\partial s}\mathbf{e}_t\\
&= \alpha_0^{1'}\left(-\sin\left(\alpha_0^2\right)\cos\left(\alpha^3\right)\mathbf{d}_1 + \sin\left(\alpha_0^2\right)\sin\left(\alpha^3\right)\mathbf{d}_2 + \cos\left(\alpha_0^2\right)\mathbf{d}_3\right)\\
&= \alpha_0^{1'}\,\mathbf{E}_3\\
&= \sqrt{\frac{F_\ell}{EI}}\mathbf{E}_3.
\end{aligned} \tag{5.155}$$

The rod in this case is said to have been bent into a helical form [213, Section 271].

With the help of the expression $(5.154)_3$ for τ, it can be shown that for values of $\Delta < 1/4$ that the helical forms are left handed (right handed) if $c > 0$ ($c < 0$). In the limiting case as $\Delta \searrow 0$, the curvature of the helical forms tends to zero and the centerline of the rod straightens. When $\Delta = 1/4$, $\tau = 0$, $\alpha_0^2 = \pm\pi/2$, and the torsion of the helical forms vanishes, so the centerline of the rod now has the shape of a circular arc of radius EI/c. It is also interesting to note that, for this value of Δ, $EIF_\ell = c^2$. For $1/4 < \Delta < 1$, the helical forms change handedness from their earlier counterparts: the helical forms are now right handed (left handed) if $c > 0$ ($c < 0$).[29] As recorded in Figure 5.15, observe that the terminal loadings change as Δ passes through $1/4$ in a manner reminiscent of a similar transition observed in the elastica (cf. Figures 4.5 and 4.6).

The moment $\mathbf{m}$ in these twisted helical states is not constant. Rather, it varies throughout the rod and has components along the tangent to the centerline of the rod as well as in the cross section:

$$\begin{aligned}\mathbf{m} &= c\mathbf{e}^1 + c\mathbf{e}^3 \\ &= c\left(\mathbf{d}_3 - \frac{1-\cos\left(\alpha_0^2\right)}{\sin\left(\alpha_0^2\right)}\left(\cos\left(\alpha^3\right)\mathbf{d}_1 - \sin\left(\alpha^3\right)\mathbf{d}_2\right)\right) \\ &= c\left(\mathbf{E}_3 + \frac{1-\cos\left(\alpha_0^2\right)}{\sin\left(\alpha_0^2\right)}\left(\cos\left(\alpha^1\right)\mathbf{E}_1 + \sin\left(\alpha^1\right)\mathbf{E}_2\right)\right). \end{aligned} \tag{5.156}$$

These representations can be used to determine the moments $\mathbf{M}_0$ and $\mathbf{M}_\ell$ applied to the ends of the rod. With the help of the identity (5.142), we are able to conclude that the moment in the twisted helical states asymptotes to the moment in the straight rod. While this result is satisfying on physical grounds, given the singularity in the Euler angle parameterization when $\alpha^2 = 0, \pi$, it is also surprising. For the case when $\Delta = 1/4$ and the helical forms have no torsion, the contact moment in the rod can be found from the expression (5.156):

$$\mathbf{m} = c\mathbf{E}_3 + c\sin\left(\alpha_0^2\right)\left(\cos\left(\alpha^1\right)\mathbf{E}_1 + \sin\left(\alpha^1\right)\mathbf{E}_2\right). \tag{5.157}$$

Observe that the circular arc formed by $\mathbf{r}(\xi)$ lies in the $X-Y$ plane and the moment $\mathbf{m}$ will have a component in the $X-Y$ plane. This component is needed to balance the moment due to terminal loadings $\mathbf{F}_\ell = F_\ell\mathbf{E}_3 = -\mathbf{F}_0$.

In summary, if $\Delta < 1$, then 3 types of equilibria are possible. As shown in Figure 5.15, one of equilibria corresponds to the straight rod, while the second and third correspond to a pair of helical forms whose handedness depends on the sign of $c = \mathbf{m}\cdot\mathbf{E}_3 = \mathbf{m}\cdot\mathbf{d}_3$ and the value of Δ. When $\Delta = 1/4$, the helical forms degenerate to circular forms (i.e., the centerline of the rod forms an circular arc). What distinguishes the two twisted helical rods is a phase offset in their twist angles (see Eqn. $(5.154)_1$). For a given value of Δ, these twisted helical states have a value of

[29] This observation on the change in handedness as Δ varies does not appear to have been previously recorded in the literature.

the energy function U that is lower than their straight counterpart and this suggests that the straight configuration for a rod of infinite length becomes unstable as Δ decreases past 1 and can be said to have buckled.

Much of what we have just described on the equilibrium states of the top and their correspondence to straight and twisted helical rods dates to Kirchhoff's seminal work from 1859. Our exposition has been heavily influenced by Love [213, Section 270] and the more recent work on this topic by Coyne [75] and Thompson and his coworkers [164, 340]. With the help of numerical integration capabilities that were not available to Love et al., the latter authors were able to examine the nonequilibrium solutions of (5.148) and discuss the corresponding deformed configurations of a rod. The picture they present, and which we will presently examine, is one with a remarkably rich range of deformed rod shapes.

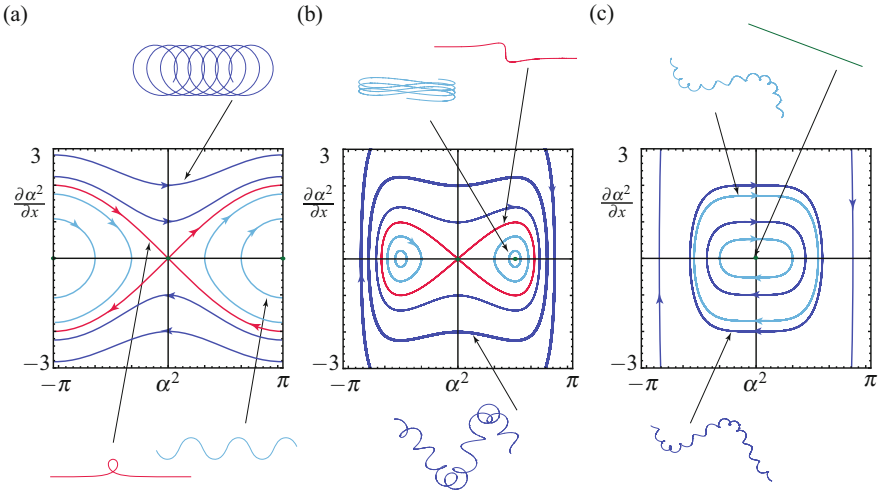

Fig. 5.16 Phase portraits of the differential equation (5.159) for three different values of the parameter $\frac{F_\ell EI}{c^2}$. In (a), $c^2 = 0$; in (b), $c^2 = 0.50 F_\ell EI$; and in (c), $c^2 = 8F_\ell EI$. The inset images correspond to the deformed material curve of a terminally loaded rod of finite length where $\alpha^2(\xi)$ corresponds to a portion of a trajectory in the phase portrait. For the pair of nontrivial equilibria in (b), the corresponding helical forms of the centerline of the rod are shown in Figure 5.15. The case $c^2 = 0$ corresponds to the terminally loaded planar elastica discussed in Section 4.4 of Chapter 4.

5.15.3 Nontrivial and Localized Equilibrium States of the Rod

To explore additional solutions to the terminally loaded rod beyond the straight and helical forms discussed earlier, we non-dimensionalize the differential equations (5.148) using Eqn. (5.147) by choosing $\hat{\ell}$ so that $\hat{F}_\ell = 1$:

$$\hat{\ell} = \sqrt{\frac{EI}{F_\ell}}. \tag{5.158}$$

The resulting dimensionless form of the differential equation (5.148) is

$$\frac{\partial^2\alpha^2}{\partial x^2}+\frac{4\Delta\left(\left(1-\cos\left(\alpha^2\right)\right)^2\right.}{\sin^3\left(\alpha^2\right)}=\sin\left(\alpha^2\right). \tag{5.159}$$

The bifurcation shown in Figure 5.15 is evident in changes to the phase portrait of the second-order differential equation (5.159) as $\frac{F_\ell EI}{c^2}$ is varied that are observed in Figure 5.16. The solutions shown in these phase portraits can be classified as fixed points (corresponding to the solutions discussed in the previous section), closed orbits, a figure ∞ loop that contains the origin, and a pair of orbits that asymptote to the fixed point in Figure 5.16(a). The figure ∞ loop and the latter orbit are pairs of homoclinic orbits.

Representative examples of $\mathbf{r}(\xi)$ corresponding to portions of the orbits and fixed points are shown in Figure 5.16. As evident from the deformed shapes of the centerline of the rod, there is a rich variety of solutions. While some recent progress has been made to establish a classification for all these solutions[30] we focus attention here on those solutions which correspond to the homoclinic orbits. Explicit solutions for $\alpha^2(x)$ for the homoclinic orbits can be found using conservation of an energy-like function e:

$$e=\frac{1}{2}\left(\frac{\partial\alpha^2}{\partial x}\right)^2+\frac{2\Delta\left(1-\cos\left(\alpha^2\right)\right)}{\left(1+\cos\left(\alpha^2\right)\right)}+\cos\left(\alpha^2\right). \tag{5.160}$$

This energy-like function is inferred from the differential equation (5.145) by nondimensionalizing U: $U\to U/F_\ell\hat{\ell}$. We can easily compute the value of the level set of the energy-like function e that passes through the origin in the phase plane to find that it is $e=1$. Thus,

$$\int_{x_1}^{x_2}dv=\int_{\alpha_2^2}^{\alpha_1^2}\frac{\sin(\chi)}{\sqrt{(2-2\cos(\chi))\sin^2(\chi)-4\Delta\left(1-\cos(\chi)\right)^2}}d\chi. \tag{5.161}$$

Using the change of variables, $u=\cos(\chi)$, the integral on the right-hand side of this equation simplifies and can be evaluated:

$$\begin{aligned}x_2-x_1&=-\int_{u_2}^{u_1}\frac{du}{\sqrt{2}(1-u)\sqrt{1-2\Delta+u}}\\&=\frac{1}{\sqrt{1-\Delta}}\operatorname{Arctanh}\left(\sqrt{\frac{1+u-2\Delta}{2(1-\Delta)}}\right)\Bigg|_{u_1}^{u_2},\end{aligned} \tag{5.162}$$

[30] See the works of Goriely [222, 249], Maddocks [86, 169, 178], Thompson [164, 340], and their coworkers.

where $u_\beta = \cos\left(\alpha_\beta^2\right)$. We choose $u_1 = \cos\left(\alpha_0^2\right) = 2\sqrt{\Delta} - 1$ and $x_1 = 0$.[31] Whence,

$$\cos\left(\alpha^2(x)\right) = 2\Delta - 1 + 2(1-\Delta)\tanh^2\left(x\sqrt{1-\Delta} + \operatorname{Arctanh}\left(\sqrt{\frac{\sqrt{\Delta}-\Delta}{1-\Delta}}\right)\right). \tag{5.163}$$

This expression can be used to determine $\alpha^1(x)$ and $\alpha^3(x)$ by integrating the differential equations (5.143). A further integration of an expression for $\mathbf{d}_3$ in terms of the Euler angles (see Eqn. (5.15)) provides the deformed shape $\mathbf{r}(\xi)$ of the centerline:

$$\frac{\partial \mathbf{r}}{\partial \xi} = \cos\left(\alpha^2(\xi)\right)\mathbf{E}_3 + \sin\left(\alpha^2(\xi)\right)\left(\cos\left(\alpha^1(\xi)\right)\mathbf{E}_1 + \sin\left(\alpha^1(\xi)\right)\mathbf{E}_2\right). \tag{5.164}$$

Observe that as $\xi \to \pm\infty$, $\alpha^2(\xi) \to 0$ and $\mathbf{d}_3 = \frac{\partial \mathbf{r}}{\partial \xi} \to \mathbf{E}_3$. It is also helpful to recall that $\xi = \sqrt{\frac{EI}{F_\ell}}x$ when interpreting these results.

A pair of examples of computing the deformed shapes of the rod corresponding to the homoclinic orbits is presented in Figure 5.17. For these examples, the parameter $\Delta = 0.25$ and the solutions are integrated numerically using the initial values $\cos\left(\alpha_0^2\right) = 2\sqrt{\Delta} - 1$ and $\frac{\partial \alpha^2}{\partial x}(x=0) = 2\left(1-\sqrt{\Delta}\right)$. In its entirety, each orbit pertains to a rod of infinite length, so only a portion of the centerline corresponding to each orbit is shown. Different initial values of $\mathbf{r}(x=0)$ are chosen to distinguish the two sets of results. As can be seen from the figure, $\mathbf{d}_3$ asymptotes to $\mathbf{E}_3$, as expected. We also note that the twist angle $\phi(x) = \alpha^3(x)$ increases monotonically throughout the length of the deformed rod. For a rod of finite length $x \in (x_1, x_2)$, if the loading parameters and boundary conditions are chosen so that $\alpha^2(x)$ lies on the homoclinic orbit, then, in addition to terminal forces $\mathbf{F}_\ell = F_\ell \mathbf{E}_3 = -\mathbf{F}_0$, moments

$$\begin{aligned}
\mathbf{M}_A &= -\mathbf{m}\left(\xi_1^+\right) = -c\left(\mathbf{e}^1\left(\xi_1^+\right) + \mathbf{e}^3\left(\xi_1^+\right)\right) - EI\frac{\partial \alpha^2}{\partial \xi}\left(\xi_1^+\right)\mathbf{e}_2\left(\xi_1^+\right), \\
\mathbf{M}_B &= \mathbf{m}\left(\xi_2^-\right) = c\left(\mathbf{e}^1\left(\xi_2^-\right) + \mathbf{e}^3\left(\xi_2^-\right)\right) + EI\frac{\partial \alpha^2}{\partial \xi}\left(\xi_2^-\right)\mathbf{e}_2\left(\xi_2^-\right),
\end{aligned} \tag{5.165}$$

must be applied at the respective ends of the rod. If the rod has an infinite length, then, after invoking the limit (5.142), we would find that the terminal moments needed are $\mathbf{M}_{-\infty} = -c\mathbf{E}_3$ and $\mathbf{M}_\infty = c\mathbf{E}_3$.

The problem of looping and hockling of cables prompted Coyne [75] to examine the deformed shape of an infinitely long rod subject to combined torsion and thrust. He made the important observation that as Δ decreased below 1, the deformed shapes of the rod corresponding to the homoclinic orbits that arise exhibited loops. These loops are easiest to see in the $Y-Z$ projections of the deformed shapes and examples are shown in Figure 5.18 and are similar to the planar loops found by

[31] It is useful to note that this choice implies that $\frac{\partial \alpha^2}{\partial x}(x = x_1 = 0) = \pm 2\left(1-\sqrt{\Delta}\right)$. To see this result, it suffices to set $e = 1$ in Eqn. (5.160) and then solve for $\frac{\partial \alpha^2}{\partial x}$ when $\cos\left(\alpha_0^2\right) = 2\sqrt{\Delta} - 1$.

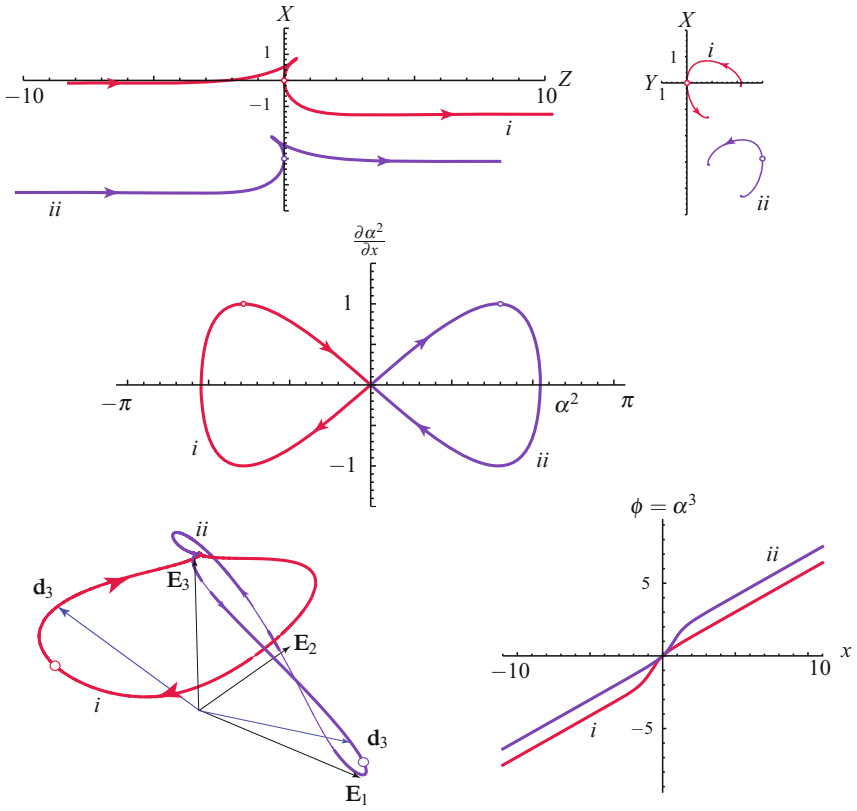

Fig. 5.17 The pair (*i* and *ii*) of homoclinic orbits of the differential equation (5.159) for values of the parameters $\Delta = \frac{c^2}{4F_\ell EI} = 0.250$ and $\frac{EI}{\mathscr{D}} = 1.3$. Corresponding to each of the orbits, the inset images show plots of the twist angle $\phi(\xi) = \alpha^3(\xi)$, the tangent indicatrices of $\mathbf{d}_3$, and the components of the position vector $\mathbf{r}(x) = X(x)\mathbf{E}_1 + Y(x)\mathbf{E}_2 + Z(x)\mathbf{E}_3$ for a finite section of a rod of infinite length that is loaded at its ends by forces and moments. The circle in the images is intended to help indicate the correspondence between points on the various graphs and the arrows indicate the direction of increasing ξ.

Euler in 1744 that we discussed in Section 4.4 of Chapter 4. Coyne then noted that, because a rod has a given diameter, self-contacting of the rod during this loop formation might be possible. Trying to remove the loop in marine cables by changing F_ℓ or c is problematic and often leads to a smaller loop with large permanent strains which damage the marine cable - a process known as hockling.

To explore the onset of the loop formation, we examine an infinitely long rod which is subject to terminal forces $\mathbf{F}_\ell = -\mathbf{F}_0 = F_\ell \mathbf{E}_3$ and moments $\mathbf{M}_\ell = -\mathbf{M}_0 = c\mathbf{E}_3$ and assume that the loading is such that $\Delta < 1$ and $\alpha^2(x)$ and its derivative trace out a homoclinic orbit in the phase plane. The displacement of the ends of the rod can be found using Eqn. (5.163) and used to calculate the shortening s_ℓ of the rod as Δ varies:

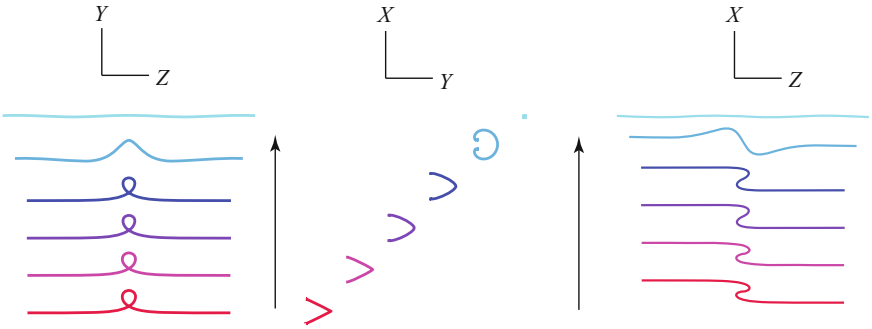

Fig. 5.18 Planar projections of the deformed centerline of the rod shown in Figure 5.14. For these projections, $\Delta = 0.00025, 0.0025, 0.025, 0.25, 0.75, 0.9995$, and $\frac{EI}{\mathscr{D}} = 1.3$. The arrow indicates the direction of decreasing Δ. The initial values of $\mathbf{r}(x=0)$ are chosen to be different for each of the curves in order to distinguish the solutions, and $\alpha^2(0) = -\arccos\left(-1+2\sqrt{\Delta}\right)$, $\frac{\partial \alpha^2}{\partial x}(x=0) = 0$. The variable $x \in [-10, 10]$ for all the solutions and the behavior of the twist angle $\phi(x)$ and strain $v_2(x)$ for these solutions are shown in Figure 5.19.

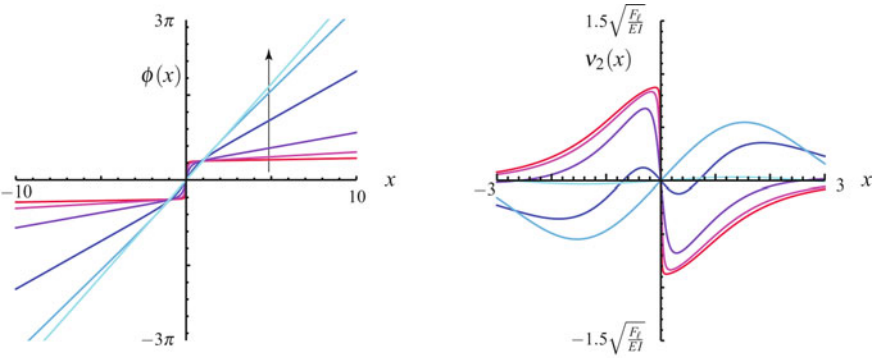

Fig. 5.19 The twist angle $\phi = \phi(x)$ and strain $v_2(x)$ for the deformed rods whose centerlines are shown in Figure 5.14. The arrow indicates the direction of decreasing Δ. In contrast to the bending strain v_2 (and v_1), because of the conservation, $\mathbf{m} \cdot \mathbf{d}_3 = c_s$, the strain v_3 is uniform throughout the rod.

$$
\begin{aligned}
s_\ell &= 2\int_0^\infty \left(1 - \cos\left(\alpha^2(\xi)\right)\right) d\xi \\
&= 2\hat{\ell}\int_0^\infty \left(1 - \cos\left(\alpha^2(x)\right)\right) dx \\
&= 4\sqrt{\frac{EI}{F_\ell}}\sqrt{1-\Delta}\left[1 - \sqrt{\frac{\sqrt{\Delta}}{1+\sqrt{\Delta}}}\right].
\end{aligned}
\tag{5.166}
$$

From the final expression, with some rearranging, we can write the change in length as a function of the terminal loadings as

$$s_\ell = 8\left(\frac{EI}{c}\right)\sqrt{\Delta - \Delta^2}\left[1 - \sqrt{\frac{\sqrt{\Delta}}{1+\sqrt{\Delta}}}\right]. \tag{5.167}$$

This expression is used to determine the shortening s_ℓ as a function of Δ for various values of c. The results are shown in Figure 5.20.

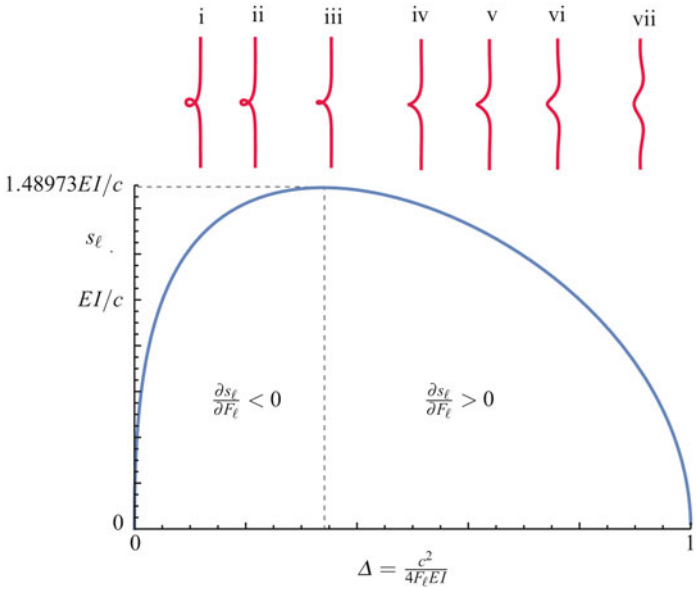

Fig. 5.20 The shortening s_ℓ of a rod of infinite length as a function of the loading parameter Δ as described by Eqn. (5.167). The inset images are projections on the $Y-Z$ plane of a portion of the deformed centerline $\mathbf{r}(\xi)$: (i), $\Delta = 0.1$; (ii), $\Delta = 0.2$; (iii), $\Delta \approx 0.3389388$; (iv), $\Delta = 0.5$; (v), $\Delta = 0.6$; (vi), $\Delta = 0.75$; and (vii), $\Delta = 0.90$. The maximum shortening $s_\ell \approx 1.48973\frac{EI}{c}$ occurs when $\Delta \approx 0.3389388$.

To see why the loop formation can be problematic, suppose we impose terminal forces $\mathbf{F}_\ell = F_\ell \mathbf{E}_3$ and $\mathbf{F}_0 = -F_\ell \mathbf{E}_3$ and terminal moments $\mathbf{M}_\ell = -\mathbf{M}_0 = c\mathbf{E}_3$ on the infinitely long rod.[32] Initially, we assume that the rod is straight and twisted and that $\Delta > 1$. We now increase F_0 so that Δ becomes smaller than 1 and assume that the rod deforms so that $\alpha^2(\xi)$ and its derivative lie on one of the homoclinic orbits (and remain there as this orbit changes with changing F_ℓ). Referring to Figure 5.20, eventually, as Δ decreases past 0.5 the rod will develop a loop. Because of the thickness

[32] Our discussion here, while also based on the behavior of s_ℓ as F_0 varies, is different from Coyne's. In particular, his discussion has statements on stability and instability that we have not been able to follow.

of the rod, self-contact becomes possible. This may lead to the rod supercoiling but our model is insufficient to predict this phenomenon. Ignoring the possibility of self-contact, as F_ℓ is increased further so that $\Delta < 0.3389388$, the shortening starts to decrease and the loop (in the $Y-Z$ plane) grows. As can be seen from Figure 5.19, the rate of change in the angle of twist of the rod also increases and becomes unbounded at $\xi = 0$ as $\Delta \to 0$. However, the strain ν_3 remains constant, while the bending strains ν_1 and ν_2 increase dramatically as F_0 increases. The concomitant large strains in the rod render our model unrealistic because plastic deformation (or hockling) now becomes likely.

5.15.4 Comments

While a configuration of the rod having a loop is present for the infinitely long rod where $\alpha^2(\xi)$ and its derivative describe a homoclinic orbit, other configurations, many with multiple loops, are also present and can be seen in Figure 5.16(b)-(c). These configurations have not received as much attention in the literature in part because analytical solutions for $\mathbf{r}(\xi)$ (which can be found in [319]) are not as tractable as those for the homoclinic case (cf. Eqn. (5.163)). While analytical solutions for $\mathbf{r}(\xi)$ are available in a handful of the aforementioned special cases and have proven to be very helpful in categorizing the rich array of possible shapes $\mathbf{r}(\xi)$, in general one cannot expect such good fortune. Indeed, it has been recently shown by Mielke and Holmes [238] that small perturbations in the form of terminal forces or inhomogeneities to the case of a rod with $EI_1 \neq EI_2$ that is terminally loaded by end moments (such as discussed in Section 5.14) can lead to spatially complex (chaotic) $\mathbf{r}(\xi)$. Examples of such complex shapes can be seen in a work by Davies and Moon [84] that was inspired by [238]. A recent perspective on, and extensions to, [238] can be found in [165].

Hopefully, a sufficient variety of spatial forms for $\mathbf{r}(\xi)$ have been presented in this chapter for the reader to appreciate the richness of the problem of a terminally loaded rod. What we have not touched upon is the manner in which $\mathbf{r}(\xi)$ changes (even in a quasistatic manner) as the loading parameters are varied. Several works, such as [340], present experiments on these transitions and there are papers such as [75, 162, 164] which discuss the transitions from an analytical perspective using a quasistatic analysis. Motivated in part by the additional application to DNA supercoiling, the papers by Bergou et al. [22], Clauvelin et al. [61], van der Heijden et al. [162], and Jawed et al. [173] also include the effects of self-contact. The results in [162] (and others) have been explored using numerical methods (and including dynamical effects) by Goyal et al. [124–126]. The analyses of Coleman et al. [67, 68] on closed loops of rod as models for DNA minicircles are also noteworthy. Despite the large body of work on the application of rod theory to looping, hockling, physical knots, and the related problem of DNA supercoiling, much remains to be discovered in this rich application of rod theory.

5.16 Rods with Intrinsic Curvature: Tendril Perversion, Helical Solutions, and Buckling

Throughout the literature one finds a large focus on the analysis of twisted rods where the centerline is in the form of a helix. These analyses are frequently motivated by the use of rod-based models to determine the static behavior of double-stranded DNA molecules. Another biomechanical application of rod theories occurs in studies on the static behavior of plant tendrils and branches. In this area of application, one finds segments of the plant tendril which are in the form both of left-handed and right-handed helices. An example of such a situation is shown in Figure 5.21 which is reproduced from Charles Darwin's (1809–1882) celebrated and lucid work [81] on climbing plants. The tendril connecting the helices of opposite handedness is known, following Goriely and Tabor [123], as a perversion and the phenomenon of the changing handedness of the helical structures formed by the tendril is known as tendril perversion.[33] For instance, referring to Figure 5.21, the tendril connects the plant stem to a support and has three perversions, a pair of left-handed helices, and a pair of right-handed helices. Related examples where a rod-like body has segments of its length taking on helical structures with varying handedness occur in telephone cords, umbilical cords, and embryonic heart loops.[34]

The rod model used to examine tendril perversions consists of an intrinsically curved rod where $\nu_{0_1} = 1/R$. That is, the reference configuration of the centerline of the rod is circular. An easy visualization of such a reference configuration is to imagine a slinky of infinitesimal thickness. By applying forces, the slinky expands out into a helical shape that is similar to a telephone cord. In plant stems, it is well known that intrinsic curvatures of the type $\nu_{0_1} = 1/R$ are induced by differential growth where one side of the plant stems grows at a faster rate than the other. The growth-induced intrinsic curvature assists in enabling plant stems to retain their form in the presence of gravitational and wind loading.[35] This intrinsic curvature can also be induced in the laboratory by stretching strips of rubber

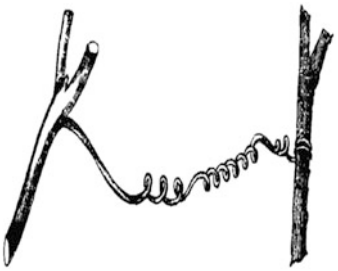

Fig. 5.21 Examples of tendril perversion in the plant *Bryonia dioica*. This figure is copied with permission from Darwin [81, Figure 13].

[33] The terminology is based on the use of the word perversion (or "Verkehrung" (= reversal)) by the famed topologist Johann B. Listing (1808–1882) for a transformation that changes the handedness of a helix (see [208, Page 22]).

[34] For additional discussions on tendril perversion, the reader is referred to Domokos and Healey [90], Keller [179], Männer [223], and McMillen and Goriely [235].

[35] For additional references on this topic, the reader is referred to [121, 273, 295, 323, 365] and references therein.

of different initial length to the same length and then gluing them together.[36] In this section, we explore various problems associated with intrinsically curved rods. These range from simple deformation of the rod to buckling instabilities and perversions. First, we examine various representations of the balance laws.

5.16.1 Balance Laws for an Intrinsically Curved Rod

We consider a terminally loaded elastic rod where $\mathbf{v}_0 \neq \mathbf{0}$. To explore some of the issues of interest it is useful to express the balance laws for this rod using the Frenet triad $\{\mathbf{e}_t, \mathbf{e}_n, \mathbf{e}_b\}$:

$$\mathbf{n} = n_t\mathbf{e}_t + n_n\mathbf{e}_n + n_b\mathbf{e}_b, \qquad \mathbf{m} = m_t\mathbf{e}_t + m_n\mathbf{e}_n + m_b\mathbf{e}_b. \tag{5.168}$$

Thus, the balance laws, $\mathbf{n}' = \mathbf{0}$ and $\mathbf{m}' + \mathbf{r}' \times \mathbf{n} = \mathbf{0}$, can be expressed as six first-order differential equations:

$$\begin{bmatrix} n_t' \\ n_n' \\ n_b' \end{bmatrix} = \begin{bmatrix} 0 & \kappa & 0 \\ -\kappa & 0 & \tau \\ 0 & -\tau & 0 \end{bmatrix} \begin{bmatrix} n_t \\ n_n \\ n_b \end{bmatrix},$$

$$\begin{bmatrix} m_t' \\ m_n' \\ m_b' \end{bmatrix} = \begin{bmatrix} 0 & \kappa & 0 \\ -\kappa & 0 & \tau \\ 0 & -\tau & 0 \end{bmatrix} \begin{bmatrix} m_t \\ m_n \\ m_b \end{bmatrix} + \begin{bmatrix} 0 \\ n_b \\ -n_n \end{bmatrix}. \tag{5.169}$$

To establish these equations, the Serret-Frenet relations (1.13) were used. It is also convenient to recall the definition of the Darboux vector $\boldsymbol{\omega}_{\mathrm{SF}} = \tau\mathbf{e}_t + \kappa\mathbf{e}_b$.

The representation (5.169) will prove useful for some, but not all, of the subsequent developments. Indeed two other representations will appear in the sequel: (5.270) which projects the balance laws onto the $\mathbf{d}_i$ basis vectors, and (5.194) which is the linearization of the balance laws about an equilibrium configuration. For the latter, a set of 1-2-3 Euler angles are used to parameterize the rotation tensor $\mathbf{P}$.[37]

5.16.2 Helical Solutions: Solving for the Geometric Torsion, Curvature, and Angle of Twist

Tacitly ignoring boundary conditions and constitutive relations for the present, we seek equilibria of Eqn. (5.169). That is, solutions to these equations where the

[36] The interested reader is referred to the paper by Liu et al. [209] where an example of such an intrinsically curved body is used to help analyze perversions.

[37] In the interests of brevity, the developments of these two representations of the balance laws are discussed in Exercises 5.14 and 5.15.

components of $\mathbf{n}$ and $\mathbf{m}$ in terms of the Frenet triad are constant: $n_t' = n_n' = n_b' = 0$ and $m_t' = m_n' = m_b' = 0$. Based on the recent works of Goriely et al. [123, 235], we show that two solutions are present: a straight possibly twisted configuration and a configuration where the centerline takes the shape of a helix and the rod is twistless.[38]

We first consider solutions where the centerline is straight: $\kappa = 0$ and $\tau = 0$. Thus, we find the expected results that $\mathbf{n} = n\mathbf{e}_t$ and $\mathbf{m}$ is constant. For the more interesting case where $\kappa \neq 0$, we find that κ and τ are constants and that

$$n_n = 0, \qquad \kappa n_t = \tau n_b, \qquad m_n = 0, \qquad \kappa m_t - \tau m_b = n_b. \tag{5.170}$$

Thus, the centerline of the rod is in the form of a helical space curve. In addition, we can also conclude that $\mathbf{n}$ is parallel to the Darboux vector:

$$\begin{aligned}\mathbf{n} &= n_t\mathbf{e}_t + n_b\mathbf{e}_b \\ &= n_b\left(\frac{\tau}{\kappa}\mathbf{e}_t + \mathbf{e}_b\right) \\ &= (\kappa m_t - \tau m_b)\left(\mathbf{e}_b + \frac{\tau}{\kappa}\mathbf{e}_t\right) \\ &= \left(m_t - \frac{\tau}{\kappa}m_b\right)\boldsymbol{\omega}_{\mathrm{SF}}.\end{aligned} \tag{5.171}$$

For a circular helix, the Darboux vector is parallel to the axis of the helix.[39] If we assume that the rod has end points at $\xi = \pm\ell$, then, as $\mathbf{n}$ is constant throughout the rod, the terminal loadings define the axis of the helix:

$$\mathbf{F}_{-\ell} = F_0\mathbf{E}, \qquad \mathbf{F}_{\ell} = -F_0\mathbf{E}, \qquad \mathbf{n}(\xi) = -F_0\mathbf{E}, \tag{5.172}$$

where $\mathbf{E}$ is a unit vector that is parallel to $\boldsymbol{\omega}_{\mathrm{SF}}$. In general, terminal moments will also need to be applied to the rod and we leave it as an exercise for the reader to determine these moments.

To proceed further, we need to make some assumptions about the constitution of the rod. We assume that the rod has a nontrivial intrinsic curvature $\boldsymbol{\nu}_0 = \nu_{0_1}\mathbf{D}_1 + \nu_{0_2}\mathbf{D}_2 + \nu_{0_3}\mathbf{D}_3$ and a strain energy function

$$2\rho_0\psi = EI_1\nu_1^2 + EI_2\nu_2^2 + \mathscr{D}\nu_3^2. \tag{5.173}$$

We presume that ν_{0_k} and the moduli EI_1, EI_2, and $\mathscr{D}$ are constants. With the help of the constitutive relations (5.93) and the Bonnet-Meusnier relations (5.102) we find that

[38] A complementary perspective on solutions of this type can be found in the discussion of Ericksen's uniform states in Section 6.6 in Chapter 6.

[39] This result was discussed in an earlier chapter of this text and the reader is referred to Eqn. (1.34) for details.

$$\mathbf{m} = \mathscr{D}\left(\tau + \frac{\partial \phi}{\partial s} - \nu_{0_3}\right)\mathbf{e}_t + \left(EI_1\nu_1\cos(\phi) - EI_2\nu_2\sin(\phi)\right)\mathbf{e}_n + \left(EI_1\nu_1\sin(\phi) + EI_2\nu_2\cos(\phi)\right)\mathbf{e}_b, \tag{5.174}$$

where

$$\nu_1 = \kappa\sin(\phi) - \nu_{0_1}, \qquad \nu_2 = \kappa\cos(\phi) - \nu_{0_2}. \tag{5.175}$$

The condition $m_n = 0$ is satisfied if

$$(EI_1 - EI_2)\,\kappa\sin(\phi)\cos(\phi) = EI_1\nu_{1_0}\cos(\phi) - EI_2\nu_{2_0}\sin(\phi). \tag{5.176}$$

This can be considered as an equation for the twist angle ϕ. Except for the trivial case where the rod is symmetric ($EI_1 = EI_2$) and $\nu_{0_1} = \nu_{0_2} = 0$, this angle must be a constant. We henceforth assume that ϕ is constant: $\phi = \phi_0$. With the help of Eqns. (5.172) and (5.174), we see that the remaining condition $(5.170)_4$ yields the identity

$$\left(\mathscr{D}\left(\tau - \nu_{0_3}\right) - \frac{\tau}{\kappa}\left(EI_1\nu_1\sin(\phi_0) + EI_2\nu_2\cos(\phi_0)\right)\right)\boldsymbol{\omega}_{\mathrm{SF}}\cdot\mathbf{E} = -F_0. \tag{5.177}$$

In conclusion, we have two equations, Eqns. (5.176) and (5.177), for the unknown parameters κ, ϕ_0, and τ of the rod solution.

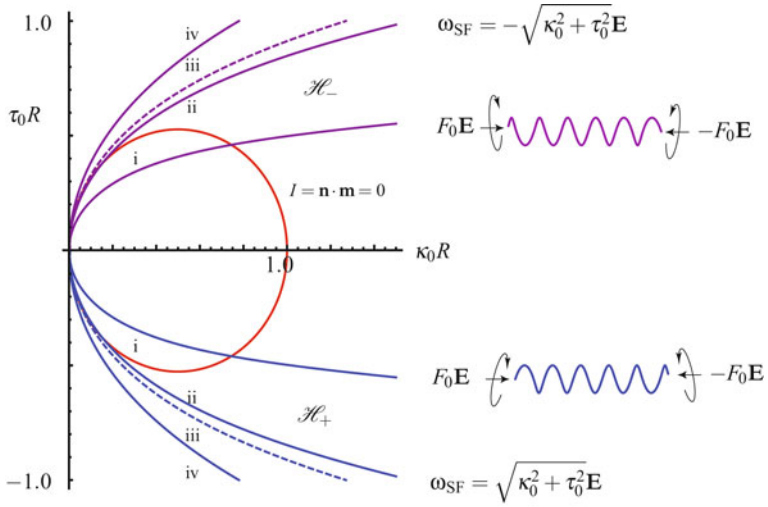

Fig. 5.22 Solutions (κ_0, τ_0) of Eqn. (5.180) with the angle of twist $\phi = \phi_0 = \frac{\pi}{2}$ for various values of $f_0 = \frac{F_0R^2}{EI_1}$. For the solutions shown, $\frac{\mathscr{D}}{EI_1} = 0.9$ and a critical value of $f_0 = 1/\mathscr{D}$: (i), $f_0 = 0.5$; (ii), $f_0 = 1.0$; (iii), $f_0 = 1/0.9$; and (iv), $f_0 = 1.5$. The zero level set of the integral $I = \mathbf{n}\cdot\mathbf{m}$ is also shown.

To illustrate the above solution procedure, we follow the literature on tendril perversion models and assume that the rod is curved into a constant radius circle in

its reference configuration (cf. [90, 123, 235]):

$$v_{0_1} = \frac{1}{R}, \qquad v_{0_2} = 0, \qquad v_{0_3} = 0. \tag{5.178}$$

In this case, the condition (5.174) is identically satisfied when[40]

$$\phi_0 = \pm\frac{\pi}{2}. \tag{5.179}$$

Finally, we find an equation for κ and τ from Eqn. (5.176):

$$\left(\mathscr{D} - \frac{EI_1 \sin(\phi_0)}{\kappa}\left(\kappa\sin(\phi_0) - \frac{1}{R}\right)\right)(\tau\boldsymbol{\omega}_{\mathrm{SF}})\cdot\mathbf{E} = -F_0. \tag{5.180}$$

Given $\frac{F_0R^2}{EI_1}$, $\frac{\mathscr{D}}{EI_1}$, and ϕ_0, we can solve Eqn. (5.180) for the pair (τ_0, κ_0). We denote a solution to Eqn. (5.180) by the pair (τ_0, κ_0) and representative cases for a range of values of F_0 are shown in Figure 5.22. Because of the possibilities

$$\boldsymbol{\omega}_{\mathrm{SF}} = \pm\sqrt{\kappa^2 + \tau^2}\mathbf{E}, \tag{5.181}$$

each solution (τ_0, κ_0) with $\boldsymbol{\omega}_{\mathrm{SF}} = \sqrt{\kappa_0^2 + \tau_0^2}\mathbf{E}$ has a counterpart $(-\tau_0, \kappa_0)$ with $\boldsymbol{\omega}_{\mathrm{SF}} = -\sqrt{\kappa_0^2 + \tau_0^2}\mathbf{E}$. This pair of helical solutions, which we respectively denote by $\mathscr{H}_+$ and $\mathscr{H}_-$, will have opposite handedness. While the terminal forces on these solutions will be identical, it is straightforward to show that the terminal moments will be different.

5.16.2.1 Tendril Perversion in an Infinitely Long Rod

We conclude from the analysis that was just discussed that, for a given rod and applied force F_0, a pair of helical solutions, $\mathscr{H}_+$ and $\mathscr{H}_-$, can be found which, apart from their handedness, are qualitatively identical. If a solution to the differential equations (5.169) can be found that connects the pair, then the corresponding solution corresponds to a perversion. Goriely et al. [123, 235] assumed that the rod is of infinite length and so they sought the so-called heteroclinic orbits that connect the pairs of fixed points corresponding to $\mathscr{H}_+$ and $\mathscr{H}_-$. To help find the solution, they cleverly exploited the fact that the solutions to (5.169) conserve $I = \mathbf{n}\cdot\mathbf{m}$. Evaluating this integral of motion at one end of the orbit, say at $\mathscr{H}_+$, we would find, after imposing the conditions (5.170), (5.174), and (5.179), that

$$\mathbf{n}\cdot\mathbf{m} = \left(\frac{\mathscr{D}\tau_0^2}{\kappa_0} + m_b\right)(\mathscr{D}\kappa_0 - m_b)\,\tau_0, \tag{5.182}$$

[40] In the sequel, our numerical results pertain to $\phi_0 = \frac{\pi}{2}$. We found that the solutions of Eqn. (5.180) for $\phi_0 = -\frac{\pi}{2}$ are qualitatively similar and so, in the interests of brevity, they are not mentioned.

where $m_b = EI_1\left(\kappa_0 \sin(\phi_0) - \frac{1}{R}\right)\sin(\phi_0)$. On the other hand, evaluating $\mathbf{n}\cdot\mathbf{m}$ at the other end of the orbit, we find that

$$\mathbf{n}\cdot\mathbf{m} = -\left(\frac{\mathscr{D}\tau_0^2}{\kappa_0} + m_b\right)\left(\mathscr{D}\kappa_0 - m_b\right)\tau_0. \tag{5.183}$$

Consequently, $I = \mathbf{n}\cdot\mathbf{m} = 0$ on the heteroclinic orbit. That is, remarkably, the force and moment are orthogonal along the orbit. For fixed points with $\phi_0 = \frac{\pi}{2}$, if $0 < F_0 \le (EI_1)^2/\mathscr{D}R^2$, then we can always find a pair of fixed points for a given F_0 and $I = 0$ at both points (cf. Figure 5.23).[41] When $\phi_0 = -\frac{\pi}{2}$, the set of suitable fixed points with $I = 0$ is empty and these solutions are not discussed any further.

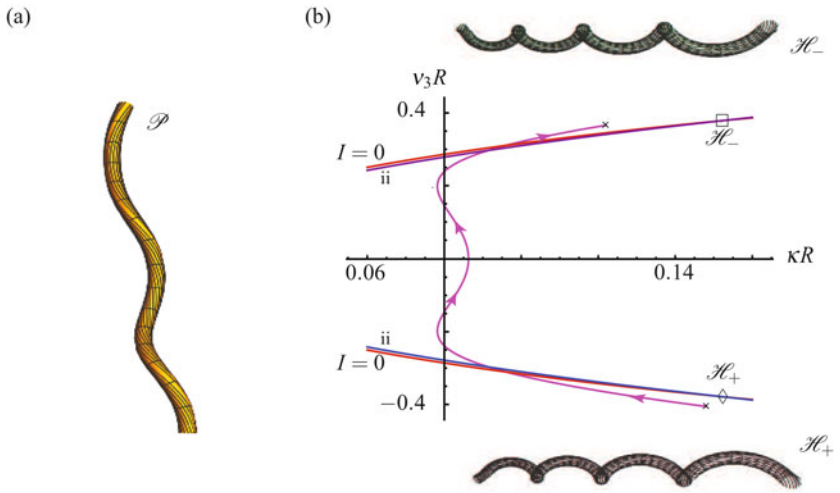

Fig. 5.23 (a) The deformed rod corresponding to an approximation $\mathscr{P}$ to the perversion connecting a pair of helical solutions $\mathscr{H}_+$ and $\mathscr{H}_-$. The pair of solutions $\mathscr{H}_+$ and $\mathscr{H}_-$ satisfy Eqn. (5.180) with the angle of twist $\phi = \phi_0 = \frac{\pi}{2}$ for a given value of $f_0 = \frac{F_0R^2}{EI_1} = 1$ and have a value of the integral $I = \mathbf{n}\cdot\mathbf{m} = 0$. (b) The evolution of $\kappa(\xi)$ and $\nu_3(\xi)$ along $\mathscr{P}$. The level set $I = 0$ of the integral $\mathbf{n}\cdot\mathbf{m}$ in the $\kappa - \nu_3$ parameter plane and the points $\mathscr{H}_+$ (labeled with a ◊) and $\mathscr{H}_-$ (labeled with a □) are also shown. The parameter values and labels are identical to those for Figure 5.22.

For a given F_0, and a pair $\mathscr{H}_\pm$, the next task is to see if there is a solution to the differential equations (5.169) that connects the pair of fixed points. To progress, the form (5.169) is not convenient to use. Instead, we use the $\mathbf{d}_i$ components of the balances of linear and angular momenta.[42] The resulting set of eighteen first-order

[41] Whence our reference to the critical value $f_0 = \frac{1}{\mathscr{D}}$ in the caption for Figure 5.22.

[42] The derivation of this form of $\mathbf{m}' + \mathbf{r}' \times \mathbf{n} = \mathbf{0}$ is similar to the derivation of Eqn. (5.119) and is discussed in Exercise 5.14.

differential equations are[43]

$$\mathbf{r}^{'} = \mathbf{d}_3, \qquad \mathbf{d}_1^{'} = v_3\mathbf{d}_2 - v_2\mathbf{d}_3, \qquad \mathbf{d}_2^{'} = -v_3\mathbf{d}_1 + \left(v_1 + \frac{1}{R}\right)\mathbf{d}_3,$$
$$\mathbf{d}_3^{'} = v_2\mathbf{d}_1 - \left(v_1 + \frac{1}{R}\right)\mathbf{d}_2, \tag{5.184}$$

and

$$n_1^{'} = -v_2 n_3 + v_3 n_2, \qquad n_2^{'} = -v_3 n_1 + \left(v_1 + \frac{1}{R}\right) n_3,$$
$$n_3^{'} = -\left(v_1 + \frac{1}{R}\right) n_2 + v_2 n_1,$$

$$EI_1 v_1^{'} - EI_2 v_2 v_3 + \mathscr{D} v_2 v_3 = n_2,$$
$$EI_2 v_2^{'} - \mathscr{D}\left(v_1 + \frac{1}{R}\right) v_3 + EI_1 v_3 v_1 = -n_1,$$
$$\mathscr{D} v_3^{'} - EI_1 v_2 v_1 + EI_2\left(v_1 + \frac{1}{R}\right) v_2 = 0. \tag{5.185}$$

In these equations,

$$\mathbf{n} = n_1\mathbf{d}_1 + n_2\mathbf{d}_2 + n_3\mathbf{d}_3 = -F_0\mathbf{E}. \tag{5.186}$$

Subject to the appropriate boundary conditions, we then solve the six first-order differential equations (5.185) to determine the heteroclinic orbit connecting the fixed points $\mathscr{H}_+$,

$$v_1(-\infty) = \kappa_0 - \frac{1}{R}, \qquad v_2(-\infty) = 0, \qquad v_3(-\infty) = \tau_0,$$
$$\mathbf{n}(-\infty) = \left(\mathscr{D}\tau_0 - EI\left(\frac{\tau_0}{\kappa_0}\right)\left(\kappa_0 - \frac{1}{R}\right)\right)\left(\mathbf{d}_1(-\infty) + \tau_0\mathbf{d}_3(-\infty)\right), \tag{5.187}$$

and $\mathscr{H}_-$,

$$v_1(\infty) = \kappa_0 - \frac{1}{R}, \qquad v_2(\infty) = 0, \qquad v_3(\infty) = -\tau_0,$$
$$\mathbf{n}(\infty) = \left(-\mathscr{D}\tau_0 + EI\left(\frac{\tau_0}{\kappa_0}\right)\left(\kappa_0 - \frac{1}{R}\right)\right)\left(\mathbf{d}_1(-\infty) - \tau_0\mathbf{d}_3(-\infty)\right). \tag{5.188}$$

We have restricted attention to an isotropic rod, i.e., $I = I_1 = I_2$, in writing the above expressions for the fixed points. One can choose $\mathbf{d}_j(-\infty) = \mathbf{E}_j$. If an orbit can be found connecting these two fixed points, then this orbit will correspond to a

[43] Note that we can express each of the vector equations $\mathbf{d}_i^{'} = (\mathbf{P}(\mathbf{v} + \mathbf{v}_0)) \times \mathbf{d}_i$ in terms of their $\mathbf{E}_k$ components to form three first-order differential equations. However, in the interests of brevity, we refrain from writing out the components.

perversion connecting two helical solutions with opposite handedness. These orbits can only be found numerically, and the numerical computations are challenging.

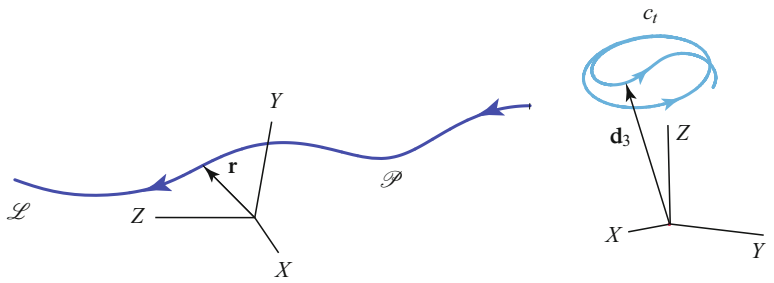

Fig. 5.24 The centerline $\mathbf{r}(\xi)$ and tangent indicatrix c_t for the approximation $\mathscr{P}$ to a perversion that is shown in Figure 5.23. The arrows indicate the direction of increasing ξ.

An example of an approximation to the heteroclinic orbit is shown in Figure 5.23(a). The procedure used to compute this solution is taken from [235].[44] The solution is supposed to connect the point $(\kappa_0, \tau_0) \approx (0.15193, -0.37837)$ to the point $(\kappa_0, \tau_0) \approx (0.15193, +0.37837)$. However, owing to the approximation procedure used, the solution asymptotes to and from points in the $\kappa - \nu_3$ parameter plane that are distinct from $\mathscr{H}_{\pm}$. The centerline $\mathbf{r}(\xi)$ and the tangent indicatrix c_t corresponding to $\mathscr{P}$ are shown in Figure 5.24. Observe that the tangent indicatrix starts off as a circle (as expected for a helical space curve[45]) but does not quite transition to a circle (for the tangent indicatrix corresponding to $\mathscr{H}_-$). The behavior of the indicatrix is also in stark contrast to the seemingly straight shape of the centerline. Indeed, the approximate perversions $\mathscr{P}$ found by McMillen and Goriely's method are surprisingly straight given that they connect two helices of opposite handedness (cf. the examples shown in [235, Figure 16]). However, examining the perversions in Figure 5.21, this also appears to be the case for tendril perversions.

5.17 Buckling of a Clamped Rod

The work we have just discussed on tendril perversion suffers from the deficiencies that it applies only to infinitely long rods and only a single perversion is found. In nature, just as in telephone cords, multiple perversions are present in rods of finite length. To address this problem, Domokos and Healey [90] examined the problem of a rod of finite length, say ℓ, that has a constant intrinsic curvature ν_{0_1}. The ends of the rod are clamped and with the appropriate terminal moments and an arbitrary

[44] We are grateful to Tyler McMillen and Alain Goriely for generously supplying the code needed to construct the solutions shown in Figures 5.23 and 5.24.

[45] See Figure 3.7 on Page 99 in Chapter 3.

force, the rod is straightened (cf. Figure 5.25). It is then of interest to examine what happens to the rod when the force is varied. As noted in [90] and also demonstrated in the experiments in Liu et al. [209] it is not unusual to find multiple perversions. In [90], it is shown explicitly how these perversions are related to bifurcations from the straight configuration. Subsequent work by Healey and his students in [159, 190] addressed the stability of some of these solutions.

While we do not explore the bifurcations, we examine the linearized buckling modes found by Domokos and Healey in [90]. Central to the analysis is the establishment of a set of equations governing supposedly small perturbations to a static deformed configuration of the rod. These developments fall into the category of "small-on-large" in the continuum mechanics literature. As we shall see, when we confine our work to the case where the rod is initially straight (i.e., $\nu_{0_1} = 0$), then we would recover a pair of familiar differential equations for the flexural perturbations and an equation for the twist. These three equations correspond to the linearized equations for Kirchhoff's rod theory and the (expected) decoupling will also appear in other linearized theories from Green et al. [131, 138] that we present in Chapter 7.

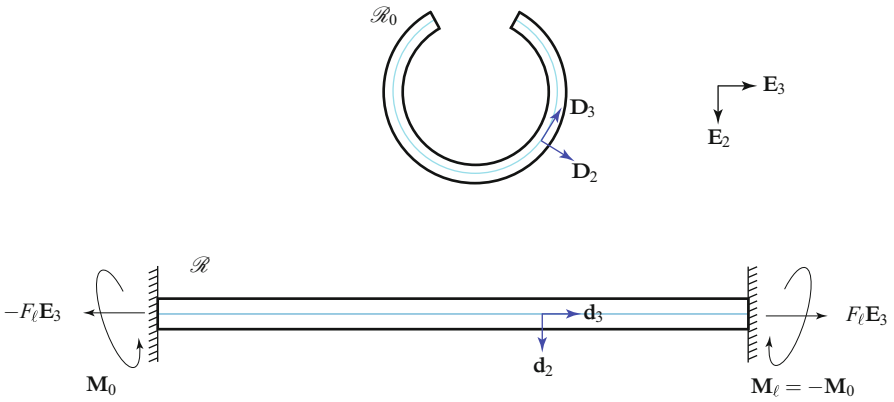

Fig. 5.25 Reference $\mathscr{R}_0$ and present $\mathscr{R}$ configurations of an intrinsically curved rod with $\nu_{0_1} = \frac{1}{R} > 0$. The centerline of the rod has a length ℓ and the rod is deformed by terminal moments into a straight line. The ends of the rod are then clamped as shown and subject to a pair of balanced terminal loadings.

We return to the intrinsically curved rod of the previous section but now assume that it is of finite length ℓ. As shown in Figure 5.25, we presume the rod is straightened by the application of terminal moments,

$$\mathbf{M}_0 = M_0\mathbf{D}_1 = EI_1\nu_{1_0}\mathbf{E}_1, \qquad \mathbf{M}_\ell = -M_0\mathbf{D}_1 = -EI_1\nu_{1_0}\mathbf{E}_1, \tag{5.189}$$

and the ends of the rod are then clamped:

$$\begin{gathered}\mathbf{r}(\xi=0)=\mathbf{0}, \qquad \mathbf{r}(\xi=\ell)\cdot\mathbf{E}_1=0, \qquad \mathbf{r}(\xi=\ell)\cdot\mathbf{E}_2=0,\\ \mathbf{d}_k(\xi=0)=\mathbf{E}_k, \qquad \mathbf{d}_k(\xi=\ell)=\mathbf{E}_k, \qquad \mathbf{n}(\xi=\ell)=F_\ell\mathbf{E}_3.\end{gathered} \tag{5.190}$$

Note that $\mathbf{P}(\xi=0)=\mathbf{P}_0^T(\xi=0)$ and $\mathbf{P}(\xi=\ell)=\mathbf{P}_0^T(\xi=0)$. We shall use a set of 1-2-3 Euler angles to parameterize $\mathbf{P}$:

$$\begin{aligned}\mathbf{P}\mathbf{P}_0 &= \sum_{i=1}^{3}\mathbf{d}_i\otimes\mathbf{E}_i=\mathbf{Q}_{\mathbf{E}}\left(\vartheta^3,\mathbf{e}_3\right)\mathbf{Q}_{\mathbf{E}}\left(\vartheta^2,\mathbf{e}_2\right)\mathbf{Q}_{\mathbf{E}}\left(\vartheta^1,\mathbf{e}_1\right)\mathbf{Q}_{\mathbf{E}}\left(\vartheta^0,\mathbf{D}_1\right),\\ \mathbf{P}_0 &= \sum_{i=1}^{3}\mathbf{D}_i\otimes\mathbf{E}_i=\cos\left(\vartheta^0\right)(\mathbf{I}-\mathbf{E}_1\otimes\mathbf{E}_1)+\sin\left(\vartheta^0\right)\operatorname{skew}(\mathbf{E}_1)+\mathbf{E}_1\otimes\mathbf{E}_1.\end{aligned} \tag{5.191}$$

Further details on these angles are presented in Exercise 5.15. It should be apparent from the reference configuration shown in Figure 5.25 that $\vartheta_0'=\nu_{0_1}=\frac{1}{R}>0$.

The straight configuration $\mathscr{R}$ shown in Figure 5.25 is defined by $\mathbf{r}=\xi\mathbf{E}_3$, $\mathbf{n}=F_\ell\mathbf{E}_3$, and $\mathbf{m}=-M_0\mathbf{E}_1$. We leave it as an exercise to show that the balance laws are satisfied. We next consider perturbations to this configuration while preserving the boundary conditions (5.190):

$$\begin{gathered}\mathbf{r}=\xi\mathbf{E}_3+\varepsilon u_1\mathbf{E}_1+\varepsilon u_2\mathbf{E}_2+\varepsilon u_3\mathbf{E}_3,\\ \vartheta^1=-\vartheta^0+\varepsilon\bar{\theta}_1, \qquad \vartheta^2=0+\varepsilon\bar{\theta}_2, \qquad \vartheta^3=0+\varepsilon\bar{\theta}_3,\\ n_1=0+\varepsilon\bar{n}_1, \qquad n_2=0+\varepsilon\bar{n}_2, \qquad n_3=F_\ell+\varepsilon\bar{n}_3,\end{gathered} \tag{5.192}$$

where ε is assumed to be small. Evaluating $\boldsymbol{\nu}$ and $\mathbf{P}$ with the help of Eqns. (5.274) and (5.278), we find that

$$\begin{gathered}\nu_1=-\nu_{0_1}+\varepsilon\bar{\theta}_1', \qquad \nu_2=\varepsilon\bar{\theta}_2', \qquad \nu_3=\varepsilon\bar{\theta}_3',\\ \mathbf{d}_1=\mathbf{E}_1+\varepsilon\bar{\theta}_3\mathbf{E}_2-\varepsilon\bar{\theta}_2\mathbf{E}_3, \qquad \mathbf{d}_2=\mathbf{E}_2-\varepsilon\bar{\theta}_3\mathbf{E}_1+\varepsilon\bar{\theta}_1\mathbf{E}_3,\\ \mathbf{d}_3=\mathbf{E}_3+\varepsilon\bar{\theta}_2\mathbf{E}_1-\varepsilon\bar{\theta}_1\mathbf{E}_2=\left(1+\varepsilon u_3'\right)\mathbf{E}_3+\varepsilon u_1'\mathbf{E}_1+\varepsilon u_2'\mathbf{E}_2.\end{gathered} \tag{5.193}$$

While $\|\mathbf{d}_3\|=1$, this inextensibility constraint is only approximately satisfied to $\mathscr{O}(\varepsilon)$. Substituting the ansatzen (5.193) into the balance law (5.185) and ignoring terms of $\mathscr{O}\left(\varepsilon^2\right)$ we find the following differential equations:

$$\left.\begin{aligned}\bar{\theta}_1&=-u_2',\\ EI_1\bar{\theta}_1''&=F_\ell\bar{\theta}_1,\end{aligned}\right\}\longleftarrow\text{flexural modes}$$

$$\left.\begin{aligned}\bar{\theta}_2&=u_1',\\ EI_2\bar{\theta}_2''-M_0\bar{\theta}_3'&=F_\ell\bar{\theta}_2,\\ \mathscr{D}\bar{\theta}_3''+M_0\bar{\theta}_2'&=0.\end{aligned}\right\}\longleftarrow\text{flexural-torsional modes} \tag{5.194}$$

The boundary conditions associated with these equations are

$$u_\alpha(\xi=0)=0, \qquad u_\alpha(\xi=\ell)=0, \qquad \bar{\theta}_\alpha(\xi=0)=0, \qquad \bar{\theta}_\alpha(\xi=\ell)=0, \tag{5.195}$$

where $\alpha = 1,2$. Observe that the flexural (or bending) modes described by u_2 are uncoupled from the flexural-torsional modes $u_1 - \bar{\theta}_3$.

By differentiating Eqn. $(5.194)_2$ once and then using Eqn. $(5.194)_1$, we arrive at a canonical equation for u_2. Similarly, by differentiating Eqn. $(5.194)_4$ once, eliminating $\bar{\theta}_3$ using Eqn. $(5.194)_5$, and then using Eqn. $(5.194)_3$, we arrive at an equation for u_1. The respective equations and their associated boundary conditions are

$$\begin{aligned} u_2'''' - \frac{F_\ell}{EI_1} u_2'' = 0, \quad u_2(\xi = 0, \ell) = 0, \quad u_2'(\xi = 0, \ell) = 0, \\ u_1'''' + \left(\frac{M_0^2}{\mathscr{D} EI_2} - \frac{F_\ell}{EI_2} \right) u_1'' = 0, \quad u_1(\xi = 0, \ell) = 0, \quad u_1'(\xi = 0, \ell) = 0. \end{aligned} \tag{5.196}$$

The general solution $u(\xi)$ to this pair of differential equations, associated characteristic equation (5.200) and modes (5.201) can be found in classic texts on elastic stability (see [345, Section 2.2]):

$$u = A_1 \cos(\upsilon\xi) + A_2 \sin(\upsilon\xi) + A_3\xi + A_4, \tag{5.197}$$

where $\upsilon^2 = -\frac{F_\ell}{EI_1}$ or $\left(\frac{M_0^2}{\mathscr{D} EI_2} - \frac{F_\ell}{EI_2} \right)$, and $A_{1,2,3,4}$ are determined by the boundary and initial conditions.

The coupled torsional-flexural modes can be solely attributed to the nonvanishing intrinsic curvature. Indeed, if we set $\nu_{0_1} = 0$, then we find three sets of equations for the pair of flexures u_1 and u_2 and the torsion $\bar{\theta}_3$ about a straight undeformed equilibrium configuration:

$$EI_1 u_2'''' = F_\ell u_2'', \qquad EI_2 u_1'''' = F_\ell u_1'', \qquad \mathscr{D}\bar{\theta}_3'' = 0. \tag{5.198}$$

This decoupling is also a consequence of the choice of constitutive relations and the geometry of the undeformed rod. Later, in Chapter 7, we shall find an instance of a similar decoupling for extensional, torsional, and flexural deformations in a more general rod theory. In all of these instances, if appropriate geometric and constitutive symmetries are imposed, then the linearized equations for flexure reduce to those for a strut that were first proposed by Euler [106] and occupy a prominent place in texts on elastic stability.[46]

Imposing the four boundary conditions on $u_{1,2}$ and their derivatives produces the following set of linear equations for $A_{1,2,3,4}$:

[46] A translation of Euler's comments on stability can be found in [254, Pages 102–103]. Timoshenko and Gere [345, Chapter 2] contains a comprehensive discussion of the buckling of a strut and the dependency of the critical loads on the boundary conditions. The text by Ziegler [375] is also highly recommended.

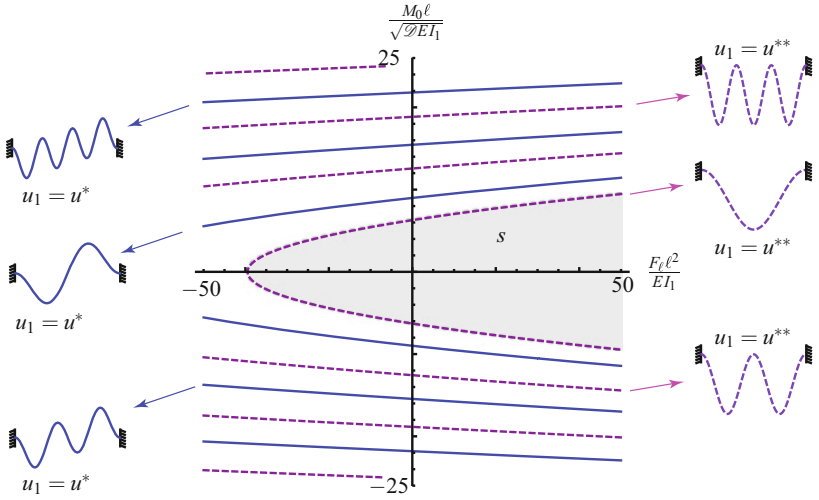

Fig. 5.26 Solutions to the characteristic equations $\tan\left(\frac{\upsilon\ell}{2}\right) = \frac{\upsilon\ell}{2}$ (dashed lines) and $\sin\left(\frac{\upsilon\ell}{2}\right) = 0$ (solid lines) in the $\frac{F_\ell\ell^2}{EI_1}$-$\frac{M_0\ell}{\sqrt{\mathscr{D}EI_1}}$ parameter plane. The associated modes shapes, from Eqns. (5.201) and (5.202), for the flexural components $u_1(\xi)$ (and the readily inferred torsional components $\bar{\theta}_3(\xi) = -\frac{M_0}{\mathscr{D}}u_1(\xi)$) of the associated coupled flexural-torsional modes are also shown.

$$\begin{bmatrix} 1 & 0 & 0 & 1 \\ \cos(\upsilon\ell) & \sin(\upsilon\ell) & \ell & 1 \\ 0 & \upsilon & 1 & 0 \\ -\upsilon\sin(\upsilon\ell) & \upsilon\cos(\upsilon\ell) & 1 & 0 \end{bmatrix} \begin{bmatrix} A_1 \\ A_2 \\ A_3 \\ A_4 \end{bmatrix} = \begin{bmatrix} 0 \\ 0 \\ 0 \\ 0 \end{bmatrix}. \tag{5.199}$$

For nontrivial solutions, the determinant of the matrix in this equation must be zero. The resulting equation, which will be solved for $\upsilon\ell$, is known as the characteristic equation:

$$\sin\left(\frac{\upsilon\ell}{2}\right)\left(\cos\left(\frac{\upsilon\ell}{2}\right) - \frac{2}{\upsilon\ell}\sin\left(\frac{\upsilon\ell}{2}\right)\right) = 0. \tag{5.200}$$

Observe that this equation can be split into a pair of equations for $\upsilon\ell$: $\sin(\upsilon\ell/2) = 0$ and $\tan(\upsilon\ell/2) = \upsilon\ell/2$. In addition, we can solve for $A_{2,3,4}$ in terms of A_1 to find that

$$u(\xi) = \begin{cases} u^*(\xi) = A_1\left(\cos(\upsilon\xi) - 1 + \cot\left(\frac{\upsilon\ell}{2}\right)(\upsilon\xi - \sin(\upsilon\xi))\right) \text{ when} \\ \qquad\qquad \tan\left(\frac{\upsilon\ell}{2}\right) = \frac{\upsilon\ell}{2} \neq 0, \\ \\ u^{**}(\xi) = A_1(\cos(\upsilon\xi) - 1) \text{ when } \sin\left(\frac{\upsilon\ell}{2}\right) = 0. \end{cases} \tag{5.201}$$

For the case $(5.194)_2$ involving coupled flexure and torsion, we find the surprisingly simple results

$$\bar{\theta}_3(\xi) = \begin{cases} \bar{\theta}_3^*(\xi) = -\frac{M_0}{\mathscr{D}} u^*(\xi) = -\nu_{0_1} u^*(\xi) \text{ when } \tan\left(\frac{\upsilon\ell}{2}\right) = \frac{\upsilon\ell}{2} \neq 0, \\ \bar{\theta}_3^{**}(\xi) = -\frac{M_0}{\mathscr{D}} u^{**}(\xi) = -\nu_{0_1} u^*(\xi) \text{ when } \sin\left(\frac{\upsilon\ell}{2}\right) = 0. \end{cases} \tag{5.202}$$

For the rod shown in Figure 5.25, $\nu_{0_1} = +1/R$ and so we have $\bar{\theta}_3 = -u_1/R$. The results (5.201) enable us to return to the equations $(5.196)_1$ for the flexural perturbations in the $\mathbf{E}_2$ direction and find the buckling loads F_ℓ for the rods. The results are similar to those we presented earlier in Chapter 4 (see Section 4.9.2 in particular) and are not mentioned any further.

For the coupled flexural-torsion modes, the characteristic equation (5.200) provides two sets of values for $\upsilon\ell$ (one of which is $\upsilon\ell = 2\pi, 4\pi, \ldots$) and two sets of modes (cf. Eqns. (5.201) and (5.202)). Referring to Figure 5.26, we solve the equations $\tan(\upsilon\ell/2) = \upsilon\ell/2$ and $\sin(\upsilon\ell/2) = 0$ for the corresponding values of M_0 and F_ℓ. Based on this linearized analysis, buckling of the clamped rod is said to have occurred when the pairing $M_0 - F_\ell$ are such that they no longer lie in the shaded region labeled s in this figure. When $M_0 = 0$, the associated critical value of the compressive load $F_\ell = -4\pi^2 EI_1/\ell^2$ is well known.[47] When the rod has an intrinsic curvature (i.e., $M_0 \neq 0$), then it is easy to see from Figure 5.26 an observation made by Domokos and Healey in [90]: the rod can buckle even when $F_\ell > 0$ (i.e., the rod is in tension) if $\nu_{0_1} = \pm 1/R$ is sufficiently large.

5.18 Spiral Springs and a Stiffness Matrix

A natural extension to the analysis just presented would be to consider a rod whose centerline in its undeformed state has the shape of a circular helix. Such an analysis is needed to determine the behavior of a helical spring under external loading. The simplest model for such a spring is to consider a thin circular inextensible rod of length ℓ whose centerline forms a circular helix of radius R and pitch angle ς (cf. Figure 5.27):

$$\mathbf{R}(\xi) = R\mathbf{e}_{\theta_0} + R\theta_0(\xi)\tan(\varsigma)\mathbf{E}_3, \tag{5.203}$$

where $\mathbf{e}_{\theta_0} = \cos(\theta_0(\xi))\mathbf{E}_1 + \sin(\theta_0(\xi))\mathbf{E}_2$. This configuration is chosen as the reference configuration of the rod and we assume that $\theta_0' > 0$. The rod is loaded at its ends by a force and moment combination that is known as a wrench:

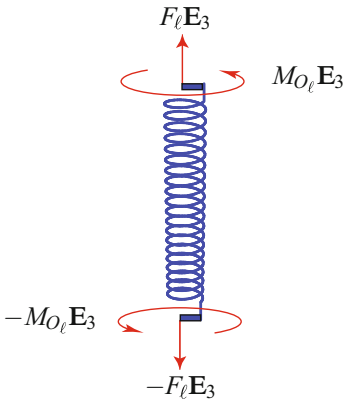

Fig. 5.27 A helical spring loaded by a terminal force $\mathbf{F}_\ell = F_\ell \mathbf{E}_3$ and a terminal moment $\mathbf{M}_{O_\ell} = M_{O_\ell}\mathbf{E}_3 = \mathbf{M}_\ell + \mathbf{r}(\ell) \times \mathbf{F}_\ell$.

[47] See [213, Section 264] or [345, Chapter 2].

$$\mathbf{n}\left(\ell^{-}\right)=F_{\ell}\mathbf{E}_{3},\qquad \mathbf{m}\left(\ell^{-}\right)=M_{O_{\ell}}\mathbf{E}_{3}-\mathbf{r}\left(\ell^{-}\right)\times F_{\ell}\mathbf{E}_{3}. \tag{5.204}$$

For such combinations, the force $\mathbf{F}_{\ell}$ and moment $\mathbf{M}_{O_{\ell}}$ are parallel. As shown in Figure 5.27, rigid attachments can be added to the ends of the spring so that an applied force and an applied moment which act in the same direction can be applied to the spring. Following the classical theory of spiral (helical) springs that is discussed in Love [213, Section 271], we seek to determine expressions for the change in height of the spring and the change in a cylindrical polar angle. These changes determine the gross extensional and torsional stiffnesses of the spring - the microscopic stiffnesses for these effects would be infinity and $\mathscr{D}$.

The model we discuss here dates to the 19th century. However, as has been recently pointed out by Đuričković et al. [89] it serves as a very useful model for studying the twist-stretch coupling observed in experiments on DNA strands that we shall discuss in Section 6.5 of Chapter 6.

5.18.1 The Reference Configuration

In the reference configuration $\mathscr{R}_0$ the position vector of a point on the centerline of the rod is assumed to have a representation (5.203). We choose the directors $\mathbf{D}_1$ and $\mathbf{D}_2$ so the rod is untwisted in its reference state. The rotation tensor $\mathbf{P}_0$ can be decomposed into the product of two simple rotations[48]:

$$\mathbf{P}_0=\mathbf{Q}_{\mathbf{E}}\left(\varphi^2,\cos\left(\varphi^1\right)\mathbf{E}_1+\sin\left(\varphi^1\right)\mathbf{E}_2\right)\mathbf{Q}_{\mathbf{E}}\left(\varphi^1,\mathbf{E}_3\right), \tag{5.205}$$

where

$$\theta_0\left(\xi\right)=\varphi^1\left(\xi\right)-\pi,\qquad \varsigma=\frac{\pi}{2}-\varphi^2. \tag{5.206}$$

A quick calculation shows that the intrinsic strains for the rod are

$$\boldsymbol{\nu}_0=\nu_{0_2}\mathbf{D}_2+\nu_{0_3}\mathbf{D}_3=\frac{\partial\varphi^1}{\partial\xi}\cos\left(\varphi^2\right)\mathbf{D}_3+\frac{\partial\varphi^1}{\partial\xi}\sin\left(\varphi^2\right)\mathbf{D}_2. \tag{5.207}$$

Using Eqn. (1.33), it can be shown that the strains are related to the curvature κ_0 and torsion τ_0 of the helical space curve defined by $\mathbf{R}(\xi)$:

$$\kappa_0=\frac{\cos^2\left(\varsigma\right)}{R}=\frac{\partial\varphi^1}{\partial\xi}\sin\left(\varphi^2\right),\qquad \tau_0=\frac{\cos\left(\varsigma\right)\sin\left(\varsigma\right)}{R}=\frac{\partial\varphi^1}{\partial\xi}\cos\left(\varphi^2\right). \tag{5.208}$$

The following identities will be particularly useful in the sequel:

$$\tau_0^2+\kappa_0^2=\frac{\kappa_0}{R},\qquad \tan\left(\varsigma\right)\kappa_0=\tau_0. \tag{5.209}$$

[48] Our comments here are intimately related to the discussion on $\mathbf{Q}_{\mathrm{SF}}$ and $\boldsymbol{\omega}_{\mathrm{SF}}$ in Section 5.10.

For the helical space curve defined by $\mathbf{R}(\xi)$, the corresponding tangent vector $\mathbf{e}_{t_0}$, normal vector $\mathbf{e}_{n_0}$, and binormal vector $\mathbf{e}_{b_0}$ are

$$\mathbf{e}_{t_0} = \mathbf{D}_3, \qquad \mathbf{e}_{n_0} = \mathbf{D}_1, \qquad \mathbf{e}_{b_0} = \mathbf{D}_2. \tag{5.210}$$

Helpful expressions for the Frenet triad basis vectors can be found in Eqn. (1.31).

5.18.2 The Balance Laws

We assume that the cross sections of the rod are circular, $I_1 = I_2 = I$, and that the strain energy function of the rod is

$$2\rho_0\psi = EI\nu_1^2 + EI\nu_2^2 + \mathscr{D}\nu_3^2. \tag{5.211}$$

The balance laws for the rod are $\mathbf{n}' = \mathbf{0}$ and $\mathbf{m}' + \mathbf{r}' \times \mathbf{n} = \mathbf{0}$. With the help of the terminal loading conditions,

$$\mathbf{n}\left(\ell^-\right) = F_\ell \mathbf{E}_3, \qquad \mathbf{m}\left(\ell^-\right) = M_{O_\ell}\mathbf{E}_3 - \mathbf{r}\left(\ell^-\right) \times F_\ell \mathbf{E}_3, \tag{5.212}$$

we find that the contact force and a moment are parallel to $\mathbf{E}_3$ throughout the length of the spring:

$$\mathbf{n}(\xi) = F_\ell \mathbf{E}_3, \qquad \mathbf{m}(\xi) + \mathbf{r}(\xi) \times \mathbf{n}(\xi) = M_{O_\ell}\mathbf{E}_3. \tag{5.213}$$

Projecting the balance of angular momentum onto the basis vectors $\{\mathbf{d}_1, \mathbf{d}_2, \mathbf{d}_3\}$ and using the constitutive relations for $\mathbf{m}$, the following differential equations can be established[49]:

$$\begin{aligned} EI\nu_1' - EI\nu_2\left(\nu_3 + \nu_{0_3}\right) + \mathscr{D}\left(\nu_2 + \nu_{0_2}\right)\nu_3 &= \mathbf{d}_2 \cdot F_\ell \mathbf{E}_3, \\ EI\nu_2' - \mathscr{D}\nu_1\nu_3 + EI\left(\nu_3 + \nu_{0_3}\right)\nu_1 &= -\mathbf{d}_1 \cdot F_\ell \mathbf{E}_3, \\ \mathscr{D}\nu_3' EI\nu_{0_2}\nu_1 &= 0. \end{aligned} \tag{5.214}$$

In writing this form of the equations we have exploited the symmetry $EI_1 = EI_2$ and the fact that $\nu_{0_1} = 0$.

We seek solutions to Eqn. (5.214) where the centerline of the deformed rod forms a helical space curve:

$$\mathbf{r}(\xi) = r\left(\cos(\theta(\xi))\mathbf{E}_1 + \sin(\theta(\xi))\mathbf{E}_2\right) + r\theta(\xi)\tan(\sigma)\mathbf{E}_3, \tag{5.215}$$

with $\theta' > 0$. The directors lie in the osculating plane,

$$\mathbf{e}_t = \mathbf{d}_3, \qquad \mathbf{e}_n = \mathbf{d}_1, \qquad \mathbf{e}_b = \mathbf{d}_2, \tag{5.216}$$

[49] Further details on the procedure to establish equations of this form are discussed in Exercise 5.14.

and the strains v_k are related to the curvature, $\kappa = \frac{\cos^2(\sigma)}{r}$, and torsion, $\tau = \frac{\cos(\sigma)\sin(\sigma)}{r}$, of the curve formed by the centerline in $\mathscr{R}$ in the following manner:

$$v_1 = 0, \qquad v_2 = \kappa - v_{0_2} = \kappa - \kappa_0, \qquad v_3 = \tau - v_{0_3} = \tau - \tau_0. \tag{5.217}$$

For the sought-after solution,

$$\mathbf{PP}_0 = \mathbf{Q}_{\mathbf{E}} \left(\frac{\pi}{2} - \sigma, \cos(\theta + \pi)\, \mathbf{E}_1 + \sin(\theta + \pi)\, \mathbf{E}_2 \right) \mathbf{Q}_{\mathbf{E}}(\theta + \pi, \mathbf{E}_3). \tag{5.218}$$

This tensor, just like its counterpart for the reference configuration, is an example of the tensor $\mathbf{Q}_{\mathrm{SF}}$.

Setting $v_1' = 0$, $v_2' = 0$, and $v_3' = 0$ in Eqn. (5.214), we see that this balance law is satisfied provided

$$\begin{gathered} \mathbf{d}_1 \cdot F_\ell \mathbf{E}_3 = 0, \qquad v_1 = 0, \\ EI_2 v_2 \left(v_3 + v_{0_3} \right) - \mathscr{D} \left(v_2 + v_{0_2} \right) v_3 + \mathbf{e}_b \cdot F_\ell \mathbf{E}_3 = 0. \end{gathered} \tag{5.219}$$

The first two of these equations are trivially satisfied and the third simplifies to

$$\cos(\sigma) F_\ell = \mathscr{D} \kappa (\tau - \tau_0) - EI \tau (\kappa - \kappa_0). \tag{5.220}$$

The contact moment in the rod is

$$\mathbf{m} = EI (\kappa - \kappa_0) \mathbf{d}_2 + \mathscr{D} (\tau - \tau_0) \mathbf{d}_3. \tag{5.221}$$

Using the boundary condition $(5.212)_2$ and Eqn. (1.31), we find that

$$M_{O_\ell} = EI (\kappa - \kappa_0) \cos(\sigma) + \mathscr{D} (\tau - \tau_0) \sin(\sigma). \tag{5.222}$$

The relations (5.220) and (5.222) provide equations to determine the moment and force needed to generate a given helical centerline and a twistless rod.

5.18.3 A Stiffness Matrix

Consider applying the wrench $\left(F_\ell \mathbf{E}_3, M_{O_\ell} \mathbf{E}_3 \right)$ to the rod in its reference state. The deformation of the rod as a result of this system deforms the rod's centerline into a helix and the twist of the rod remains 0. Changes in the scalars F_ℓ and M_{O_ℓ} alter the radius r and pitch angle σ of the helix and the position vector $\mathbf{r}(\xi = \ell)$:

$$\begin{aligned} \Delta\theta &= \theta(\xi = \ell) - \theta_0(\xi = \ell) = \ell \left(\frac{\cos(\sigma)}{r} - \frac{\cos(\varsigma)}{R} \right), \\ \Delta z &= z(\xi = \ell) - z_0(\xi = \ell) = \ell (\sin(\sigma) - \sin(\varsigma)). \end{aligned} \tag{5.223}$$

We define the following perturbations:

$$\Delta\sigma = \sigma - \varsigma, \qquad \Delta r = r - R, \qquad \Delta\kappa = \kappa - \kappa_0, \qquad \Delta\tau = \tau - \tau_0, \tag{5.224}$$

and define the concomitant changes to F_ℓ and M_{O_ℓ}:

$$F_\ell = 0 + \Delta F_\ell, \qquad M_{O_\ell} = 0 + \Delta M_{O_\ell}. \tag{5.225}$$

By considering Taylor series expansions of κ and τ and assuming that all quantities of the form $\Delta\kappa, \Delta r, \ldots$ are small, it should not be difficult to verify that[50]

$$\begin{aligned}
\begin{bmatrix} \Delta\kappa \\ \Delta\tau \end{bmatrix} &= \begin{bmatrix} -\kappa_0 & -2\tau_0 \\ -\tau_0 & 2\kappa_0 - \frac{1}{R} \end{bmatrix} \begin{bmatrix} \frac{\Delta r}{R} \\ \Delta\sigma \end{bmatrix}, \\
\begin{bmatrix} \frac{\Delta z}{R} \\ \Delta\theta \end{bmatrix} &= \frac{\ell}{R} \begin{bmatrix} 0 & \cos(\varsigma) \\ -\cos(\varsigma) & -\sin(\varsigma) \end{bmatrix} \begin{bmatrix} \frac{\Delta r}{R} \\ \Delta\sigma \end{bmatrix}.
\end{aligned} \tag{5.226}$$

Combining these two results, one finds that

$$\begin{bmatrix} \Delta\kappa \\ \Delta\tau \end{bmatrix} = \frac{R\sec(\varsigma)}{\ell} \begin{bmatrix} -\tau_0 & \kappa_0 \\ \kappa_0 & \tau_0 \end{bmatrix} \begin{bmatrix} \frac{\Delta z}{R} \\ \Delta\theta \end{bmatrix}. \tag{5.227}$$

These expressions can be used to quantify changes to the end point of any helical space curve as the torsion and curvature are varied.

Expanding the expressions (5.220) and (5.222) for F_ℓ and M_{O_ℓ} about their equilibrium values of 0 as functions of changing κ, τ, and σ, using Eqn. (5.227) and performing some minor rearranging, we find that the changes to these quantities can be related to the geometric changes at the end $\xi = \ell$ by a symmetric stiffness matrix:

$$\begin{bmatrix} \frac{\Delta F_\ell R^2}{EI} \\ \frac{\Delta M_{O_\ell} R}{EI} \end{bmatrix} = \begin{bmatrix} k_{11} & k_{12} \\ k_{12} & k_{22} \end{bmatrix} \begin{bmatrix} \frac{\Delta z}{R} \\ \Delta\theta \end{bmatrix}. \tag{5.228}$$

The components $k_{\alpha\beta}$ of the stiffness matrix have the compact representations

$$\begin{aligned}
\begin{bmatrix} k_{11} & k_{12} \\ k_{12} & k_{22} \end{bmatrix} &= \frac{R^2}{\ell} \begin{bmatrix} \frac{\mathscr{D}}{EI}\kappa_0 + \frac{\tau_0^2}{\kappa_0} & \left(\frac{\mathscr{D}}{EI} - 1\right)\tau_0 \\ \left(\frac{\mathscr{D}}{EI} - 1\right)\tau_0 & \frac{\mathscr{D}}{EI}\frac{\tau_0^2}{\kappa_0} + \kappa_0 \end{bmatrix} \\
&= \frac{R^2}{\ell} \begin{bmatrix} -\frac{\tau_0}{\kappa_0} & \frac{\mathscr{D}}{EI} \\ 1 & \frac{\mathscr{D}}{EI}\frac{\tau_0}{\kappa_0} \end{bmatrix} \begin{bmatrix} -\tau_0 & \kappa_0 \\ \kappa_0 & \tau_0 \end{bmatrix}.
\end{aligned} \tag{5.229}$$

As discussed in Love [213, Section 271], relations of the form (5.228) are classic and can be found in Kelvin and Tait [180, Section 607].[51] We emphasize that the stiffness matrix pertains to small perturbations from the trivial equilibrium

[50] The identities (5.209) are particularly helpful in establishing several of the results which follow and enabling comparisons with [89, Eqns. (9) and (10)].

[51] The representation (5.228) is a dimensionless form of [213, Eqn. (42), Section 271].

configuration. If perturbations from another helical configuration are of interest, then the components of this matrix are expected to change and it is a straightforward exercise to establish the stiffness matrix in this case.

Observe that the components of the stiffness matrix are combinations of the geometric (κ_0, τ_0, I, R, ℓ) and material (E and ν) properties of the rod. The stiffness matrix is symmetric, has a determinant $\frac{\mathscr{D}R^2}{EI\ell^2}$, and is positive definite. Indeed, it is possible to form an energy function E_{spring} consisting of a quadratic form composed of $\Delta\theta$, $\frac{\Delta z}{R}$ and the following stiffness matrix:

$$E_{\text{spring}} = \frac{1}{2}k_{11}\left(\frac{\Delta z}{R}\right)^2 + k_{12}\frac{\Delta z}{R}\Delta\theta + \frac{1}{2}k_{22}\Delta\theta^2. \tag{5.230}$$

Functions of this type would appear in rigid body dynamics problems when the spring is treated as a discrete element. As astutely discussed by Đuričković et al. [89] such a function provides a model to interpret recent works, such as [120, 177, 207, 227], on the twist-stretch coupling in the mechanical testing of DNA strands. Particular focus is placed on a term that is equivalent to k_{12} in these works. Remarkably, Gore et al. [120] have been able to quantify this term for strands of B-DNA and estimate this quantity in the range of -90×10^{-21} Nm.

We can invert the linear relations (5.228) to find the useful results

$$\begin{aligned}\begin{bmatrix}\frac{\Delta z}{R}\\ \Delta\theta\end{bmatrix} &= \frac{EI\ell}{\mathscr{D}}\begin{bmatrix}\frac{\mathscr{D}}{EI}\frac{\tau_0^2}{\kappa_0}+\kappa_0 & -\left(\frac{\mathscr{D}}{EI}-1\right)\tau_0\\ -\left(\frac{\mathscr{D}}{EI}-1\right)\tau_0 & \frac{\mathscr{D}}{EI}\kappa_0+\frac{\tau_0^2}{\kappa_0}\end{bmatrix}\begin{bmatrix}\frac{\Delta F_\ell R^2}{EI}\\ \frac{\Delta M_{O_\ell}R}{EI}\end{bmatrix}\\ &= 2\pi\begin{bmatrix}\frac{\sin(\varsigma)}{\cos^2(\varsigma)}+\frac{EI}{\mathscr{D}}\cos(\varsigma) & \left(\frac{EI}{\mathscr{D}}-1\right)\sin(\varsigma)\\ \left(\frac{EI}{\mathscr{D}}-1\right)\sin(\varsigma) & \cos(\varsigma)+\frac{EI}{\mathscr{D}}\frac{\sin(\varsigma)}{\cos^2(\varsigma)}\end{bmatrix}\begin{bmatrix}\frac{\Delta F_\ell R^2}{EI}\\ \frac{\Delta M_{O_\ell}R}{EI}\end{bmatrix}.\end{aligned} \tag{5.231}$$

For rods with circular cross sections, $\frac{EI}{\mathscr{D}} = 1+\nu$, where ν is Poisson's ratio. Thus, $EI > \mathscr{D}$. Consequently, we can attribute twist-stretch coupling to the helical nature of the spring: if the spring were circular, $\varsigma = 0$ and this coupling would be absent. It is easy to see from Eqn. (5.231) that the application of a positive increment ΔF_ℓ to the force acting on the end will result in a positive Δz and, assuming $\tau_0 > 0$, a positive $\Delta\theta$. Thus the spring will appear to overwind (as opposed to underwind for $\Delta\theta < 0$).[52] In addition, we can also conclude with the help of the relations $(5.228)_2$ that the radius of the helix will shrink ($\Delta r < 0$). This shrinkage is in compliance with the fact that the centerline of the helical rod is inextensible (and so $\ell = 2\pi r\sec(\sigma) = 2\pi R\sec(\varsigma)$).

Our discussion has been limited to the case considered in the classic work of Kelvin and Tait. Recently, Đuričković et al. [89] have extended this analysis to consider helical springs where $EI_1 \neq EI_2$ and linearized stiffness matrices for more general cases than the one we have presented.

[52] The terminology we use here is from the literature on DNA testing (cf. Đuričković et al. [89]).

5.19 Closing Remarks

We have only the space and opportunity to touch upon a small fraction of the work that has been published on the terminally loaded rod where $EI_1 = EI_2$. To do full justice to these works would fill hundreds of pages. In addition, many of the problems considered in the earlier chapters have nonplanar counterparts where bending and torsion are significant which remain to be explored. If this chapter has both motivated the reader to further explore some of the papers mentioned (and the works they inspired) and provided sufficient background to read and appreciate these works, then it will have achieved one of its primary purposes.

5.20 Exercises

Exercise 5.1: Recall the expression (5.54) for the kinetic energy T of the rod. Using the symmetries $y^{\alpha\beta} = y^{\beta\alpha}$, show that

$$\dot{T} = \dot{\mathbf{r}} \cdot \dot{\mathbf{G}} + \dot{\mathbf{d}}_1 \cdot \dot{\mathbf{L}}^1 + \dot{\mathbf{d}}_2 \cdot \dot{\mathbf{L}}^2. \tag{5.232}$$

In a similar fashion, starting from (5.56), show that

$$\dot{\mathbf{h}}_O = \mathbf{r} \times \dot{\mathbf{G}} + \mathbf{d}_1 \times \dot{\mathbf{L}}^1 + \mathbf{d}_2 \times \dot{\mathbf{L}}^2. \tag{5.233}$$

Exercise 5.2: Show that the local form of (5.77) reduces to $(5.80)_5$ with the help of (5.233).

Exercise 5.3: Show that the local form of (5.79) reduces to $(5.80)_7$ with the help of (5.232).

Exercise 5.4: Consider the jump condition associated with the balance of material momentum for a rod. Show that this jump condition has the representation

$$\{\mathbf{n}\} \cdot \left[\left[\mathbf{r}'\right]\right]_\gamma + \{\mathbf{m}\}_\gamma \cdot [\![\mathbf{P}(\mathbf{v} + \mathbf{v}_0)]\!]_\gamma - [\![\rho_0 \psi]\!]_\gamma = \mathbf{M}_\gamma \cdot \{\mathbf{P}(\mathbf{v} + \mathbf{v}_0)\}_\gamma + \mathbf{F}_\gamma \cdot \{\mathbf{r}'\}_\gamma + \mathsf{B}_\gamma. \tag{5.234}$$

Exercise 5.5: Consider the local form of the balance of material momentum for a rod where $\mathbf{v}_0 = \mathbf{0}$. Show that this law is identically satisfied if $\mathsf{b} = \mathsf{b}_\mathrm{p}$ where

$$\mathsf{b}_\mathrm{p} = -\rho_0 \mathbf{f} \cdot \mathbf{r}' - \mathbf{m}_a \cdot (\mathbf{P}\mathbf{v}) - \left(\frac{\partial (\rho_0 \psi)}{\partial \xi} - \frac{\partial T}{\partial \xi} \right)_{\text{exp.}}. \tag{5.235}$$

This result is used to help demonstrate when C is conserved in static boundary-value problems.

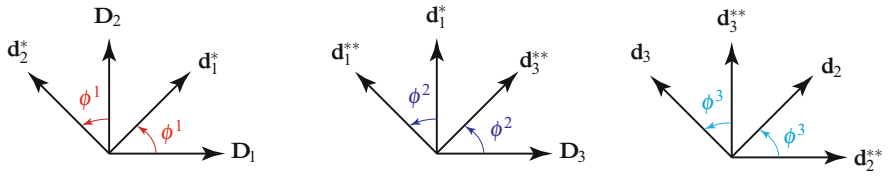

Fig. 5.28 Schematic of the three rotations used to define the 3-2-1 set of Euler angles (cf. Eqn. (5.236)).

Exercise 5.6: Consider the case where a set of 3-2-1 Euler angles are used to parameterize the rotation tensor $\mathbf{P} = \sum_{i=1}^{3} \mathbf{d}_i \otimes \mathbf{D}_i$:

$$\mathbf{P} = \mathbf{Q}_{\mathbf{E}}\left(\phi^3, \mathbf{e}_3\right) \mathbf{Q}_{\mathbf{E}}\left(\phi^2, \mathbf{e}_2\right) \mathbf{Q}_{\mathbf{E}}\left(\phi^1, \mathbf{e}_1\right). \tag{5.236}$$

(a) With the help of the intermediate results shown in Figure 5.28, show that the Euler basis vectors for the 3-2-1 set of Euler angles have the representations

$$\begin{aligned}
\mathbf{e}_1 &= \mathbf{D}_3 \\
&= \cos\left(\phi^2\right)\cos\left(\phi^3\right)\mathbf{d}_3 + \cos\left(\phi^2\right)\sin\left(\phi^3\right)\mathbf{d}_2 - \sin\left(\phi^2\right)\mathbf{d}_1, \\
\mathbf{e}_2 &= \cos\left(\phi^1\right)\mathbf{D}_2 - \sin\left(\phi^1\right)\mathbf{D}_1 \\
&= \cos\left(\phi^3\right)\mathbf{d}_2 - \sin\left(\phi^3\right)\mathbf{d}_3, \\
\mathbf{e}_3 &= \cos\left(\phi^2\right)\cos\left(\phi^1\right)\mathbf{D}_1 + \cos\left(\phi^2\right)\sin\left(\phi^1\right)\mathbf{D}_2 - \sin\left(\phi^2\right)\mathbf{D}_3 \\
&= \mathbf{d}_1.
\end{aligned} \tag{5.237}$$

(b) Why is this set of Euler angles subject to the restrictions $\phi^1 \in [0, 2\pi)$, $\phi^2 \in (-\pi/2, \pi/2)$, and $\phi^3 \in [0, 2\pi)$?

(c) Show that the components $P_{ik} = (\mathbf{P}\mathbf{D}_k) \cdot \mathbf{D}_i$ of $\mathbf{P}$ have the representations

$$\begin{bmatrix} P_{11} & P_{12} & P_{13} \\ P_{21} & P_{22} & P_{23} \\ P_{31} & P_{32} & P_{33} \end{bmatrix} = \begin{bmatrix} c_2c_1 & -c_3s_1 - c_1s_2s_3 & -c_1c_3s_2 + s_1s_3 \\ c_2s_1 & c_3c_1 - s_1s_2s_3 & -c_3s_1s_2 - c_1s_3 \\ s_2 & c_2s_3 & c_2c_3 \end{bmatrix}. \tag{5.238}$$

In writing expressions for the components P_{ik}, we have employed the abbreviations $c_k = \cos\left(\phi^k\right)$ and $s_k = \sin\left(\phi^k\right)$.

(d) Show that the dual Euler basis vectors for the 3-2-1 set of Euler angles have the representations

$$\begin{bmatrix} \mathbf{e}^1 \\ \mathbf{e}^2 \\ \mathbf{e}^3 \end{bmatrix} = \begin{bmatrix} 0 & \sin\left(\phi^3\right)\sec\left(\phi^2\right) & \cos\left(\phi^3\right)\sec\left(\phi^2\right) \\ 0 & \cos\left(\phi^3\right) & -\sin\left(\phi^3\right) \\ 1 & \sin\left(\phi^3\right)\tan\left(\phi^2\right) & \cos\left(\phi^3\right)\tan\left(\phi^2\right) \end{bmatrix} \begin{bmatrix} \mathbf{d}_1 \\ \mathbf{d}_2 \\ \mathbf{d}_3 \end{bmatrix}. \tag{5.239}$$

Establish the corresponding representations for $\mathbf{e}^k$ in terms of $\mathbf{D}_1, \mathbf{D}_2$, and $\mathbf{D}_3$.

(e) Show that the components $v_i = \mathbf{v} \cdot \mathbf{D}_i$ of the strain vector $\mathbf{P}\mathbf{v} = \sum_{i=1}^{3} v_i \mathbf{d}_i$ have the following representations in terms of the 3-2-1 set of Euler angles:

$$\begin{bmatrix} v_1 \\ v_2 \\ v_3 \end{bmatrix} = \begin{bmatrix} -\sin\left(\phi^2\right) & 0 & 1 \\ \cos\left(\phi^2\right)\sin\left(\phi^3\right) & \cos\left(\phi^3\right) & 0 \\ \cos\left(\phi^2\right)\cos\left(\phi^3\right) & -\sin\left(\phi^3\right) & 0 \end{bmatrix} \begin{bmatrix} \frac{\partial \phi^1}{\partial \xi} \\ \frac{\partial \phi^2}{\partial \xi} \\ \frac{\partial \phi^3}{\partial \xi} \end{bmatrix}. \tag{5.240}$$

In addition, show that the inverses of these relations are

$$\begin{bmatrix} \frac{\partial \phi^1}{\partial \xi} \\ \frac{\partial \phi^2}{\partial \xi} \\ \frac{\partial \phi^3}{\partial \xi} \end{bmatrix} = \begin{bmatrix} 0 & \sin\left(\phi^3\right)\sec\left(\phi^2\right) & \cos\left(\phi^3\right)\sec\left(\phi^2\right) \\ 0 & \cos\left(\phi^3\right) & -\sin\left(\phi_3\right) \\ 1 & \sin\left(\phi^3\right)\tan\left(\phi^2\right) & \cos\left(\phi^3\right)\tan\left(\phi^2\right) \end{bmatrix} \begin{bmatrix} v_1 \\ v_2 \\ v_3 \end{bmatrix}. \tag{5.241}$$

(f) Show that the vector $\mathbf{d}_3 = \mathbf{r}'$ has the representation

$$\mathbf{d}_3 = \sin\left(\phi^2\right)\mathbf{D}_1 + \cos\left(\phi^2\right)\sin\left(\phi^3\right)\mathbf{D}_2 + \cos\left(\phi^2\right)\cos\left(\phi^3\right)\mathbf{D}_3. \tag{5.242}$$

With the help of this expression for $\mathbf{r}'$, compute representations for the curvature κ and torsion τ of the centerline of a rod whose rotation tensor $\mathbf{P}$ is parameterized using a set of 3-2-1 Euler angles.

(g) Consider an initially straight homogeneous rod which is subject to terminal moments and terminal forces and deforms into a twisted rod whose centerline remains straight (see Figure 5.6(b)). For this rod, we assume that $\mathbf{P} = \mathbf{Q}_{\mathbf{E}}\left(\phi_0, \mathbf{E}_3\right)$ where $\frac{\partial \phi_0}{\partial \xi}$ is a constant and choose $\mathbf{D}_k = \mathbf{E}_k$. To examine the stability of the deformed configuration, we consider perturbations to the straight twisted state:

$$\mathbf{P} = \mathbf{Q}_{\mathbf{E}}\left(\delta\phi^3, \mathbf{e}_3\right)\mathbf{Q}_{\mathbf{E}}\left(\delta\phi^2, \mathbf{e}_2\right)\mathbf{Q}_{\mathbf{E}}\left(\delta\phi^1, \mathbf{e}_1\right)\mathbf{Q}_{\mathbf{E}}\left(\phi_0, \mathbf{E}_3\right), \tag{5.243}$$

where $\delta\phi^k$ are assumed to be small.[53] Show that

$$\mathbf{P}\mathbf{v} \approx \frac{\partial \delta\phi^3}{\partial \xi}\mathbf{i}_1 + \frac{\partial \delta\phi^2}{\partial \xi}\mathbf{i}_2 + \left(\frac{\partial \delta\phi^1}{\partial \xi} + \frac{\partial \phi_0}{\partial \xi}\right)\mathbf{E}_3, \tag{5.244}$$

where $\mathbf{i}_1 = \mathbf{Q}_{\mathbf{E}}\left(\phi_0, \mathbf{E}_3\right)\mathbf{E}_1$ and $\mathbf{i}_2 = \mathbf{Q}_{\mathbf{E}}\left(\phi_0, \mathbf{E}_3\right)\mathbf{E}_2$. By considering the deformed centerline of the rod, show that the following identifications can be made:

$$\delta\phi^2 \approx \frac{\partial \hat{X}}{\partial s}, \qquad \delta\phi^3 \approx \frac{\partial \hat{Y}}{\partial s}, \qquad \frac{\partial Z}{\partial s} \approx 1, \tag{5.245}$$

where $\mathbf{r} = \hat{X}\mathbf{i}_1 + \hat{Y}\mathbf{i}_2 + Z\mathbf{E}_3$.

(h) Suppose $\mathbf{P}$ is given by Eqn. (5.243). Show that

$$\mathbf{r}' \times \mathbf{r}'' = \mathbf{d}_3 \times \mathbf{d}_3' \approx -\frac{\partial \delta\phi^3}{\partial \xi}\mathbf{i}_1 + \frac{\partial \delta\phi^2}{\partial \xi}\mathbf{i}_2. \tag{5.246}$$

[53] That is, we are considering a set of three infinitesimal rotations superposed on a finite rotation.

Noting that $\kappa \mathbf{e}_b = \mathbf{r}' \times \mathbf{r}''$, give an interpretation of the perturbation that the infinitesimal rotations $\delta\phi^k$ provide.

(i) Suppose the strain energy function of the rod is given by Eqn. (5.64). Determine an expression for the moment $\mathbf{m}$ in the rod when $\mathbf{P}$ is given by Eqn. (5.243).

Exercise 5.7: To establish the alternative form (5.87) of the jump condition $(5.81)_7$ a variety of identities were employed. To this end, show that

$$[\![\mathbf{G}]\!]_\gamma \cdot \mathbf{v}_\gamma = \left[\!\left[\mathbf{G} \cdot \left(\dot{\mathbf{r}} + \dot{\gamma}\mathbf{r}'\right)\right]\!\right]_\gamma,$$

and that

$$\left[\!\left[\mathbf{d}_\beta \times \mathbf{L}^\beta\right]\!\right]_\gamma \cdot \boldsymbol{\omega}_\gamma = \left[\!\left[\left((\boldsymbol{\omega} + \dot{\gamma}\mathbf{P}(\mathbf{v} + \mathbf{v}_0)) \times \mathbf{d}_\beta\right) \times \mathbf{L}^\beta\right]\!\right]_\gamma, \qquad (\beta = 1,2). \tag{5.247}$$

With the help of the preceding results, show that

$$[\![2T]\!]_\gamma \dot{\gamma} = [\![\mathsf{P}\dot{\gamma}]\!]_\gamma \dot{\gamma} + [\![\mathbf{G}\dot{\gamma}]\!]_\gamma \cdot \mathbf{v}_\gamma + \left[\!\left[\mathbf{d}_1 \times \mathbf{L}^1 + \mathbf{d}_2 \times \mathbf{L}^2\right]\!\right]_\gamma \cdot \boldsymbol{\omega}_\gamma. \tag{5.248}$$

The continuity of $\mathbf{d}_1$ and $\mathbf{d}_2$ as well as the identities (1.58) and (5.50) should be used to arrive at your solution.

Exercise 5.8: Verify that the equations (5.138) for the rod problem discussed in Section 5.15 are equivalent to Lagrange's equations of motion,

$$\frac{\partial}{\partial \xi}\left(\frac{\partial L}{\partial \alpha^{k\prime}}\right) - \frac{\partial L}{\partial \alpha^k} = 0, \qquad (k = 1,2,3), \tag{5.249}$$

where

$$L = \frac{EI}{2}\left(\frac{\partial \alpha^2}{\partial \xi}\frac{\partial \alpha^2}{\partial \xi} + \frac{\partial \alpha^1}{\partial \xi}\frac{\partial \alpha^1}{\partial \xi}\sin^2\left(\alpha^2\right)\right) + \frac{\mathscr{D}}{2}\left(\frac{\partial \alpha^1}{\partial \xi}\cos\left(\alpha^2\right) + \frac{\partial \alpha^3}{\partial \xi}\right)^2 - F_\ell \cos\left(\alpha^2\right). \tag{5.250}$$

Exercise 5.9: Consider the differential equation (5.148) discussed in Section 5.15. Show that the equilibria $\left(\alpha^2 = \alpha_0^2, \frac{\partial \alpha^2}{\partial \xi} = 0\right)$ of this equation are governed by a quartic equation for $\cos\left(\alpha_0^2\right)$. For $\frac{F_\ell EI}{c^2} > \frac{1}{4}$, show that 3 equilibria are present and for $\frac{F_\ell EI}{c^2} < \frac{1}{4}$ the only equilibrium present is $\alpha_0^2 = 0$. In contrast, show that the differential equation (5.251) has a single equilibrium $\left(\alpha^2 = \alpha_0^2 = \pi, \frac{\partial \alpha^2}{\partial \xi} = 0\right)$ for all nonzero values of $\frac{F_\ell EI}{c^2}$.

Exercise 5.10: Consider the analytical expression (5.163) for $\alpha^2(\xi)$ corresponding to the homoclinic orbit. With the help of Eqns. (5.163) and (5.164) and the representations (5.15) for the Euler basis vectors, determine analytical expressions for the centerline of the deformed rod. Show how the shape of this centerline and the

tangent indicatrix changes as Δ increases from 0 to 1. As a check on your answers, examples of $\mathbf{r}(\xi)$ and $\mathbf{d}_3(\xi)$ can be seen in Figures 10–12 in [164].

Exercise 5.11: Consider the case of a rod where $EI_1 = EI_2$ which is loaded at its ends by terminal force and moments as in Section 5.15. Suppose that $c_S = -c_F = c$. In this case, the moment components in the directions of $\mathbf{d}_3$ and $\mathbf{F}_0$ are equal and opposite. Show that the differential equation (5.144) simplifies to

$$EI\frac{\partial^2\alpha^2}{\partial\xi^2} - \frac{c^2\left(\left(1+\cos\left(\alpha^2\right)\right)^2\right.}{EI\sin^3\left(\alpha^2\right)} = F_\ell \sin\left(\alpha^2\right). \tag{5.251}$$

The differential equation (5.251) is analogous to the equation used to demonstrate the stability of a downward pointing top (sleeping top) for any spin speed. Classify the solutions to Eqn. (5.251), show that the sole equilibrium corresponds to a twisted rod whose centerline is straight, and show that the remaining deformed shapes of the rod's centerline are qualitatively similar.

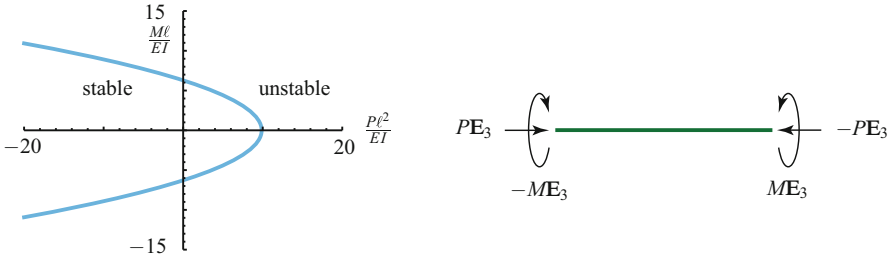

Fig. 5.29 Greenhill's stability criterion (5.252) for a straight terminally loaded rod of length ℓ. The development of the criterion was motivated by possible buckling instabilities in the drive shafts (propellor shafts) of ships some of which were over 150 feet long and close to 2 feet in diameter.

Exercise 5.12: In Greenhill [141], the following criterion for stability of a rod of length ℓ where $EI = EI_1 = EI_2$ which is subject to a thrust force P and an applied moment M was established[54]:

$$\frac{M^2}{4EI} + P \le \frac{\pi^2 EI}{\ell^2}. \tag{5.252}$$

The criterion is shown in Figure 5.29. The terminal loadings on the rod are $\mathbf{F}_0 = P\mathbf{E}_3$, $\mathbf{F}_\ell = -P\mathbf{E}_3$, $\mathbf{M}_0 = -M\mathbf{E}_3$, and $\mathbf{M}_\ell = M\mathbf{E}_3$. Thus, when $P > 0$, the rod is in compression. To establish his criterion, Greenhill derived the following pair of linearized equations for the transverse deflections u_1 and u_2 of the rod:

[54] Additional discussions of this criterion can be found in [213, Section 272] and [345, Pages 156–157]. Ziegler's delightful introductory text [375, Chapter 5, Section 3] has an informative discussion of the case where $P = 0$.

$$\begin{bmatrix} \frac{\partial^2 u_1}{\partial x^2} \\ \frac{\partial^2 u_2}{\partial x^2} \end{bmatrix} + \begin{bmatrix} 0 & \frac{M}{EI} \\ -\frac{M}{EI} & 0 \end{bmatrix} \begin{bmatrix} \frac{\partial u_1}{\partial x} \\ \frac{\partial u_2}{\partial x} \end{bmatrix} + \begin{bmatrix} \frac{P}{EI} & 0 \\ 0 & \frac{P}{EI} \end{bmatrix} \begin{bmatrix} u_1 \\ u_2 \end{bmatrix} = \begin{bmatrix} 0 \\ 0 \end{bmatrix}. \tag{5.253}$$

Here, x is the axial coordinate and the deflections u_1 and u_2 are subject to the boundary conditions

$$u_1(x=0)=0, \qquad u_2(x=0)=0, \qquad u_1(x=\ell)=0, \qquad u_2(x=\ell)=0. \tag{5.254}$$

(a) Show that $u_1(x)$ is governed by the differential equation

$$\frac{\partial^4 u_1}{\partial x^4} + \left(\left(\frac{M}{EI} \right)^2 + \frac{2P}{EI} \right) \frac{\partial^2 u_1}{\partial x^2} + \left(\frac{P}{EI} \right)^2 u_1 = 0. \tag{5.255}$$

(b) Verify that the general solution to Eqn. (5.253) is

$$\begin{aligned} u_1 &= A_1 \sin(\omega_1 x) + A_2 \cos(\omega_1 x) + A_3 \sin(\omega_2 x) + A_4 \cos(\omega_2 x), \\ u_2 &= B_1 \sin(\omega_1 x) + B_2 \cos(\omega_1 x) + B_3 \sin(\omega_2 x) + B_4 \cos(\omega_2 x), \end{aligned} \tag{5.256}$$

where $A_{1,2,3,4}$ and $B_{1,2,3,4}$ are constants, and $\omega_{1,2}$ are the roots of

$$\left(\omega^2 - \frac{P}{EI} \right)^2 - \left(\frac{M}{EI} \right)^2 \omega^2 = 0. \tag{5.257}$$

That is,

$$\omega_{1,2} = \frac{M}{2EI} \pm \sqrt{\left(\frac{M}{2EI} \right)^2 + \frac{P}{EI}}. \tag{5.258}$$

(c) Assuming $M \neq 0$, with the help of Eqn. (5.253), show that

$$B_1 = -f_1 A_2, \qquad B_2 = f_1 A_1, \qquad B_3 = -f_2 A_4, \qquad B_4 = f_2 A_3, \tag{5.259}$$

where

$$\begin{aligned} f_1 &= \left(-\omega_1^2 + \frac{P}{EI} \right) \left(\omega_1 \frac{M}{EI} \right)^{-1} = 1, \\ f_2 &= \left(-\omega_2^2 + \frac{P}{EI} \right) \left(\omega_2 \frac{M}{EI} \right)^{-1} = 1. \end{aligned} \tag{5.260}$$

(d) By forming a matrix equation for $A_{1,2,3,4}$ using the boundary conditions (5.254) and examining the determinant of the resulting matrix, show that nonzero solutions to the boundary-value problem are possible when the following equation is satisfied:

$$\sin\left(\frac{\ell}{2} (\omega_1 - \omega_2) \right) = 0. \tag{5.261}$$

Show that this equation implies Greenhill's stability criterion (5.252).

(e) Consider the case $M = 0$. Show that $\omega_1 = \omega_2 = \sqrt{\frac{P}{EI}}$ and, in order for a non-trivial solution to the boundary-value problem to exist, that

$$\sin\left(\sqrt{\frac{P}{EI}}\ell\right) = 0. \tag{5.262}$$

Verify that this condition is equivalent to the classic Euler buckling formula $\frac{P\ell^2}{EI} = \pi^2$. Why cannot this result be directly found from Eqn. (5.261)?

(f) Consider the case $P = 0$. Show that $\omega_2 = 0$ and $\omega_1 = \frac{M}{EI}$ and, in order for a nontrivial solution to the boundary-value problem to exist, that

$$\cos\left(\frac{M\ell}{EI}\right) = 1. \tag{5.263}$$

Verify that this condition is equivalent to the classic torsional instability criterion $\frac{M\ell}{EI} = 2\pi$.

(g) After non-dimensionalizing P and M, numerically determine the solutions $\frac{P\ell^2}{EI}$ and $\frac{M\ell}{EI}$ to Eqn. (5.261) such that nonzero solutions to the boundary-value can be found. It is prudent to verify that the limiting cases of your results are the solutions discussed in Eqn. (5.252) and the earlier parts (e) and (f) of this exercise. Plot representative values of the solutions $u_1(x)$ and $u_2(x)$ corresponding to the buckling modes of the shaft. For certain instances, these modes should reduce to the classic buckling modes discussed in (e) and (f).

(h) Using your results from (g), show that if the rod is in tension ($P < 0$), then by choosing P appropriately it is possible for the rod to support an arbitrarily large moment M without becoming unstable.

Exercise 5.13: Greenhill's development of the linearized equations (5.253) in [141] starts with a model for an initially straight homogenous rod whose strain energy function is given by Eqn. (5.64).

(a) For this rod show that, under loading by terminal forces $\pm P\mathbf{E}_3$ and moments $\mp M\mathbf{E}_3$ and assuming that the centerline remains straight, the angle of twist changes at a constant rate along the length of the rod.

(b) Consider an order ε perturbation to the straight state:

$$\mathbf{r} = X\mathbf{E}_1 + Y\mathbf{E}_2 + Z\mathbf{E}_3 = z\mathbf{E}_3 + \varepsilon\left(u_1\mathbf{E}_1 + u_2\mathbf{E}_2 + u_3\mathbf{E}_3\right). \tag{5.264}$$

Show that

$$\frac{\partial z}{\partial s} = 1 + \mathscr{O}(\varepsilon), \qquad \frac{\partial u_1}{\partial s} = \frac{\partial u_1}{\partial z} + \mathscr{O}(\varepsilon), \qquad \frac{\partial u_2}{\partial s} = \frac{\partial u_2}{\partial z} + \mathscr{O}(\varepsilon). \tag{5.265}$$

(c) Starting from the ansatz (5.264) and using the results (5.265), show that

$$\begin{aligned}\kappa \mathbf{e}_b &= \mathbf{r}' \times \mathbf{r}'' \\ &= -\varepsilon \frac{\partial^2 u_2}{\partial z^2}\mathbf{E}_1 + \varepsilon \frac{\partial^2 u_1}{\partial z^2}\mathbf{E}_2 + \mathscr{O}\left(\varepsilon^2\right).\end{aligned} \tag{5.266}$$

If the perturbation to the straight twisted state is such that

$$EI\kappa \mathbf{e}_b + M\mathbf{r}' - \mathbf{r} \times P\mathbf{E}_3 = \text{constant}, \tag{5.267}$$

then show how Eqn. (5.267) leads to the differential equations (5.253).

(d) Show how Eqn. (5.267) can be partially motivated by the balance laws $\mathbf{n}' = \mathbf{0}$ and $(\mathbf{m} + \mathbf{r} \times \mathbf{n})' = \mathbf{0}$ along with the appropriate boundary conditions. For assistance with this problem, the results of Exercise 5.6(g)-(i) may prove to be helpful.

Exercise 5.14: This exercise outlines the establishment of the following extension to Kirchhoff's kinetic analogue that was proposed by Joseph Larmor (1857–1942) [197, Section 8]: "That the motion of a gyroscopic pendulum (i.e., a solid rotating about a fixed point with a revolving fly-wheel mounted on an axis fixed in it) is exactly analogous to the form assumed by a wire originally helical, when deformed by any distribution of forces applied to its extremities."[55] Larmor's extension is helpful when analyzing the deformed shapes of plant tendrils and wires that have intrinsic curvatures, geometric torsion, and twist.

(a) Consider a rod which has an intrinsic curvature $\boldsymbol{\nu}_0 = \nu_{0_1}\mathbf{D}_1 + \nu_{0_2}\mathbf{D}_2 + \nu_{0_3}\mathbf{D}_3$. Under which conditions does the rod correspond to a twisted rod with a straight centerline, a twisted rod with a circular centerline, and a twisted rod where the centerline is bent into a circular helix?

(b) Show that

$$\mathbf{d}_k' = \left(\sum_{i=1}^{3}\left(\nu_i + \nu_{0_i}\right)\mathbf{d}_i\right) \times \mathbf{d}_k. \tag{5.268}$$

(c) Suppose the rod is bent by application of terminal forces $\pm\mathbf{F}_0$ and terminal moments. Using balances of linear and angular momentum, $\mathbf{n}' = \mathbf{0}$ and $\mathbf{m}' + \mathbf{r}' \times \mathbf{n} = \mathbf{0}$, and assuming a constitutive relation

$$2\rho_0\psi = EI_1\nu_1^2 + EI_2\nu_2^2 + \mathscr{D}\nu_3^2, \tag{5.269}$$

establish the equations governing $\nu_k(\xi)$:

$$\begin{aligned} EI_1\nu_1' - EI_2\nu_2\left(\nu_3 + \nu_{0_3}\right) + \mathscr{D}\left(\nu_2 + \nu_{0_2}\right)\nu_3 &= -\mathbf{d}_2 \cdot \mathbf{F}_0, \\ EI_2\nu_2' - \mathscr{D}\left(\nu_1 + \nu_{0_1}\right)\nu_3 + EI_1\left(\nu_3 + \nu_{0_3}\right)\nu_1 &= \mathbf{d}_1 \cdot \mathbf{F}_0, \\ \mathscr{D}\nu_3' - EI_1\left(\nu_2 + \nu_{0_2}\right)\nu_1 + EI_2\left(\nu_1 + \nu_{0_1}\right)\nu_2 &= 0. \end{aligned} \tag{5.270}$$

[55] This extension is presented in far greater detail in Love [213, Section 261] than in Larmor's original work [197, Section 8].

The constitutive parameters EI_1, EI_2, and $\mathscr{D}$ are assumed to be constant. HINT: the derivation of Eqn. (5.270) closely follows the developments of Eqns. (5.119).

(d) Using the conservations (5.115) and (5.116), show that the following three quantities are conserved along the length of the rod:

$$\mathbf{n}\cdot\mathbf{m}, \qquad \mathsf{C}, \qquad \mathbf{n}\cdot\mathbf{n}. \tag{5.271}$$

For the conservation of C, it is necessary to assume that ν_{k_0} are constant. This assumption is adopted for the remainder of this exercise.

(e) Show that the equations you found in (c) correspond to those for the orientation of a gyrostat which is free to rotate about a fixed point O. Give a sketch of the gyrostat and discuss how the orientation of the flywheel relative to the outer rigid casing is related to ν_{0_k}, EI_1, EI_2, $\mathscr{D}$, and the moment of inertia I of the flywheel about its axis of symmetry.

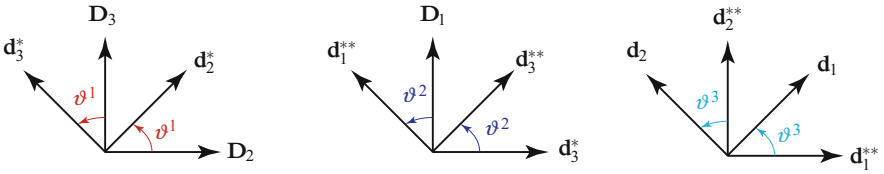

Fig. 5.30 Schematic of the three rotations used to define the 1-2-3 set of Euler angles (cf. Eqn. (5.272)).

Exercise 5.15: In many applications of rods theories, the rod has an intrinsic curvature ν_{0_1}. For these situations, it is convenient to use a 1-2-3 set of Euler angles to parameterize $\mathbf{P} = \sum_{i=1}^{3} \mathbf{d}_i \otimes \mathbf{D}_i$ (cf. Figure 5.30). Whence,[56]

$$\begin{aligned}
\mathbf{P}\mathbf{P}_0 &= \sum_{i=1}^{3} \mathbf{d}_i \otimes \mathbf{E}_i = \mathbf{Q}_{\mathbf{E}}\left(\vartheta^3, \mathbf{e}_3\right) \mathbf{Q}_{\mathbf{E}}\left(\vartheta^2, \mathbf{e}_2\right) \mathbf{Q}_{\mathbf{E}}\left(\vartheta^1, \mathbf{e}_1\right) \mathbf{Q}_{\mathbf{E}}\left(\vartheta^0, \mathbf{D}_1\right), \\
\mathbf{P}_0 &= \sum_{i=1}^{3} \mathbf{D}_i \otimes \mathbf{E}_i = \cos\left(\vartheta^0\right)\left(\mathbf{I} - \mathbf{E}_1 \otimes \mathbf{E}_1\right) + \sin\left(\vartheta^0\right) \operatorname{skew}\left(\mathbf{E}_1\right) + \mathbf{E}_1 \otimes \mathbf{E}_1.
\end{aligned} \tag{5.272}$$

Here, the angle ϑ^0 is intimately related to the sole nonvanishing intrinsic curvature:

$$\nu_{0_1} = \frac{\partial \vartheta^0}{\partial \xi}. \tag{5.273}$$

[56] Parameterizations of this type are sometimes used in studies on the dynamics of satellites in orbit. See, for example, Rumyantsev [311] and articles such as [272, 333] citing this work.

(a) Show that the components $P_{ik} = (\mathbf{P}\mathbf{D}_k)\cdot\mathbf{D}_i$ of $\mathbf{P}$ have the representations

$$\begin{bmatrix} P_{11} & P_{12} & P_{13} \\ P_{21} & P_{22} & P_{23} \\ P_{31} & P_{32} & P_{33} \end{bmatrix} = \begin{bmatrix} c_2c_3 & -c_2s_3 & s_2 \\ c_3s_1s_2+c_1s_3 & c_1c_3-s_1s_2s_3 & -c_2s_1 \\ -c_1c_3s_2+s_1s_3 & c_3s_1+c_1s_2s_3 & c_1c_2 \end{bmatrix}. \tag{5.274}$$

In writing expressions for the components P_{ik}, we have employed the abbreviations $c_k = \cos\left(\vartheta^k\right)$ and $s_k = \sin\left(\vartheta^k\right)$.

(b) Show that the Euler basis vectors used in the representations (5.272) for the rotation tensors $\mathbf{P}$ and $\mathbf{P}_0$ have the representations

$$\begin{aligned} \mathbf{e}_1 &= \mathbf{E}_1 = \mathbf{D}_1 \\ &= \cos\left(\vartheta^2\right)\cos\left(\vartheta^3\right)\mathbf{d}_1 - \cos\left(\vartheta^2\right)\sin\left(\vartheta^3\right)\mathbf{d}_2 + \sin\left(\vartheta^2\right)\mathbf{d}_3, \\ \mathbf{e}_2 &= \cos\left(\vartheta^1\right)\mathbf{D}_2 + \sin\left(\vartheta^1\right)\mathbf{D}_3 \\ &= \cos\left(\vartheta^3\right)\mathbf{d}_2 + \sin\left(\vartheta^3\right)\mathbf{d}_1, \\ \mathbf{e}_3 &= \sin\left(\vartheta^2\right)\mathbf{D}_1 - \cos\left(\vartheta^2\right)\sin\left(\vartheta^1\right)\mathbf{D}_2 + \cos\left(\vartheta^2\right)\cos\left(\vartheta^1\right)\mathbf{D}_3 \\ &= \mathbf{d}_3 = \mathbf{e}_t. \end{aligned} \tag{5.275}$$

In addition, show that

$$\begin{aligned} \mathbf{E}_3 = &\left(-\cos\left(\vartheta^1+\vartheta^0\right)\sin\left(\vartheta^2\right)\cos\left(\vartheta^3\right) + \sin\left(\vartheta^1+\vartheta^0\right)\sin\left(\vartheta^3\right)\right)\mathbf{d}_1 \\ &+ \left(\cos\left(\vartheta^1+\vartheta^0\right)\sin\left(\vartheta^2\right)\sin\left(\vartheta^3\right) + \sin\left(\vartheta^1+\vartheta^0\right)\cos\left(\vartheta^3\right)\right)\mathbf{d}_2 \\ &+ \cos\left(\vartheta^1+\vartheta^0\right)\cos\left(\vartheta^2\right)\mathbf{d}_3. \end{aligned} \tag{5.276}$$

(c) Why are the Euler angles subject to the restrictions $\vartheta^1 \in [0, 2\pi)$, $\vartheta^2 \in (-\pi/2, \pi/2)$, and $\vartheta^3 \in [0, 2\pi)$? Suppose the reference configuration of the centerline of the rod lies in the $\mathbf{E}_2 - \mathbf{E}_3$. Show that the Euler angles in this configuration are not close to the singularities associated with ϑ^2. Could the same statement be made if a set of 1-2-1 Euler angles were used to parameterize $\mathbf{P}$?

(d) Show that the dual Euler basis vectors have the following representations:

$$\begin{bmatrix} \mathbf{e}^1 \\ \mathbf{e}^2 \\ \mathbf{e}^3 \end{bmatrix} = \begin{bmatrix} \sec\left(\vartheta^2\right)\cos\left(\vartheta^3\right) & -\sec\left(\vartheta^2\right)\sin\left(\vartheta^3\right) & 0 \\ \sin\left(\vartheta^3\right) & \cos\left(\vartheta^3\right) & 0 \\ -\tan\left(\vartheta^2\right)\cos\left(\vartheta^3\right) & \tan\left(\vartheta^2\right)\sin\left(\vartheta^3\right) & 1 \end{bmatrix} \begin{bmatrix} \mathbf{d}_1 \\ \mathbf{d}_2 \\ \mathbf{d}_3 \end{bmatrix}. \tag{5.277}$$

Establish the corresponding representations for $\mathbf{e}^k$ in terms of the two set of basis vectors $\{\mathbf{E}_1, \mathbf{E}_2, \mathbf{E}_3\}$ and $\{\mathbf{D}_1, \mathbf{D}_2, \mathbf{D}_3\}$.

(e) Show that the components $v_i = \mathbf{v}\cdot\mathbf{D}_i$ of the strain vector $\mathbf{P}\mathbf{v} = \sum_{i=1}^{3} v_i\mathbf{d}_i$ have the following representations:

$$\begin{bmatrix} v_1 \\ v_2 \\ v_3 \end{bmatrix} = \begin{bmatrix} \cos\left(\vartheta^2\right)\cos\left(\vartheta^3\right) & \sin\left(\vartheta^3\right) & 0 \\ -\cos\left(\vartheta^2\right)\sin\left(\vartheta^3\right) & \cos\left(\vartheta^3\right) & 0 \\ \sin\left(\vartheta^2\right) & 0 & 1 \end{bmatrix} \begin{bmatrix} \frac{\partial\vartheta^1}{\partial\xi} \\ \frac{\partial\vartheta^2}{\partial\xi} \\ \frac{\partial\vartheta^3}{\partial\xi} \end{bmatrix}. \tag{5.278}$$

In addition, show that the inverses of these relations are

$$\begin{bmatrix} \frac{\partial \vartheta^1}{\partial \xi} \\ \frac{\partial \vartheta^2}{\partial \xi} \\ \frac{\partial \vartheta^3}{\partial \xi} \end{bmatrix} = \begin{bmatrix} \cos\left(\vartheta^3\right)\sec\left(\vartheta^2\right) & -\sin\left(\vartheta^3\right)\sec\left(\vartheta^2\right) & 0 \\ \sin\left(\vartheta^3\right) & \cos\left(\vartheta^3\right) & 0 \\ -\cos\left(\vartheta^3\right)\tan\left(\vartheta^2\right) & \sin\left(\vartheta^3\right)\tan\left(\vartheta^2\right) & 1 \end{bmatrix} \begin{bmatrix} \nu_1 \\ \nu_2 \\ \nu_3 \end{bmatrix}. \tag{5.279}$$

(f) With the help of the Bonnet-Meusnier relations (5.102) and the representations

$$\begin{aligned} \mathbf{D}_2^{'} &= \nu_{0_1}\mathbf{D}_3, \\ \mathbf{D}_3^{'} &= -\nu_{0_1}\mathbf{D}_2, \\ \mathbf{d}_3 &= \mathbf{r}^{'} = \mathbf{e}_t \\ &= \sin\left(\vartheta^2\right)\mathbf{D}_1 - \sin\left(\vartheta^1\right)\cos\left(\vartheta^2\right)\mathbf{D}_2 + \cos\left(\vartheta^2\right)\cos\left(\vartheta^1\right)\mathbf{D}_3, \end{aligned} \tag{5.280}$$

show that

$$\kappa^2 = \left(\frac{\partial \vartheta^0}{\partial \xi} + \frac{\partial \vartheta^1}{\partial \xi}\right)^2 \cos^2\left(\vartheta^2\right) + \left(\frac{\partial \vartheta^2}{\partial \xi}\right)^2. \tag{5.281}$$

With the help of this result, derive expressions for the torsion τ of the centerline and rate of change of the angle of twist $\frac{\partial \phi}{\partial s}$ of a rod whose rotation tensor $\mathbf{P}$ is parameterized using a set of 1-2-3 Euler angles. Give a physical interpretation of the conditions whereby $\frac{\partial \phi}{\partial s} = \frac{\partial \vartheta^3}{\partial s}$.